Hippo signaling instructs ectopic but not normal organ growth

Authors: W. Kowalczyk[1*], L. Romanelli[1*], M. Atkins[1,6], H. Hillen[1], C. Bravo González-Blas[2], J. Jacobs[2], J. Xie[1], S. Soheily[1], E. Verboven[1], I. M. Moya[1,3], S. Verhulst[4], M. de Waegeneer[2], L. Sansores-Garcia[1], L. van Huffel[1], R.L. Johnson[5], Leo A. van Grunsven[4], S. Aerts[2], G. Halder[1#]

Affiliations:

[1] VIB Center for Cancer Biology and KU Leuven Department of Oncology, KU Leuven; Leuven, Belgium

[2] VIB Center for Brain and Disease Research and KU Leuven Department of Neurosciences, KU Leuven; Leuven, Belgium

[3] Facultad de Ingeniería y Ciencias Aplicadas, Universidad de Las Américas; Quito, Ecuador.

[4] Department for Cell Biology, Faculty of Medicine and Pharmacy, Vrije Universiteit Brussel; Brussel-Jette, Belgium

[5] The University of Texas MD Anderson Cancer Center; Houston, TX, USA

[6] Department of Biological Sciences, Sam Houston State University; Huntsville, TX, USA

* Contributed equally

Corresponding author. Email: Georg.Halder@vib.be

Abstract: The Hippo signalling pathway is widely considered a master regulator of organ growth due to the striking overgrowth phenotypes caused by experimental manipulation of its activity. Contrary to this model, here we show that removing Hippo transcriptional output did not impair the ability of the mouse liver and *Drosophila* eyes to grow to their normal size. Moreover, the transcriptional activity of the Hippo pathway effectors Yki/Yap/Taz did not correlate with cell proliferation, and hyperactivation of Yki/Yap/Taz induced gene expression programs that did not recapitulate normal development. Concordantly, a functional screen in *Drosophila* identified several Hippo pathway target genes that were required for ectopic overgrowth but not normal growth. Thus, Hippo signalling does not instruct normal growth and the Hippo-induced overgrowth phenotypes are due to activation of abnormal genetic programs.

Main Text:

The Hippo pathway is a conserved signal transduction pathway that regulates gene expression through its downstream effectors, the transcriptional co-activators Yap and Taz (Yorkie, Yki in *Drosophila*) that bind to TEAD (Scalloped, Sd in *Drosophila*) and other transcription factors (1-5). The core of the pathway comprises a kinase cascade where the Mst1/2 kinases (Hippo, Hpo in *Drosophila*) activate the Lats1/2 kinases (Warts, Wts in *Drosophila*) which then inhibit Yap/Taz/Yki by phosphorylation (Fig.S1A). Hippo pathway activity is modulated by diverse biochemical and mechanical cell-cell and ECM-cell signals integrating information about cell shape, cell adhesion, and tissue integrity (1-5).

The Hippo pathway is thought to be a master regulator of organ growth (5-10). This model is largely based on the observation that mutations in Hippo pathway components can lead to organ overgrowth in flies and mice. In particular the mouse liver and *Drosophila* imaginal disc derived structures such as eyes and wings show dramatic overgrowth upon Hippo pathway deregulation. There, loss-of-function mutations in the core kinases or overexpression of Yap/Taz/Yki upregulates the expression of genes that induce cell proliferation, cell survival and tissue growth (6, 11-20). Accordingly, the central hypothesis of the Hippo pathway growth control model is that Yap/Taz/Yki are active and drive cell proliferation during the growth phase of an organ but are then inactivated when the organ has reached its proper size. Thus, in this model, the Hippo pathway acts instructively in that it directs cells when to proliferate and when to stop proliferation.

This model makes three key predictions: 1. Hippo pathway output is required for normal growth; 2. Hippo pathway activity is modulated during development and correlates with cell proliferation; and 3. The genetic program that drives overgrowth in Hippo mutants resembles that of normal growth. Consistent with these predictions, loss of Yki results in smaller eyes and wings (21) and hyperactivation of Yap/Taz/Yki can drive excessive cell proliferation (6, 12-20). However, some findings do not fit the model, namely that *Yap/Taz* mutant hepatocytes and *sd* mutant eye disc cells can proliferate (22-24). We therefore re-evaluated the function of Hippo signaling during organ growth. We studied *Drosophila* imaginal discs and the mouse liver, because these are major developmental paradigms where the Hippo pathway and organ growth have been investigated (10, 25, 26).

Yap/Taz are not required in liver progenitor cells for liver growth

We started by analyzing the phenotype of mouse livers where we removed Hippo pathway transcriptional output. We conditionally deleted *Yap* and *Taz* during embryonic liver development using floxed alleles (27, 28). Others and us previously reported that co-deletion of *Yap* and *Taz* from hepatoblasts, the embryonic liver progenitor cells that give rise to hepatocytes and cholangiocytes (a.k.a. biliary epithelial cells), using *Albumin-Cre (Alb-Cre)* did not affect liver

size (*23*, *24*). However, because *Alb-Cre* triggers recombination only after E15.5 when hepatoblasts are already proliferating (*29*), we used *Alfp-Cre* which is expressed earlier, before day E10.5 (*30*), at the onset of hepatoblast specification and before hepatoblasts undergo extensive proliferation (*31*)**.** *Alfp-Cre* efficiently recombined a *R26-Lox-STOP-Lox-tdTomato* reporter transgene starting at E10.5 (Fig.S1B) and knocked out *Yap/Taz* as verified by immunohistochemistry (Fig.S1D). *Alfp-Cre; Yap/Taz* double knockout mice (*Alfp-Cre; Yap/Taz*^{KO}*)* were born at Mendelian ratios but presented yellow ears and paws, and had high AST, ALT and total bilirubin serum levels, indicating liver damage (Fig.S1E). However, gross liver morphology, liver to body weight ratio and hepatocyte size and numbers were normal (Fig.1A-C, Fig.S1C). Rather, mutant mice lacked bile ducts similar to but stronger than the phenotype of *Yap* (and *Taz*) knockout by *Alb-Cre* (*23*, *24*, *32*). This was because few cholangiocytes were specified in *Alfp-Cre; Yap/Taz*^{KO} embryos (Fig.1D, Fig.S1D). Therefore, *Yap* and *Taz* are not required in hepatoblasts for their proliferation but for their differentiation into cholangiocytes.

Drosophila **eye discs can grow without Hippo pathway transcriptional output**

Unlike the ability of the mouse liver to grow in the absence of Yap and Taz, deletion of *yki* in *Drosophila* imaginal disc cells results in smaller eyes and wings (*21*). However, while this phenotype shows that Yki is required for imaginal disc development, such small tissue phenotypes result not only from mutations in genes that control growth, but also from mutations in genes required for basic cellular functions (i.e. housekeeping genes). Therefore, the *yki* loss-of-function phenotype does not reveal whether Hippo signaling acts instructively to command when and where cells proliferate or permissively to simply enable cells to function properly. We therefore turned to Sd, the main transcription factor binding to Yki. Sd is required for hyperactivated Yki to cause overgrowth (*22*, *33*, *34*), but unlike *yki* mutant cells, *sd* null mutant cells survive and can proliferate (*22*, *33*) (Fig.1E). As previously reported, this difference in phenotype is explained because Sd acts as a transcriptional repressor in the absence of Yki (*35*). Thus, *yki* mutant cells die because Sd represses cell survival genes in the absence of Yki but *sd* single or *yki;sd* double mutant cells are able to proliferate because the repressive activity of Sd is removed (Fig.1E bottom). Consequently, *sd* mutants provide a tool to eliminate Hippo pathway output without killing the cells. However, because Yki can also interact with other transcription factors (*36*, *37*), we first determined to what extent deletion of Sd reduces the ability of Yki to drive gene expression and thus Hippo pathway transcriptional output.

To this end, we studied eye imaginal discs rather than wing discs, because Sd controls the fate of wing disc cells in addition to its role in the Hippo pathway (*38*). We induced mutant clones early in eye development before the major growth phase using the *eyeless-Flipase (ey-Flp)*/FRT MARCM recombination system and inspected phenotypes in adult flies or third instar discs, after most of the eye disc cell proliferation has occurred. As reported (*22*, *33*, *34*), deletion of *sd* suppressed the overgrowth caused by loss of *hpo* (Fig.1E) and the immense overgrowth of cell

clones that overexpressed Yki^{3SA}, a constitutively active form of Yki that has all three Warts phosphorylation sites mutated to alanine (*39*) (Fig.1F-G). At the level of the transcriptome, deleting *sd* completely inhibited the ability of Yki^{3SA} overexpression to cause changes in gene expression (Fig.1H-K, Fig.S2A-C, TableS1). Thus, while Yki^{3SA} overexpression caused differential expression of 1632 genes in wild-type third instar eye discs (log2FC>1; padj<0.05) (Fig.1J, Fig.S2B), these effects were fully suppressed when Yki^{3SA} was overexpressed in *sd* mutant clones (Fig.1K, Fig.S2A-C). Such double mutant discs differentially expressed only the *rosy* gene, which is an eye color gene that does not affect growth. Therefore, Yki hyperactivation has no effect on gene expression and cell proliferation anymore when Sd is not present. In conclusion, deletion of *sd* abolishes the transcriptional output of the Hippo pathway and provides a model to study imaginal disc growth control in the absence of Hippo output.

We then analyzed *sd* mutant phenotypes in more detail in third instar eye discs, as they allow visualization of cell proliferation, tissue patterning and cellular differentiation. Third instar eye discs are flat, sac-like epithelial structures where one side, the disc proper, is a columnar epithelium (of about 40,000 cells) that gives rise to the adult eye, antenna and head cuticle, while the other side, the peripodial epithelium, comprises large squamous cells (about 2000) that are required for disc eversion during metamorphosis (Fig.2A) (*40-42*). *sd* null mutant clones in the disc proper had normal numbers and distribution of cells in S-phase and grew to normal size and without developmental delay (Fig.2B-D). They also had normal patterning and neuronal specification (Fig.2D). Similarly, knockdown of *sd* specifically in the growing retinal field by expressing UAS-RNAi transgenes using the *optix-Gal4* driver did not significantly reduce eye size or affect morphology (Fig.2E, Fig.S3A), nor did it increase the variation in eye size between the left and right eyes of individual flies, a measure of fluctuating asymmetry that evaluates the robustness of growth control (*43*) (Fig.2F). The *optix>sd^{RNAi}* knockdown was effective because co-expressing *sd*-RNAi reversed the small eye phenotype of *yki* knockdown (Fig.2E). Thus, loss of *sd* did not detectably affect the development of the disc proper. In contrast, *sd* mutant clones were not recovered in the peripodial epithelium (Fig.2B-C), and knockdown of *sd* specifically in peripodial cells with *C311-Gal4* produced eye discs without peripodial epithelium but folded retinal fields and pharate adults with severe defects in head eversion (*40*), typical for defects in peripodium function (Fig.2G-I). The lack of peripodial cells in *C311>sd^{RNAi}* eye discs was due to defects in cell proliferation and survival rather than a transformation into retinal cells, as co-expression of the anti-apoptotic protein p35 partially rescued the loss of the peripodial cells which however produced a clump of morphologically abnormal cells (Fig.S3B).

At the transcriptional level, the expression profile of eye discs with *sd* mutant clones was not significantly different from that of control discs (Fig.1L). Thus, loss of Sd did not affect the expression of cell cycle genes and the basal expression levels of Hippo target genes. Correspondingly, loss of Sd reverted the massive increase in Yki target gene expression caused by Yki^{3SA} overexpression back to wild-type levels in *sd;Yki^{3SA}* double mutants (Fig.S2A-C). We did

not observe effects on peripodial gene expression since these discs did not have *sd* clones in the peripodial epithelium (Fig.2B-C; methods). Altogether, Sd, and thus transcriptional output from the Hippo pathway, is not measurably required for the growth of the eye disc proper but for the development of the peripodial epithelium.

Yap/Taz activity during liver development

The second prediction of the model was that Hippo activity is modulated during development such that Yap/Taz/Yki activity correlates with cell proliferation. To test this, we measured the activity of Yap/Taz by analyzing the expression pattern of a stringent Yap/Taz target gene signature (for simplicity "Yap signature") of 22 genes (*44*). The Yap signature was strongly upregulated in response to Yap hyperactivation in adult hepatocytes, confirming that it reports Yap activity (Fig.S4A-E). In addition, we mapped the signature onto an extensive single-cell RNA-seq atlas of the adult mouse liver that included parenchymal cells, endothelial cells, fibroblasts, immune cells, and other cell types (*45*). The Yap signature was preferentially expressed in cholangiocytes, endothelial cells and fibroblasts, which are precisely the cell types in the liver that require Yap/Taz for their development (Fig.S4F-G) (*46*)**.** We then mapped the Yap signature and a canonical cell cycle signature onto a single cell RNA-seq data set of embryonic liver development that encompasses the stages when hepatoblasts proliferate and start to differentiate into hepatocytes and cholangiocytes (embryonic days E10.5 - E17.5) (Fig.3A-B)(*47*). As expected, expression of the cell cycle genes was strongly enriched in early (proliferating) hepatoblasts and a small cluster of proliferating cholangiocytes (Fig.3C, Fig.S5A). In contrast, the Yap signature was not enriched in hepatoblasts but in all cholangiocytes (Fig.3D, Fig.S5B-D). Yap activity was comparable in cycling and non-cycling cholangiocytes, and a single cell scatter plot further showed a general lack of correlation between Yap signature expression and cell proliferation (Fig.3E, Fig.S5C). Notably, the pattern of Yap signature expression was highly robust and driven by the majority of the Yap signature genes (Fig.S5B,D,E). The pattern of Yap activity during liver development therefore mirrors the phenotype of *Yap/Taz* mutants in cholangiocyte specification and cements that Yap/Taz drive cholangiocyte development but do not control hepatoblast proliferation and thus liver growth.

Yki activity during eye disc development

Analogously, we compared the pattern of Yki activity and cell proliferation during *Drosophila* imaginal disc development. To measure Yki activity, we generated a Yki target gene signature by assembling a list of high-quality Sd binding regions in the genome (by overlapping Sd ChIP-seq peaks and Sd binding motifs) and then selecting nearby genes that were upregulated by Yki activation in eye and wing discs. (Fig.S6A-B; see methods). The resulting gene signature contained 52 genes including the Yki target genes *ex, kibra,* and *wts* (Table S2) and the signature's expression level correlated with the strength of Yki activity in different Hippo pathway mutants (Fig.S7A-B). Therefore, the Yki signature reports Yki activity in imaginal discs.

We then analyzed the expression of the Yki signature using an RNA-seq data set of discs at different time points during development spanning from mid second instar (72h AEL, after egg laying) to late third instar (120h AEL) just before puparium formation. The expression of more than 40% of the Yki signature genes increased at later time points, but overall, the expression patterns were not uniform and poorly correlated with time (Fig.S7C, TableS3), suggesting that Yki activity is not significantly downregulated towards the end of disc growth. However, a potential downregulation of Yki activity may have been obscured because cells in the posterior eye disc already start differentiating while more anterior cells still proliferate (Fig.2D *ctrl*, Fig.S7D) thereby never providing a stage at which all cells synchronously cease proliferation. To circumvent this problem, we fed larvae a special diet that lacks precursor molecules necessary for the synthesis of the molting hormone ecdysone required for pupation, thus keeping animals in the larval stage (*48*). Importantly, the imaginal discs in these larvae grow until their terminal size is reached but they do not proceed with differentiation as this requires a pulse of ecdysone. This method thus allowed us to directly compare actively growing discs with discs at the same developmental stage that terminated proliferation after reaching their proper size. Indeed, EdU incorporation was nearly absent and RNA-seq showed that cell cycle genes were downregulated in growth completed discs from 11 days old non-pupating larvae (Fig.3F-G, Fig.S8A-D). However, from the Yki signature genes only 8 (15%) were downregulated and over 40% (23) were actually upregulated in growth completed discs (Fig.3H, Fig.S8E-F, TableS3). Moreover, knockdown of *yki* reduced the expression of the Yki reporter gene *ex-lacZ* in growing as well as growth completed discs (Fig.S9). These results show that Yki is still active in growth completed discs and not inactivated when growth ceases. This was also observed with a similar approach in wing discs (*49*).

In a second approach, we separated cell proliferation from differentiation by using a single cell gene expression atlas of third instar eye discs (*50*). This atlas reproduces the switch from proliferating precursor cells in the anterior to differentiating photoreceptor and interommatidial support cells in the posterior of the eye disc (Fig.3I). The cell cycle signature was preferentially expressed in proliferating antennal and retinal precursor cells and in cells in the second mitotic wave consistent with the proliferation pattern observed by EdU incorporation (Fig.3J left, Fig.S10A). In contrast, expression of the Yki signature was highest in peripodial cells and showed no correlation with cell proliferation (Fig.3J right, Fig.S10B-E). Likewise, the Yki signature was also preferentially expressed in peripodial cells of wing discs (Fig.3K; Fig.S11A-F).

To further scrutinize our genomics findings, we examined Yki activity in situ. Yki intracellular localization, assayed by a functional Yki-GFP genomic knock-in construct, showed a tendency for enhanced nuclear localization in peripodial cells (Fig.S11H), but this assay was not very sensitive (*51*). On the other hand, the expression of *ex-lacZ* was high in peripodial cells, but its Sd independent basal expression in disc proper cells (*22*) prevented its use to compare Yki activity in

peripodial and disc proper cells (Fig.S11I). As previously observed and shown in our RNA-seq data, *kibra* expression strongly correlated with Yki activity (Fig.S11J) (52). We thus monitored *kibra* expression with a *lacZ* enhancer trap insertion into the *kibra* gene. *kibra-lacZ* expression was strongly induced upon Yki activation by *wts* knockdown (Fig.S11K-L) indicating that it is regulated by Yki. In wild type animals, *kibra-lacZ* expression was absent in disc proper cells but high in peripodial cells, even when cell proliferation stopped after disc growth was complete (Fig.3J right, Fig.S11M). Thus, *kibra-lacZ* is a new Yki-Sd activity reporter that reports positive Yki-Sd output, and its expression pattern confirmed the predominantly peripodial activity of Yki-Sd.

The preferential activity of Yki-Sd in peripodial cells was also observed at the chromatin level. Analyzing our single cell ATAC-seq dataset of accessible chromatin in eye disc cells (50) showed that over 90% of the Sd binding regions were accessible in peripodial cells and 25% were exclusively accessible in peripodial cells (Fig.S11G). In addition, more than 20% of all peripodial-specific accessible chromatin regions were bound by Sd (Fig.3L). Therefore, peripodial specific enhancers are strongly enriched for Sd binding and Sd bound enhancers are preferentially accessible in peripodial cells. Altogether, the data presented in this section show that the activity of Yki-Sd does not correlate with the rate of cell proliferation but with the development of peripodial cells consistent with the loss-of-function phenotype of *sd* mutants.

Yap hyperactivation induces an ectopic program in hepatocytes

The third prediction of the model that the Hippo pathway is a master regulator of organ growth is that the overgrowth induced by Yap/Taz/Yki hyperactivation recapitulates growth during normal development. To test this prediction, we compared the genetic program active during Yap/Taz/Yki driven overgrowth with that of normal development. In mice, we studied how ectopic Yap activation causes liver overgrowth. We conditionally activated Yap in hepatocytes of adult mice by two different methods to assure the highest robustness of our results: we deleted the *Lats1/2* kinases via injecting AAV8-Cre into *Lats1/2* double floxed mice (*Lats1/2*^{KO}) and we overexpressed YAP via doxycycline feeding of mice that expressed the tetracycline-activated transactivator (rtTA) under the hepatocyte-specific *ApoE* promoter and human YAP from a rtTA-responsive TetO promoter (hereafter *Apo>YAP*) (6). Adult hepatocytes are normally quiescent, but Yap activation triggered cell cycle re-entry and caused the liver to more than double its size within two weeks in both mutants as previously described (Fig.S12A) (6). One week after Yap activation, purified *Lats1/2*^{KO} and *Apo>YAP* hepatocytes had massive changes in gene expression that were highly correlated (R=0.84; Fig.4A, Fig.S12B-F). The overlap comprised 1819 upregulated and 372 downregulated genes (Log2FC>1, padj<0.05; TableS4). Functions of upregulated genes (hereafter called the Yap^{hyper} program) were enriched for cell cycle regulation (113 genes, 6%), ECM regulation, cell motility and angiogenesis (306 genes, 17%), and immune functions (417 genes, 23%), (Fig.S12G-H), while the downregulated genes were enriched for

hepatocyte metabolic functions (Fig.S12I-J). Notably, the Yap^{hyper} program is different from the Yap signature in that it included all 1819 genes that were either directly or indirectly upregulated in hepatocytes in response to Yap hyperactivation, while the Yap-signature is a very select set of 22 genes that are broadly activated in response to Yap.

We then asked to what extent the Yap^{hyper} program resembled that of embryonic liver development. To answer this, we mapped the Yap^{hyper} program onto the single cell RNA-seq atlas of liver development (*47*). The average expression of Yap^{hyper} program genes was highest in proliferating cholangiocytes followed by non-cycling cholangiocytes and early (proliferating) hepatoblasts (Fig.4B). However, this pattern was a composite of the expression patterns of four gene clusters with distinct expression patterns (Fig.4C): The first cluster of 247 genes (13% of the Yap^{hyper} program) contained genes that were expressed in all proliferating cells – mostly early hepatoblasts and a few proliferating cholangiocytes. The second cluster of 312 genes (17% of the Yap^{hyper} program) was expressed specifically in all cholangiocytes regardless of the cell cycle. The other two clusters had uniform or overall low expression in embryonic liver cells. Thus, while the expression of Yap^{hyper} genes in hepatoblasts showed that Yap induces parts of the hepatoblast program, this was not because Yap induced progenitor cell characteristics but because it induced general cell cycle genes. Indeed, the Yap^{hyper} program contained less than 5% of the hepatoblast specific gene set (Fig.S12K). On the other hand, Yap activated genes that are specifically expressed in embryonic cholangiocytes. However, the Yap^{hyper} program represented only about 15% of all cholangiocyte markers (Fig.S12K). It follows that Yap hyperactivation in adult hepatocytes did not simply activate the genetic program of embryonic hepatoblasts but induced a general cell proliferation program and partially transdifferentiated hepatocytes towards cholangiocyte fate.

Another possibility was that Yap hyperactivation induced a program that is used during liver regeneration, when hepatocytes re-enter the cell cycle. To test this, we performed RNA-seq on regenerating hepatocytes that we purified 48 hours after acute injury by injection of the liver toxin CCl_4, when hepatocyte proliferation peaks. Regenerating hepatocytes upregulated 1021 genes of which over half were also present in the Yap^{hyper} program (Fig.S14A). Thus, Yap hyperactivation indeed induced a large portion of the liver regeneration program (Fig.4D,G, Fig.S13A). However, endogenous Yap/Taz were not required for hepatocyte proliferation (*23*) or the induction of the regeneration program after CCl_4 injection (Fig.4E-F; Fig.S13B-E; TableS5). This conundrum can be resolved because Yap hyperactivation and the resulting overgrowth caused liver damage, as revealed by elevated serum levels of AST (Fig.S13G), which would then induce the regeneration program as a secondary effect. Therefore, the Yap^{hyper} program comprises direct effects caused by Yap hyperactivation, and indirect effects triggered by liver damage. Concordantly, we divided it into a general regeneration part that comprised the genes induced by both Yap and CCl_4 (Yap-CCl_4), and a "Yap-specific" part that comprised the genes that were induced by Yap but not by CCl_4 (Fig.4G; TableS6). Genes in the Yap-CCl_4 set predominantly function in cell cycle and

immune system, were most active in early hepatoblasts and proliferating cholangiocytes, and their expression poorly correlated with endogenous Yap activity (Fig.4H-J). This set thus constitutes the regenerative response to the liver damage caused by Yap-induced liver overgrowth. In contrast, genes in the Yap-specific set were normally expressed in embryonic cholangiocytes (Fig.4K-L), as well as in endothelial cells, fibroblasts and cholangiocytes of adult livers (Fig.S14). These are the cells with the highest Yap activity and that require Yap/Taz for their development (*53*).

To understand the biological functions of the Yap-specific genes, we classified them according to their expression patterns in normal adult liver. A first cluster of genes (ECM cluster, Fig.4M-N) was expressed in endothelial cells, fibroblasts and cholangiocytes and was strongly enriched for functions in angiogenesis and ECM, while a second cluster was predominantly expressed in immune cells and enriched for immune functions (Immune cluster, Fig.4M-N) and a third cluster had uniform but low expression in normal livers (Signaling cluster, Fig.4M-N). Strikingly, the ECM cluster comprised more than 50% of the endothelial cell specific markers and 33% and 18% of the fibroblast and cholangiocyte specific markers, respectively, with several genes expressed in all three cell types (Fig.4O). Altogether, these data show that Yap hyperactivation in adult hepatocytes does not cause liver overgrowth because it activates a normal progenitor (hepatoblast) cell program. Rather, Yap hyperactivation ectopically induces parts of the genetic programs of endothelial cells, cholangiocytes, and fibroblasts as well as other genes that are not normally expressed in hepatocytes.

Ectopic Yki activates an abnormal genetic program in imaginal discs

Next, we asked how ectopic Yki drives tissue overgrowth in *Drosophila* imaginal discs. Like in the liver, we overexpressed the constitutively active Yki^{3SA} and deleted the *Lats1/2* homolog *wts* in clones of cells. Both conditions produced eye discs that were nearly entirely composed of mutant cells and lacked ommatidial patterning and photoreceptor differentiation (Fig.1F). Discs had massive changes in gene expression that were highly correlated between the two mutants (Fig.5A, Fig.S15A-C, TableS8). Consistent with the histological phenotype, induced genes were mainly involved in ribosome biogenesis (indicating accelerated cell growth) and DNA replication, while the downregulated genes were involved in retinal cell differentiation (Fig.S15D). This phenotype raised the possibility that hyperactivation of Yki during eye development trapped cells in an early developmental stage thereby producing an excess of precursor cells. However, three lines of evidence refuted this hypothesis.

First, we compared the Yki^{hyper} program, defined as the 222 genes overlapping between the Yki^{3SA} and wts^{-} mutant profiles, with that of wild-type eye discs from different developmental stages (*54*). 44% (98) of the Yki^{hyper} program genes were expressed at higher levels at early stages compared to later stages of eye development (Fig.5B-C). However, these genes represented less than 4% of

the genes that characterize early eye development (Fig.5B, Fig.S15E). Therefore, Yki hyperactivation did not simply extend early development.

Second, mapping the Yki^{hyper} program onto the single cell expression atlas of third instar eye discs showed that Yki^{hyper} cells downregulated genes normally expressed in differentiating photoreceptor cells consistent with their lack of retinal differentiation (Fig.5D). The upregulated genes, however, were not enriched for genes expressed in progenitor cells but for genes expressed in peripodial cells (Fig.5E-F). Expression in peripodial cells was the predominant pattern with few of the Yki^{hyper} program genes being broadly or lowly expressed in normal eye discs (Fig.5F). Because *ey-Flp* induces clones not only in disc proper but also in peripodial cells, this result may simply be the consequence of hyperactivating Yki in peripodial cells causing their overproliferation. However, driving Yki^{3SA} overexpression specifically in disc proper cells by *optix-Gal4* caused essentially the same phenotype and triggered the induction of peripodial cell specific genes (Fig.S15F-G). Likewise, in wing discs, *wts* mutant clones and Yki overexpression induced a genetic program that was most similar to that of peripodial cells (Fig.S16). Yet, Yki induced less than half of the peripodial cell markers (FigS15H-I). Therefore, Yki activation did not simply cause an expansion of retinal progenitor cells and inhibit their differentiation, but ectopically activated a portion of the peripodial cell program.

Third, we compared the Yki^{hyper} program to a gene set representative of normal growth that we generated as the difference in gene expression between actively growing and growth completed eye discs collected from larvae fed the ecdysone precursor-deficient food (Fig.S15J). There was minimal overlap between the Yki^{hyper} and normal growth programs and unlike the Yki^{hyper} program, the normal growth program was not specifically expressed in peripodial cells, but rather broadly and reflecting the pattern of cell proliferation (Fig.5G-H,K-L). On the other hand, the Yki^{hyper} program resembled abnormal growth, here defined as genes upregulated in Ras^{V12G} driven neoplastic tumors (*Ras^{V12G} scrib^{RNAi}* tumors) (*55*). Such tumors have hyperactive Yki (*55*) and their gene expression profile significantly overlapped with the Yki^{hyper} program and was enriched in peripodial cells (Fig.5I-K; Fig.S17A-G). Altogether, ectopic Yki activation did not simply stimulate extra normal growth, but partially reprogrammed disc proper cells towards a peripodial cell phenotype (Fig.5M; Fig.S17H).

Next, we asked which Yki-Sd target genes were required for Yki-driven overgrowth. To this end, we performed a genetic screen in which we assessed the role of the 322 predicted Sd target genes plus an additional 143 low confidence targets (Table S10, methods). We knocked down each of these genes in eye discs that overexpressed Yki^{1SA} under the control of the *GMR-Gal4* driver *(GMR>Yki^{1SA})* which causes massively overgrown adult eyes (*22*). We thus crossed *GMR>Yki^{1SA}* flies to a collection of 1673 fly stocks that each expressed an RNAi construct targeting one of the candidate genes under the control of a Gal4 responsive UAS-promoter (on average 3.6 different

RNAi lines per gene). Knockdown of 44 genes suppressed *GMR>Yki^{1SA}* overgrowth, while knockdown of 40 enhanced overgrowth and knockdown of the remaining 381 did not noticeably affect the adult eye phenotype (Fig.5N; TableS10). We then screened all 465 genes for requirement during normal growth using the *optix-Gal4* driver, which is active in disc proper cells during eye development. Here, knockdown of 70 genes reduced eye size, while knockdown of 8 resulted in larger eyes (Fig.5N; TableS10). Overlapping the results of the two screens showed that 25 (57%) of the 44 Yki^{1SA}-overgrowth suppressors were also required for normal growth, but knockdown of the other 19 (43%) suppressors did not affect normal growth (Fig.5N). Although RNAi knockdown can be incomplete and may not reveal full loss-of-function phenotypes, our results indicate that the *GMR>Yki^{1SA}* phenotype is preferentially sensitive to knockdown of these genes. Thus, these results further support that Yki driven overgrowth does not simply recapitulate normal growth.

Among the Yki^{1SA}-overgrowth suppressors that were also required for normal growth were RNAi lines targeting Yki as expected, EGFR and its ligands Vn and Spi, the cell cycle regulators E2f1, CyclinE, and Stg, the cell growth promoter dMyc, and components of Notch signaling (Dl, Gp150, Uif, E(spl)malpha) (Fig.5O). Overexpression of these genes can cause ectopic cell proliferation, although overexpression of any of them alone does not phenocopy the amount of overgrowth seen in Hippo mutants (*25*). On the other hand, the 17 Yki^{1SA}-overgrowth specific suppressors included Sd, confirming that it is an overgrowth specific and not a general growth gene, and several genes encoding components functioning in cytoskeleton and ECM regulation such as RhoGAP18B (a GTPase activating protein for Rho GTPases), Myosin alkali light chain 1 (Mlc1), phosphatase and actin regulator 1 (PHACTR1, CG32264), the endopeptidase Spn55B, Miles to go (Mtgo, a fibronectin type III domain containing protein), and Netrin B (NetB, a secreted ligand regulating axon outgrowth). Thus, ectopic Yki causes eye disc overgrowth through mechanisms that include effects on the cytoskeleton and on cell-cell and cell-ECM interactions.

Discussion

Here we evaluated the role of the Hippo pathway in organ growth control. We examined fly eye imaginal discs and the mouse liver, two commonly used model systems to study organ growth. Our data show that Hippo pathway output is not required for the proliferation of liver precursor cells and disc proper cells, the main parenchymal cell types whose proliferation embodies the growth of the liver and eye discs. We conclude that the Hippo pathway does not instruct cells when to proliferate and when to stop proliferation during the normal development of these organs.

How can this conclusion be coherent with the fact that loss of the Hippo core kinases causes severe overgrowth of liver and imaginal discs, thus demonstrating that proper activity of the kinases is required for normal organ growth? This seeming paradox is resolved when considering that the Hippo kinase mutant overgrowth phenotypes are the result of ectopic Yap/Taz/Yki activation and are thus gain-of-function situations. Yap/Taz and Yki-Sd are normally not active in hepatocytes

and disc proper cells, but their ectopic activation can induce the overexpression of a battery of genes that then cause overgrowth. This means that the role of the Hippo core kinases in hepatocytes and disc proper cells is to keep Yap/Taz/Yki in check in order to prevent them from triggering abnormal overgrowth. It follows that Hippo signaling is permissive but not instructive for organ growth control during the normal development of *Drosophila* eye discs and mouse liver.

So, what do Yap/Taz/Yki normally do and how does ectopic Yap/Taz/Yki induce organ overgrowth? Yap/Taz and Yki-Sd are transcriptionally active in and required for the development of cholangiocytes and peripodial cells, respectively. Others reported that Yap/Taz/Yki-Sd are also required in endothelial cells, activated fibroblasts, lung AT1 cells, the squamous retinal pigment epithelial cells of zebrafish, and the squamous follicular cells of *Drosophila* egg chambers (*51*, *56-59*). Interestingly, these cells have in common that they are either flat cells that are under mechanical or morphological stress, or that they have extra strong cell-ECM adhesion. In line with this theme, when we analyzed expression of the Yki-Sd reporter *kibra-lacZ* we found strong expression in glial cells and in particular in the two carpet cells of developing eye discs, two huge and flat cells that each covers half of the eye disc (*60*). Therefore, there is a strong correlation between cell morphology and Hippo pathway activity. Indeed, Yap/Taz are activated by mechanical stress, for example when cells stretch out on a stiff cell culture substrate (*61*) and mediate a cell's response to mechanical strain such as the reinforcement of the cytoskeleton and cell adhesion. A major function of Yap/Taz/Yki-Sd thus appears to be a homeostatic function in morphologically and mechanically challenged cells. Concordantly, we found that Yap and Yki hyperactivation induced factors involved in cytoskeleton and ECM regulation and activated genetic programs that were most similar to the programs of cells where Yap/Taz/Yki-Sd are active and required for their development. We thus hypothesize that ectopic activation of these programs changes how cells interact with their neighbors, and how they receive and interpret growth control signals. In this way, hyperactivation of Hippo pathway output can cause ectopic cell proliferation and organ overgrowth even though it is not directly involved in normal growth control.

Notably, however, while Hippo output does not play a role in growth control in liver and eye discs, it is required for the growth of other organs. In flies, modulation of Yki is required to fine tune the growth of the presumptive wing tissue, the wing pouch of the wing disc, where Yki is activated in peripheral cells due to mechanical strain exerted by the growth of cells in the center (*62*). In the mouse, Yap/Taz are required for the growth of the embryonic heart while hyperactivation of Yap causes heart enlargement and can trigger cardiomyocyte proliferation in adults (*63*). Notably, in these tissues, Yap/Taz/Yki appear to be activated by mechanical stress (e.g. heartbeat) and their activity may affect tissue growth by regulating the mechanical properties of the cells. Thus, the function of Yap/Taz/Yki in cardiomyocytes and wing pouch cells may be comparable to that in cholangiocytes, peripodial cells and other mechanically challenged cells and not reflect a role of the Hippo pathway as a master regulator of organ growth. Similarly, Yap/Taz/Yki can be activated by mechanical strain after injury and then promote tissue repair and regeneration (*2*, *3*). In the adult

fly gut for example, Yki is not required for normal homeostasis, but injury activates Yki in differentiated enterocytes, which then produce multiple cytokines and EGFR ligands that induce regenerative proliferation of intestinal stem cells (*64*). Thus also here, Yki function is permissive but not instructive for organ growth, and its effect on growth involves a specialized response that is not essential for normal development.

Our findings correct a long-standing misconception that states that the Hippo pathway is a master regulator of organ growth. Hippo signaling as a master regulator of growth control has provided a straightforward and convenient explanation for its function in regeneration and cancer. Our new model for how Hippo signaling affects organ growth in turn reveals the need to re-evaluate our understanding of Yap/Taz's function as oncogenes and in regeneration. Investigating Yap/Taz as drivers of a response to mechanical strain will identify new mechanisms that promote cancer cell phenotypes and initiate regenerative responses.

Methods summary

A full description of the methods can be found in the supplementary materials. This includes full mouse and *Drosophila* genotypes and treatment protocols, descriptions of sample processing for immunofluorescence staining and RNA sequencing, statistical tests and bioinformatics analyses.

References and Notes

1. Z. Wu, K. L. Guan, Hippo Signaling in Embryogenesis and Development. *Trends Biochem Sci* **46**, 51-63 (2021).

2. Y. Zheng, D. Pan, The Hippo Signaling Pathway in Development and Disease. *Dev Cell* **50**, 264-282 (2019).

3. I. M. Moya, G. Halder, Hippo-YAP/TAZ signalling in organ regeneration and regenerative medicine. *Nat Rev Mol Cell Biol* **20**, 211-226 (2019).

4. J. R. Davis, N. Tapon, Hippo signalling during development. *Development* **146**, (2019).

5. G. Halder, R. L. Johnson, Hippo signaling: growth control and beyond. *Development* **138**, 9-22 (2011).

6. J. Dong *et al.*, Elucidation of a universal size-control mechanism in Drosophila and mammals. *Cell* **130**, 1120-1133 (2007).

7. D. Rogulja, C. Rauskolb, K. D. Irvine, Morphogen control of wing growth through the Fat signaling pathway. *Dev Cell* **15**, 309-321 (2008).

8. T. Aegerter-Wilmsen *et al.*, Integrating force-sensing and signaling pathways in a model for the regulation of wing imaginal disc size. *Development* **139**, 3221-3231 (2012).

9. K. D. Irvine, K. F. Harvey, Control of organ growth by patterning and hippo signaling in Drosophila. *Cold Spring Harb Perspect Biol* **7**, (2015).

10. I. K. Hariharan, Organ Size Control: Lessons from Drosophila. *Dev Cell* **34**, 255-265 (2015).

11. M. Kango-Singh *et al.*, Shar-pei mediates cell proliferation arrest during imaginal disc growth in Drosophila. *Development* **129**, 5719-5730 (2002).

12. N. Tapon *et al.*, salvador Promotes both cell cycle exit and apoptosis in Drosophila and is mutated in human cancer cell lines. *Cell* **110**, 467-478 (2002).

13. K. F. Harvey, C. M. Pfleger, I. K. Hariharan, The Drosophila Mst ortholog, hippo, restricts growth and cell proliferation and promotes apoptosis. *Cell* **114**, 457-467 (2003).

14. S. Wu, J. Huang, J. Dong, D. Pan, hippo encodes a Ste-20 family protein kinase that restricts cell proliferation and promotes apoptosis in conjunction with salvador and warts. *Cell* **114**, 445-456 (2003).

15. R. S. Udan, M. Kango-Singh, R. Nolo, C. Tao, G. Halder, Hippo promotes proliferation arrest and apoptosis in the Salvador/Warts pathway. *Nat Cell Biol* **5**, 914-920 (2003).

16. D. Zhou *et al.*, Mst1 and Mst2 maintain hepatocyte quiescence and suppress hepatocellular carcinoma development through inactivation of the Yap1 oncogene. *Cancer Cell* **16**, 425-438 (2009).

17. H. Song *et al.*, Mammalian Mst1 and Mst2 kinases play essential roles in organ size control and tumor suppression. *Proc Natl Acad Sci U S A* **107**, 1431-1436 (2010).

18. F. D. Camargo *et al.*, YAP1 Increases Organ Size and Expands Undifferentiated Progenitor Cells. *Current Biology* **17**, 2054-2060 (2007).

19. L. Lu *et al.*, Hippo signaling is a potent in vivo growth and tumor suppressor pathway in the mammalian liver. *Proc Natl Acad Sci U S A* **107**, 1437-1442 (2010).

20. J. H. Lee *et al.*, A crucial role of WW45 in developing epithelial tissues in the mouse. *EMBO J* **27**, 1231-1242 (2008).

21. J. Huang, S. Wu, J. Barrera, K. Matthews, D. Pan, The Hippo signaling pathway coordinately regulates cell proliferation and apoptosis by inactivating Yorkie, the Drosophila Homolog of YAP. *Cell* **122**, 421-434 (2005).

22. S. Wu, Y. Liu, Y. Zheng, J. Dong, D. Pan, The TEAD/TEF family protein Scalloped mediates transcriptional output of the Hippo growth-regulatory pathway. *Dev Cell* **14**, 388-398 (2008).

23. E. Verboven *et al.*, Regeneration Defects in Yap and Taz Mutant Mouse Livers Are Caused by Bile Duct Disruption and Cholestasis. *Gastroenterology* **160**, 847-862 (2021).

24. L. Lu, M. J. Finegold, R. L. Johnson, Hippo pathway coactivators Yap and Taz are required to coordinate mammalian liver regeneration. *Experimental &Amp; Molecular Medicine* **50**, e423 (2018).

25. R. M. Neto-Silva, B. S. Wells, L. A. Johnston, Mechanisms of growth and homeostasis in the Drosophila wing. *Annu Rev Cell Dev Biol* **25**, 197-220 (2009).

26. B. Z. Stanger, The biology of organ size determination. *Diabetes Obes Metab* **10 Suppl 4**, 16-22 (2008).

27. M. Xin *et al.*, Hippo pathway effector Yap promotes cardiac regeneration. *Proceedings of the National Academy of Sciences* **110**, 13839-13844 (2013).

28. M. Xin *et al.*, Regulation of insulin-like growth factor signaling by Yap governs cardiomyocyte proliferation and embryonic heart size. *Sci Signal* **4**, ra70 (2011).

29. C. M. Weisend, J. A. Kundert, E. S. Suvorova, J. R. Prigge, E. E. Schmidt, Cre activity in fetal albCre mouse hepatocytes: Utility for developmental studies. *Genesis* **47**, 789-792 (2009).

30. C. Kellendonk, C. Opherk, K. Anlag, G. Schütz, F. Tronche, Hepatocyte-specific expression of Cre recombinase. *Genesis* **26**, 151-153 (2000).

31. M. Gordillo, T. Evans, V. Gouon-Evans, Orchestrating liver development. *Development* **142**, 2094-2108 (2015).

32. N. Zhang *et al.*, The Merlin/NF2 tumor suppressor functions through the YAP oncoprotein to regulate tissue homeostasis in mammals. *Dev Cell* **19**, 27-38 (2010).

33. L. Zhang *et al.*, The TEAD/TEF family of transcription factor Scalloped mediates Hippo signaling in organ size control. *Dev Cell* **14**, 377-387 (2008).

34. Y. Goulev *et al.*, SCALLOPED interacts with YORKIE, the nuclear effector of the hippo tumor-suppressor pathway in Drosophila. *Curr Biol* **18**, 435-441 (2008).

35. Laura M. Koontz *et al.*, The Hippo Effector Yorkie Controls Normal Tissue Growth by Antagonizing Scalloped-Mediated Default Repression. *Developmental Cell* **25**, 388-401 (2013).

36. H. Oh, K. D. Irvine, Cooperative regulation of growth by Yorkie and Mad through bantam. *Dev Cell* **20**, 109-122 (2011).

37. H. W. Peng, M. Slattery, R. S. Mann, Transcription factor choice in the Hippo signaling pathway: homothorax and yorkie regulation of the microRNA bantam in the progenitor domain of the Drosophila eye imaginal disc. *Genes Dev* **23**, 2307-2319 (2009).

38. G. Halder *et al.*, The Vestigial and Scalloped proteins act together to directly regulate wing-specific gene expression in Drosophila. *Genes Dev* **12**, 3900-3909 (1998).

39. H. Oh, K. D. Irvine, In vivo analysis of Yorkie phosphorylation sites. *Oncogene* **28**, 1916-1927 (2009).

40. T. Zhang, Q. Zhou, F. Pignoni, Yki/YAP, Sd/TEAD and Hth/MEIS control tissue specification in the Drosophila eye disc epithelium. *PLoS One* **6**, e22278 (2011).

41. M. C. Gibson, G. Schubiger, Peripodial cells regulate proliferation and patterning of Drosophila imaginal discs. *Cell* **103**, 343-350 (2000).

42. K. D. McClure, G. Schubiger, Developmental analysis and squamous morphogenesis of the peripodial epithelium in Drosophila imaginal discs. *Development* **132**, 5033-5042 (2005).

43. D. M. Vallejo, S. Juarez-Carreño, J. Bolivar, J. Morante, M. Dominguez, A brain circuit that synchronizes growth and maturation revealed through Dilp8 binding to Lgr3. *Science* **350**, aac6767 (2015).

44. Y. Wang *et al.*, Comprehensive Molecular Characterization of the Hippo Signaling Pathway in Cancer. *Cell Rep* **25**, 1304-1317.e1305 (2018).

45. M. Guilliams *et al.*, Spatial proteogenomics reveals distinct and evolutionarily conserved hepatic macrophage niches. *Cell* **185**, 379-396.e338 (2022).

46. S. Manmadhan, U. Ehmer, Hippo Signaling in the Liver - A Long and Ever-Expanding Story. *Front Cell Dev Biol* **7**, 33 (2019).

47. L. Yang *et al.*, A single-cell transcriptomic analysis reveals precise pathways and regulatory mechanisms underlying hepatoblast differentiation. *Hepatology* **66**, 1387-1401 (2017).

48. T. Katsuyama, R. Paro, Innate immune cells are dispensable for regenerative growth of imaginal discs. *Mechanisms of development* **130**, 112-121 (2013).

49. K. Strassburger, M. Lutz, S. Müller, A. A. Teleman, Ecdysone regulates Drosophila wing disc size via a TORC1 dependent mechanism. *Nature communications* **12**, 6684 (2021).

50. C. Bravo González-Blas *et al.*, Identification of genomic enhancers through spatial integration of single-cell transcriptomics and epigenomics. *Mol Syst Biol* **16**, e9438 (2020).

51. G. C. Fletcher *et al.*, Mechanical strain regulates the Hippo pathway in Drosophila. *Development* **145**, (2018).

52. A. Genevet, M. C. Wehr, R. Brain, B. J. Thompson, N. Tapon, Kibra is a regulator of the Salvador/Warts/Hippo signaling network. *Dev Cell* **18**, 300-308 (2010).

53. S. Manmadhan, U. Ehmer, Hippo Signaling in the Liver – A Long and Ever-Expanding Story. *Frontiers in Cell and Developmental Biology* **7**, (2019).

54. M. Torres-Oliva, J. Schneider, G. Wiegleb, F. Kaufholz, N. Posnien, Dynamic genome wide expression profiling of Drosophila head development reveals a novel role of Hunchback in retinal glia cell development and blood-brain barrier integrity. *PLoS genetics* **14**, e1007180 (2018).

55. M. Atkins *et al.*, An Ectopic Network of Transcription Factors Regulated by Hippo Signaling Drives Growth and Invasion of a Malignant Tumor Model. *Curr Biol* **26**, 2101-2113 (2016).

56. X. Wang *et al.*, YAP/TAZ Orchestrate VEGF Signaling during Developmental Angiogenesis. *Dev Cell* **42**, 462-478.e467 (2017).

57. I. Mannaerts *et al.*, The Hippo pathway effector YAP controls mouse hepatic stellate cell activation. *J Hepatol*, (2015).

58. J. B. Miesfeld *et al.*, Yap and Taz regulate retinal pigment epithelial cell fate. *Development* **142**, 3021-3032 (2015).

59. L. B. Nantie *et al.*, Lats1/2 inactivation reveals Hippo function in alveolar type I cell differentiation during lung transition to air breathing. *Development* **145**, (2018).

60. M. Silies *et al.*, Glial cell migration in the eye disc. *J Neurosci* **27**, 13130-13139 (2007).

61. S. Dupont *et al.*, Role of YAP/TAZ in mechanotransduction. *Nature* **474**, 179-183 (2011).

62. C. Rauskolb, S. Sun, G. Sun, Y. Pan, K. D. Irvine, Cytoskeletal tension inhibits Hippo signaling through an Ajuba-Warts complex. *Cell* **158**, 143-156 (2014).

63. S. Liu, J. F. Martin, The regulation and function of the Hippo pathway in heart regeneration. *Wiley Interdiscip Rev Dev Biol* **8**, e335 (2019).

64. P. Zhang, B. A. Edgar, Insect Gut Regeneration. *Cold Spring Harb Perspect Biol* **14**, (2022).

65. C. Postic *et al.*, Dual roles for glucokinase in glucose homeostasis as determined by liver and pancreatic beta cell-specific gene knock-outs using Cre recombinase. *J Biol Chem* **274**, 305-315 (1999).

66. J. Yi *et al.*, Large tumor suppressor homologs 1 and 2 regulate mouse liver progenitor cell proliferation and maturation through antagonism of the coactivators YAP and TAZ. *Hepatology* **64**, 1757-1772 (2016).

67. S. Hayashi *et al.*, GETDB, a database compiling expression patterns and molecular locations of a collection of Gal4 enhancer traps. *Genesis* **34**, 58-61 (2002).

68. B. A. Hay, T. Wolff, G. M. Rubin, Expression of baculovirus P35 prevents cell death in Drosophila. *Development* **120**, 2121-2129 (1994).

69. T. Lee, L. Luo, Mosaic analysis with a repressible cell marker (MARCM) for Drosophila neural development. *Trends Neurosci* **24**, 251-254 (2001).

70. H. Oh, K. D. Irvine, In vivo regulation of Yorkie phosphorylation and localization. *Development* **135**, 1081-1088 (2008).

71. M. I. Love, W. Huber, S. Anders, Moderated estimation of fold change and dispersion for RNA-seq data with DESeq2. *Genome biology* **15**, 550 (2014).

72. J. Bageritz *et al.*, Gene expression atlas of a developing tissue by single cell expression correlation analysis. *Nature Methods* **16**, 750-756 (2019).

73. M. Deng *et al.*, Single cell transcriptomic landscapes of pattern formation, proliferation and growth in Drosophila wing imaginal discs. *Development* **146**, (2019).

74. I. Korsunsky *et al.*, Fast, sensitive and accurate integration of single-cell data with Harmony. *Nat Methods* **16**, 1289-1296 (2019).

75. Y. Hao *et al.*, Integrated analysis of multimodal single-cell data. *Cell* **184**, 3573-3587.e3529 (2021).

76. T. Wu *et al.*, clusterProfiler 4.0: A universal enrichment tool for interpreting omics data. *Innovation (Camb)* **2**, 100141 (2021).

77. C. Herrmann, B. Van de Sande, D. Potier, S. Aerts, i-cisTarget: an integrative genomics method for the prediction of regulatory features and cis-regulatory modules. *Nucleic Acids Res* **40**, e114 (2012).

78. H. Imrichová, G. Hulselmans, Z. K. Atak, D. Potier, S. Aerts, i-cisTarget 2015 update: generalized cis-regulatory enrichment analysis in human, mouse and fly. *Nucleic Acids Res* **43**, W57-64 (2015).

79. J. Pascual *et al.*, Hippo Reprograms the Transcriptional Response to Ras Signaling. *Dev Cell* **42**, 667-680.e664 (2017).

80. A. Ikmi *et al.*, Molecular evolution of the Yap/Yorkie proto-oncogene and elucidation of its core transcriptional program. *Mol Biol Evol* **31**, 1375-1390 (2014).

Acknowledgments:

We thank Duojia Pan for providing the *sd*, *hpo* and *yki* mutant fly stocks and the *ApoE>hYAP* mice, and Kenneth D. Irvine for the *yki*^{3SA} stock. The gp-anti-Ato antibody was donated by Hugo Bellen. We thank the Transgenic RNAi Project (TRiP) at Harvard Medical School, the Vienna Drosophila Resource Center, and the Bloomington Drosophila Stock Center for providing transgenic RNAi and other fly stocks. We thank Natalia Alves Souza Carvalhais, Elena Kesikiadou and Jana Mach for help with experiments.

Funding: This work was funded by The Research Foundation – Flanders (FWO, Odysseus Type I grant and Project grants G.0954.16N and G.030616N to G.H.).

Author contributions: G.H. conceived the project. G.H., W.K., L.R., I.M.M. and M.A wrote the manuscript. G.H., W.K., L.R., M.A. designed the experiments and analyzed the data. W.K. and L.R. organized and performed most of the experiments. M.A. contributed to *Drosophila* experiments. W.K., C.B.G.-B., J.J., M.deW. and S.A. performed the bioinformatics analyses. H.H., I.M.M., E.V., S.S., S.V., L.S.-G., L.vH., R.J., L.A.vG. contributed to the mouse experiments.

Competing interests: Authors declare that they have no competing interests.

Data and materials availability: All sequencing data generated in this study have been deposited in the Gene Expression Omnibus (GEO) under the accession GSE211461 with the following SubSeries: GSE211457 (Drosophila – non-pupating larvae), GSE211458 (Drosophila – Yki hyperactivation), GSE211459 (Liver – Yap hyperactivation) and GSE211460 (Liver – CCl4 in Yap/Taz KO). Processed data and analyses results are provided in the supplementary tables.

Supplementary Materials

Materials and Methods

Figs. S1 to S17

References (*65–80*)

Fig. 1. Loss of Hippo signaling output does not affect developmental growth. (**A**) Control and *Aflp-Cre; Yap/Taz KO* whole liver pictures from adult mice (6 months; scale bars 1cm). (**B**) Average liver to body weight ratios from postnatal day 5 to adulthood (N=3). (**C**-**D**) Liver sections of indicated genotypes stained for nuclei (DAPI, blue), adherens junctions (β-catenin, green in C), hepatocytes (HNF4α, red in C, green in D) and cholangiocytes (Sox9, red in D). (**E**) Lateral views of mosaic adult Drosophila eyes with mutant clones of the indicated genotypes; mutant cells are marked by the absence of red pigment. (**F**-**G**) Immunofluorescent images and quantification of clone size of eye imaginal discs with clones of cells of the indicated genotypes marked by GFP expression. (**H**) Heatmap showing relative expression levels of genes differentially expressed between Yki3SA and control eye discs (Padj < 0.05; |log2FC|>1) of the indicated genotypes. (**I**) PCA plot showing all samples of indicated genotypes. (**J**-**L**) MA plots for indicated comparisons; upregulated genes (Padj < 0.05; log2FC > 1) are shown in red, downregulated genes (Padj < 0.05; log2FC < -1) are shown in blue. DAPI, 4′,6-diamidino-2-phenylindole; GFP, green fluorescent protein; **** P < 0.0001; n.s., not significant; error bars indicate SD.

Fig. 2. Sd is required for the development of the peripodial epithelium but not for the disc proper. (**A**) Top-view and cross section schematic representation of a wild-type 3rd instar eye-antennal disc showing the location of its major cell types; PRs – photoreceptors, MF – morphogenetic furrow, AMF and PMF – anterior and posterior to the morphogenetic furrow. (**B**-**C**) Representative images and size quantification of control and sd- mutant clones in disc proper and peripodium, clones marked by GFP (green); N=10. (**D**) Eye imaginal discs with mutant clones of the indicated genotypes marked by the absence of GFP (green) expression. EdU (red) incorporation labels cells in S-phase. Details of eye imaginal discs with anti-Atonal (Ato; blue) and anti-ELAV (red) staining illustrates neuronal patterning and photoreceptor differentiation. (**E**) Lateral views of adult *Drosophila* eyes of the indicated genotypes. (**F**) Quantification of asymmetry (difference in the number of ommatidia between the two eyes of the same animal) in control and *sd*- mutant retinae; N=10, P = 0.25. (**G**-**H**) Lateral views of an adult head and a pupa lacking a head, and confocal images of eye imaginal discs of the indicated genotypes stained with DAPI (blue) and anti-ELAV (red) to label nuclei and photoreceptors, respectively. (**I**) Cross-section view of the eye imaginal discs shown in G and H, arrow and arrowheads point to the peripodium and disc proper, respectively.

Fig. 3. Yap/Taz/Yki activity does not correlate with cell proliferation. (**A**-**B**) UMAP plot of single cell RNA-seq data from embryonic murine livers colored by developmental time point (A) and cell type (B); HB – hepatoblasts, Hep – hepatocytes, Chol - cholangiocytes. (**C**-**D**) Average expression of cell cycle (C) and Yap signature genes (D). (**E**) Scatter plot showing the correlation between Yap signature and cell cycle gene expression in single cells colored by cell identity. (**F**) Actively growing (day 5 after egg laying – AEL) and growth-completed (day 11 AEL) eye imaginal discs from animals feed a pupation-preventing diet, stained for nuclei (DAPI, blue) and EdU (yellow) marking cells in S-phase. (**G**-**H**) Heatmaps showing relative expression and log2 fold changes (green sidebar marks statistically significant changes; Padj < 0.05) in cell cycle (G)

and Yki signature genes (H) between actively growing and growth completed eye imaginal discs. (**I**) UMAP plot of single cell RNA-seq data with 2596 cells colored by assigned cell type together with a schematic visualization of an eye imaginal disc; lat – lateral, med – medial, morpho – morphogenetic, photorec – photoreceptors, (**J**) Left column: cell proliferation in an eye disc shown by EdU incorporation (yellow) in disc proper (top) and peripodium (bottom) and average expression of cell cycle genes on the UMAP (middle); right column: Yki activity shown by kibra-lacZ staining (green) in disc proper (top) and peripodium (bottom) and average expression of Yki signature genes on the UMAP (middle). The arrows point to corresponding groups of cells. (**K**) Violin plot showing average expression of Yki signature genes in single cells of the wing imaginal disc, grouped by cell type. (**L**) Venn diagram showing the proportion of all chromatin regions specifically accessible in peripodial cells overlapping with those that also show enrichment for Sd binding motifs.

Fig. 4. Yap hyperactivation drives an ectopic growth program in hepatocytes. (**A**) Overlap between the up- (top) and downregulated (bottom) genes in hepatocytes with YAP overexpression and *Lats1/2 KO*. (**B**) Average expression of Yap^{hyper} program genes in the developing liver. (**C**) Clustering of Yap^{hyper} program genes by their normal expression pattern during liver development. Cells (columns) are grouped by cell type, cell cycle phase and developmental time; genes (rows) are grouped by similar expression pattern. (**D**) Correlation of changes in gene expression between *Apo>YAP* and CCl4 (compared to their relative controls); cell cycle and Yap signature genes are marked in green and red, respectively, and their distribution is shown by the density plot on the right side. (**E**) Correlation of changes in hepatocyte gene expression induced by CCl4 injection into control (*ctrl*) and *Yap/Taz KO* animals. (**F**) log2 fold changes (log2FC) of Yap signature genes for comparisons between the indicated conditions and their respective controls; values rounded to the nearest integer. (**G**) log2FC of genes (rows) induced by Yap hyperactivation or CCl4 injection for comparisons (columns) between the indicated conditions and their respective controls. (**H**) Barplot showing the percentage of genes in the Yap-specific or Yap-CCl4 subsets of the Yap^{hyper} program that belong to the given GO term categories. (**I-L**) Average expression of the Yap-CCl4 (I) and Yap-specific (K) parts of the Yap^{hyper} program in single cells of the embryonic liver and its correlation with the expression of cell cycle (J) and Yap signature (L) genes, respectively. (**M-N**) Subclustering of the Yap-specific genes by their co-expression in different cell types of the adult liver; (M) heatmap shows the absolute expression (log10 CPM, counts per million) in single cells aggregated by cell type; (N) treeplot shows the top 5 GO terms enriched for each cluster; dot size corresponds to the number of genes and its color reflects the proportion of genes in each cluster. (**O**) Overlap between genes in the ECM cluster and marker genes of fibroblasts, cholangiocytes and endothelial cells.

Fig. 5. Yki hyperactivation driven overgrowth resembles tumor, but not normal growth. (**A**) Correlation of changes in gene expression between Yki^{3SA} overexpression and *wts KO* (compared to their respective controls); Yki^{hyper} program genes are in green. (**B**) Relative expression levels of the Yki^{hyper} program genes at different time points of larval growth (72h, 96h and 120h AEL) and

after growth completion (11 days AEL). (**C**) Overlap between the Yki^{hyper} program and the genes upregulated (Padj < 0.05, log2FC > 1) at 72h (compared to 120h, which is the time point of Yki^{hyper} samples and their controls). (**D-E**) Average expression of the overlap of the genes downregulated in Yki^{3SA} overexpression and *wts KO* (D) and the genes in Yki^{hyper} program (E) in the single cells of imaginal eye discs. (**F**) Expression of the Yki^{hyper} program in eye disc cell types: heatmap (top) shows the absolute expression (log10 CPM) in single cells aggregated by cell type and violin plot (bottom) shows average expression in single cells grouped by cell type. (**G-J**) Average expression of the genes upregulated in actively growing compared to growth completed eye discs (G) and genes upregulated in *Ras^{G12V} scrib^{RNAi}* tumors (I) and its correlation with the expression of cell cycle (H) and Yki signature (J) genes, respectively. (**K**) Overlap between the Yki^{hyper} program and genes upregulated in actively growing compared to growth completed eye discs and genes upregulated in *Ras^{G12V} scrib^{RNAi}* tumors (Padj. < 0.05, log2FC > 1). (**L**) Correlation of log2 fold changes in gene expression between Yki^{3SA} overexpression relative to control and growth completed discs relative to growing discs; cell cycle and Yki signature genes are marked in blue and red, respectively, and their distribution along the axes is shown by the density plots. (**M**) Correlation between the average expression of the indicated gene sets in single cells of the eye disc, "peripodium" refers to the marker genes (Padj. < 0.05; log2FC > 0.5) of all peripodial cells. (**N**) Schematic representation of the results of the *in vivo* RNAi screens. (**O**) The suppressors of Yki-induced overgrowth listed in 9 functional categories.

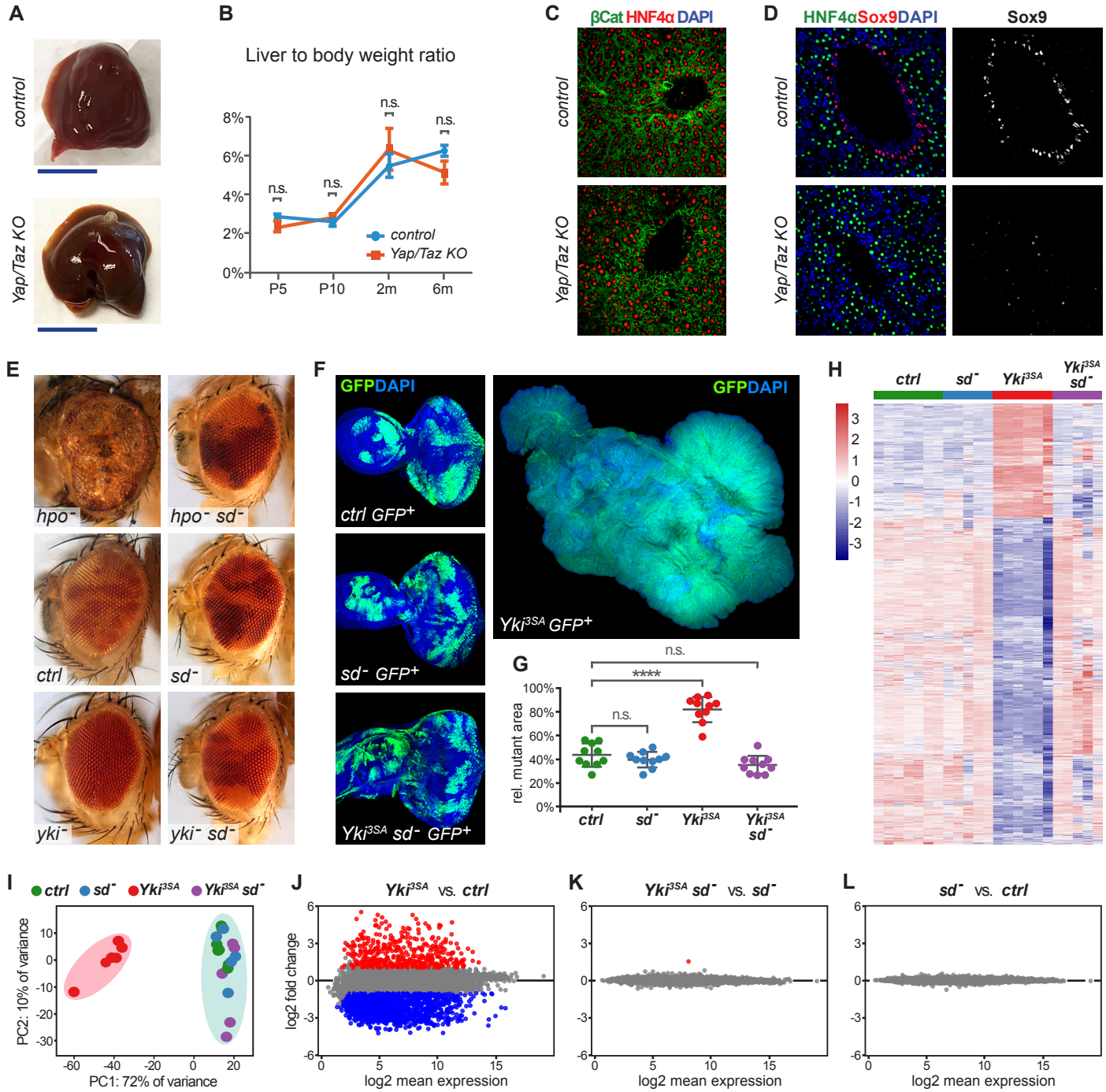
A
control
Yap/Taz KO
B
Liver to body weight ratio
8%
6%
4%
2%
0%
n.s.
n.s.
n.s.
n.s.
control
Yap/Taz KO
P5
P10
2m
6m
C
βCat HNF4α DAPI
control
Yap/Taz KO
D
HNF4αSox9DAPI
Sox9
control
Yap/Taz KO
E
hpo⁻
hpo⁻ sd⁻
ctrl
sd⁻
yki⁻
yki⁻ sd⁻
F
GFPDAPI
ctrl GFP+
sd⁻ GFP+
Yki3SA sd⁻ GFP+
GFPDAPI
Yki3SA GFP+
G
n.s.
****
n.s.
100%
80%
60%
40%
20%
0%
rel. mutant area
ctrl
sd⁻
Yki3SA
Yki3SA sd⁻
H
ctrl
sd⁻
Yki3SA
Yki3SA sd⁻
3
2
1
0
-1
-2
-3
I
ctrl
sd⁻
Yki3SA
Yki3SA sd⁻
PC2: 10% of variance
PC1: 72% of variance
J
Yki3SA vs. ctrl
log2 fold change
log2 mean expression
K
Yki3SA sd⁻ vs. sd⁻
log2 mean expression
L
sd⁻ vs. ctrl
log2 mean expression

Figure 1

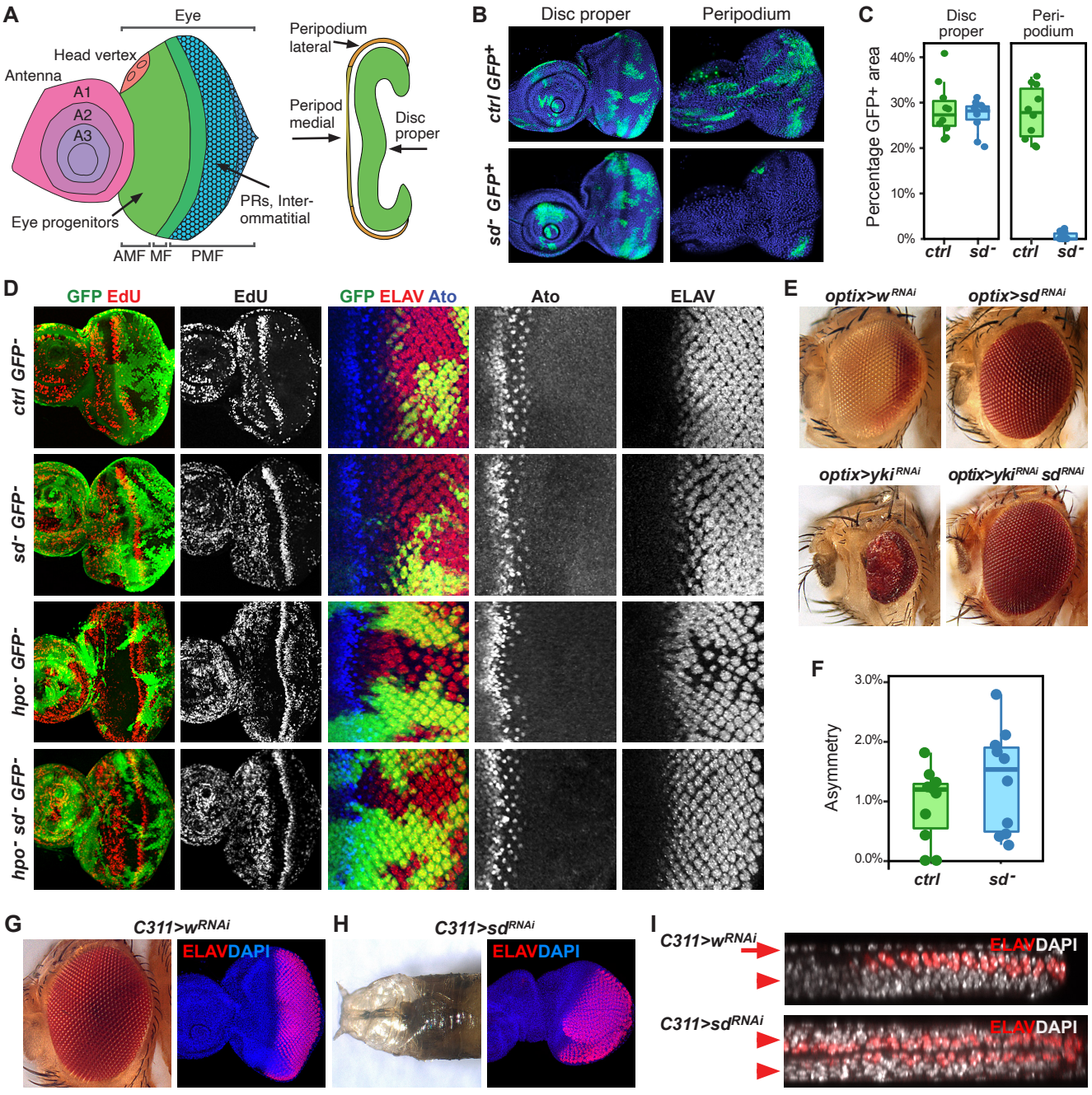
A
Eye
Head vertex
Antenna
A1
A2
A3
Eye progenitors
AMF MF PMF
Peripodium lateral
Peripod medial
Disc proper
PRs, Inter-ommatitial
B
Disc proper
Peripodium
ctrl GFP+
sd- GFP+
C
Disc proper
Peri-podium
Percentage GFP+ area
40%
30%
20%
10%
0%
ctrl
sd-
ctrl
sd-
D
GFP EdU
EdU
GFP ELAV Ato
Ato
ELAV
ctrl GFP-
sd- GFP-
hpo- GFP-
hpo- sd- GFP-
E
optix>wRNAi
optix>sdRNAi
optix>ykiRNAi
optix>ykiRNAi sdRNAi
F
Asymmetry
3.0%
2.0%
1.0%
0.0%
ctrl
sd-
G
C311>wRNAi
ELAVDAPI
H
C311>sdRNAi
ELAVDAPI
I
C311>wRNAi
ELAVDAPI
C311>sdRNAi
ELAVDAPI

Figure 2

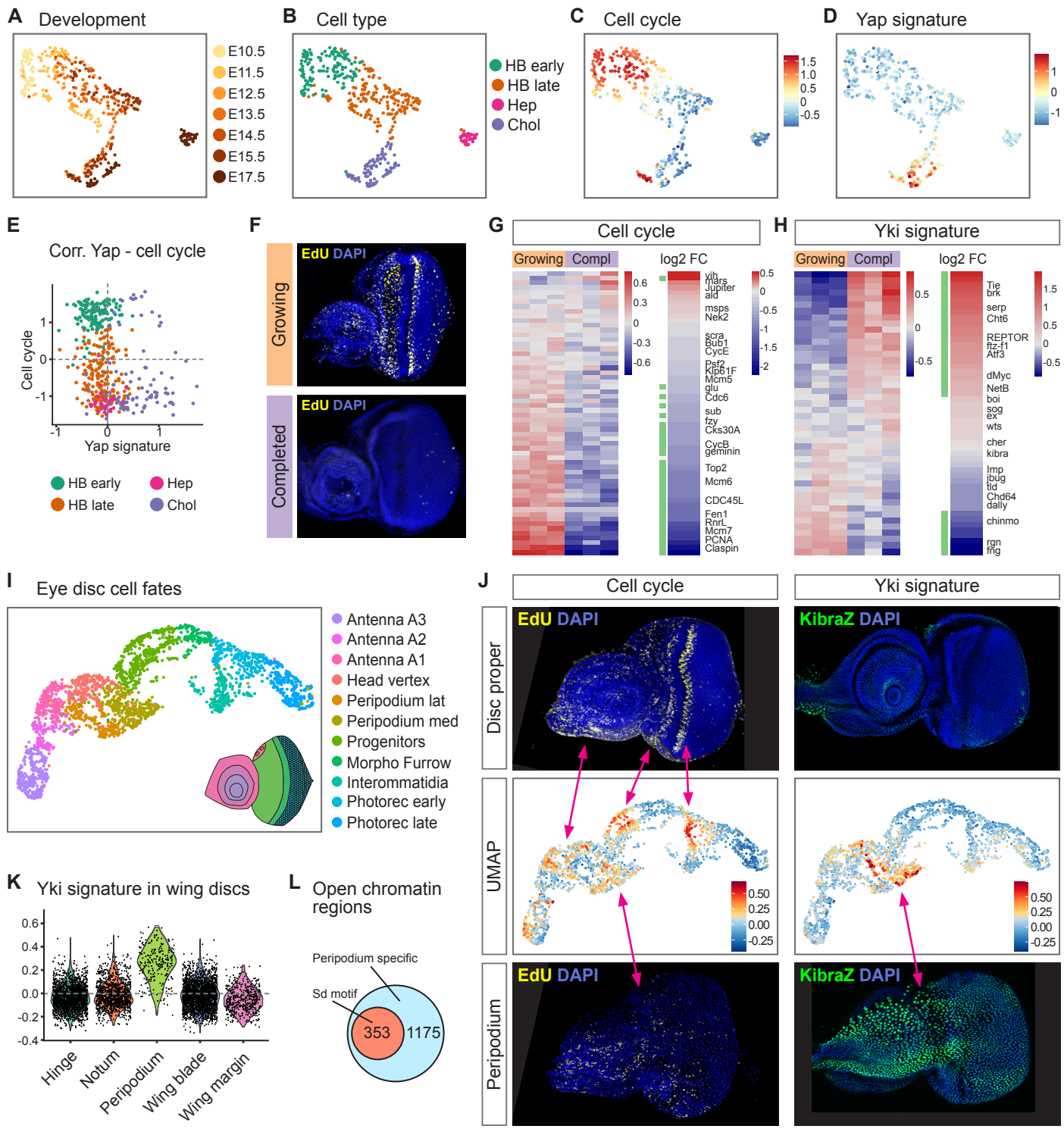
A
Development
E10.5
E11.5
E12.5
E13.5
E14.5
E15.5
E17.5
B
Cell type
HB early
HB late
Hep
Chol
C
Cell cycle
1.5
1.0
0.5
0
-0.5
D
Yap signature
1
0
-1
E
Corr. Yap - cell cycle
Cell cycle
Yap signature
HB early
HB late
Hep
Chol
F
Growing
Completed
EdU DAPI
EdU DAPI
G
Cell cycle
Growing
Compl
log2 FC
vih
rhars
Jupiter
ald
msps
Nek2
scra
Bub1
CycE
Psf2
Kif61F
Mcm5
glu
Cdc6
sub
fzy
Cks30A
CycB
geminin
Top2
Mcm6
CDC45L
Fen1
RnrL
Mcm7
PCNA
Claspin
H
Yki signature
Growing
Compl
log2 FC
Tie
brk
serp
Cht6
REPTOR
ftz-f1
Atf3
dMyc
NetB
boi
sog
ex
wts
cher
kibra
Imp
ibug
tld
Chd64
dally
chinmo
rgn
fng
I
Eye disc cell fates
Antenna A3
Antenna A2
Antenna A1
Head vertex
Peripodium lat
Peripodium med
Progenitors
Morpho Furrow
Interommatidia
Photorec early
Photorec late
J
Cell cycle
Yki signature
Disc proper
UMAP
Peripodium
EdU DAPI
KibraZ DAPI
EdU DAPI
KibraZ DAPI
0.50
0.25
0.00
-0.25
K
Yki signature in wing discs
Hinge
Notum
Peripodium
Wing blade
Wing margin
L
Open chromatin regions
Peripodium specific
Sd motif
353
1175

Figure 3

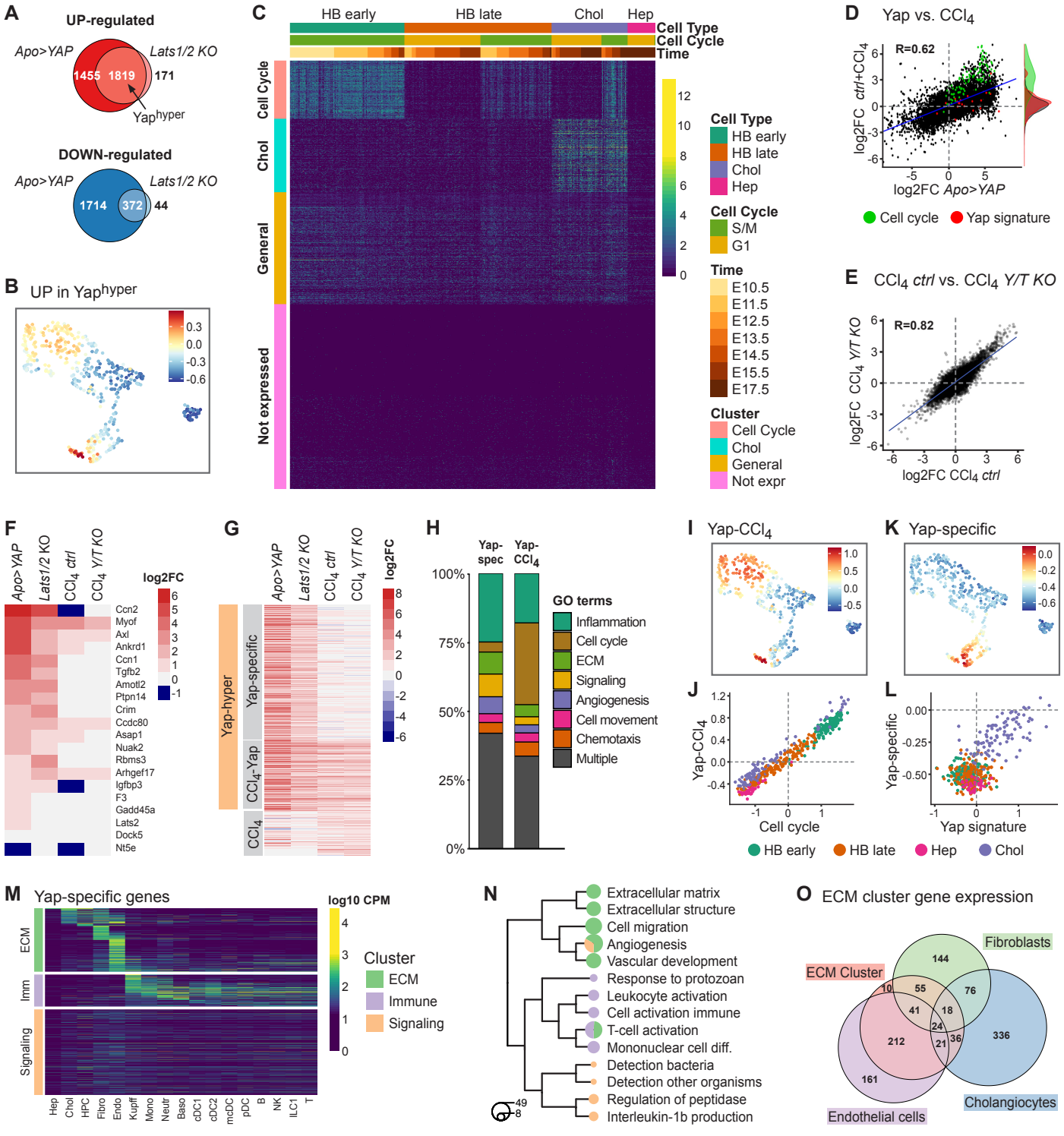
A
UP-regulated
Apo>YAP
Lats1/2 KO
1455
1819
171
Yaphyper
DOWN-regulated
Apo>YAP
Lats1/2 KO
1714
372
44
B
UP in Yaphyper
0.3
0.0
-0.3
-0.6
C
HB early
HB late
Chol
Hep
Cell Type
Cell Cycle
Time
Cell Cycle
Chol
General
Not expressed
12
10
8
6
4
2
0
Cell Type
HB early
HB late
Chol
Hep
Cell Cycle
S/M
G1
Time
E10.5
E11.5
E12.5
E13.5
E14.5
E15.5
E17.5
Cluster
Cell Cycle
Chol
General
Not expr
D
Yap vs. CCl4
R=0.62
log2FC ctrl+CCl4
log2FC Apo>YAP
Cell cycle
Yap signature
E
CCl4 ctrl vs. CCl4 Y/T KO
R=0.82
log2FC CCl4 Y/T KO
log2FC CCl4 ctrl
F
Apo>YAP
Lats1/2 KO
CCl4 ctrl
CCl4 Y/T KO
log2FC
Ccn2
Myof
Axl
Ankrd1
Ccn1
Tgfb2
Amotl2
Ptpn14
Crim
Ccdc80
Asap1
Nuak2
Rbms3
Arhgef17
Igfbp3
F3
Gadd45a
Lats2
Dock5
Nt5e
G
Apo>YAP
Lats1/2 KO
CCl4 ctrl
CCl4 Y/T KO
log2FC
Yap-hyper
Yap-specific
CCl4-Yap
CCl4
H
Yap-spec
Yap-CCl4
100%
75%
50%
25%
0%
GO terms
Inflammation
Cell cycle
ECM
Signaling
Angiogenesis
Cell movement
Chemotaxis
Multiple
I
Yap-CCl4
J
Yap-CCl4
Cell cycle
K
Yap-specific
L
Yap-specific
Yap signature
HB early
HB late
Hep
Chol
M
Yap-specific genes
log10 CPM
ECM
Imm
Signaling
Hep
Chol
HPC
Fibro
Endo
Kupff
Mono
Neutr
Baso
cDC1
cDC2
mcDC
pDC
B
NK
ILC1
T
Cluster
ECM
Immune
Signaling
N
Extracellular matrix
Extracellular structure
Cell migration
Angiogenesis
Vascular development
Response to protozoan
Leukocyte activation
Cell activation immune
T-cell activation
Mononuclear cell diff.
Detection bacteria
Detection other organisms
Regulation of peptidase
Interleukin-1b production
49
8
O
ECM cluster gene expression
Fibroblasts
ECM Cluster
Endothelial cells
Cholangiocytes
144
10
55
76
41
18
24
212
21
36
336
161

Figure 4

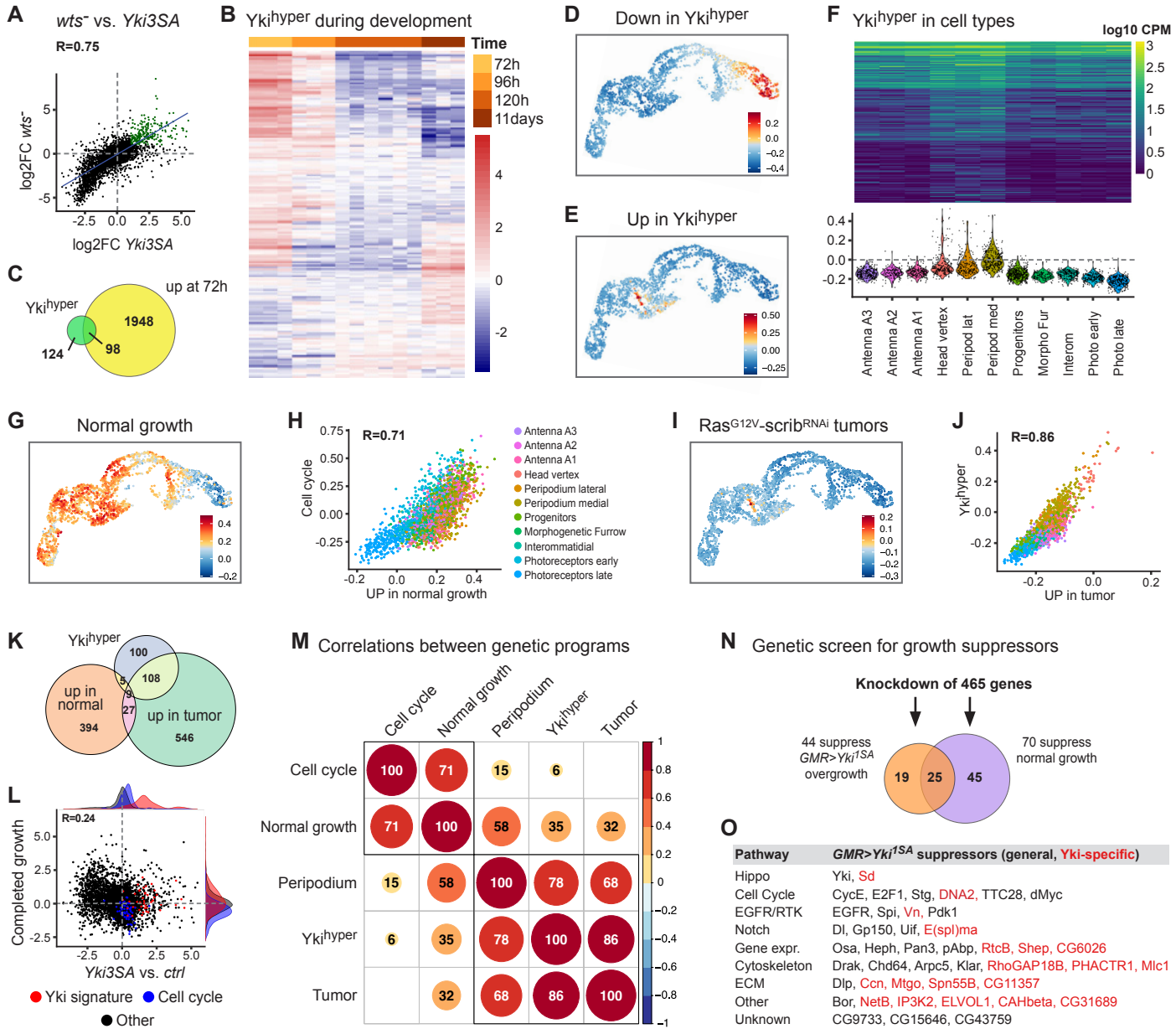
A
wts- vs. Yki3SA
R=0.75
log2FC wts-
log2FC Yki3SA
B
Yki^hyper during development
Time
72h
96h
120h
11days
C
Yki^hyper
up at 72h
1948
124
98
D
Down in Yki^hyper
E
Up in Yki^hyper
F
Yki^hyper in cell types
log10 CPM
Antenna A3
Antenna A2
Antenna A1
Head vertex
Peripod lat
Peripod med
Progenitors
Morpho Fur
Interom
Photo early
Photo late
G
Normal growth
H
R=0.71
Cell cycle
UP in normal growth
Antenna A3
Antenna A2
Antenna A1
Head vertex
Peripodium lateral
Peripodium medial
Progenitors
Morphogenetic Furrow
Interommatidial
Photoreceptors early
Photoreceptors late
I
Ras^G12V-scrib^RNAi tumors
J
R=0.86
Yki^hyper
UP in tumor
K
Yki^hyper
100
108
up in normal
394
27
up in tumor
546
L
R=0.24
Completed growth
Yki3SA vs. ctrl
Yki signature
Cell cycle
Other
M
Correlations between genetic programs
Cell cycle
Normal growth
Peripodium
Yki^hyper
Tumor
100 71 15 6
71 100 58 35 32
15 58 100 78 68
6 35 78 100 86
32 68 86 100
N
Genetic screen for growth suppressors
Knockdown of 465 genes
44 suppress GMR>Yki^1SA overgrowth
19
25
45
70 suppress normal growth
O
Pathway | GMR>Yki^1SA suppressors (general, Yki-specific)
Hippo | Yki, Sd
Cell Cycle | CycE, E2F1, Stg, DNA2, TTC28, dMyc
EGFR/RTK | EGFR, Spi, Vn, Pdk1
Notch | Dl, Gp150, Uif, E(spl)ma
Gene expr. | Osa, Heph, Pan3, pAbp, RtcB, Shep, CG6026
Cytoskeleton | Drak, Chd64, Arpc5, Klar, RhoGAP18B, PHACTR1, Mlc1
ECM | Dlp, Ccn, Mtgo, Spn55B, CG11357
Other | Bor, NetB, IP3K2, ELVOL1, CAHbeta, CG31689
Unknown | CG9733, CG15646, CG43759

Figure 5

Science
AAAS

Supplementary Materials for

Hippo signaling instructs ectopic but not normal organ growth

W. Kowalczyk[*], L. Romanelli[*], M. Atkins, H. Hillen, C. Bravo González-Blas, J. Jacobs, J. Xie, S. Soheily, E. Verboven, I. M. Moya, S. Verhulst, M. de Waegeneer, L. Sansores-Garcia, L. van Huffel, R.L. Johnson, Leo A. van Grunsven, S. Aerts, G. Halder[#]

*These authors contributed equally to this work.

#Correspondence to: Georg.Halder@vib.be

This PDF file includes:

Materials and Methods

Figs. S1 to S17

Other Supplementary Materials for this manuscript include the following:

Tables S1 to S10

Materials and Methods

Mouse genotypes

Alfp-Cre; Yap$^{flox/flox}$*; Taz*$^{flox/flox}$ mice were generated by crossing *Yap (28)* and *Taz* (*27*) floxed mice with the *Alfp-Cre* (*65*) line. The *Yap*$^{flox/flox}$ and *Taz*$^{flox/flox}$ mouse lines were generated by E. N. Olson. The *ApoE-rtTA, TRE-hYAP* mouse line was generated and gifted by D. Pan (*6*). *Lats1*$^{flox/flox}$*; Lats2*$^{flox/flox}$ was generated by R. L. Johnson (*66*). C57BL/6 mice were purchased from Charles River. Controls matched for sex and age were littermates. Mice were housed, fed and treated in accordance with protocols approved by the committee for animal research at KULeuven. All mouse experiments were approved by the institutional ethical commission at KULeuven and were performed in accordance with relevant institutional and national guidelines and regulations.

Genotypes in Fig.1(A-D):

control: *Yap*$^{flox/flox}$*; Taz*$^{flox/flox}$

Yap/Taz KO: *Alfp-Cre/+; Yap*$^{flox/flox}$*; Taz*$^{flox/flox}$.

Doxycycline, CCl_4 and AAV8-Cre administration

To activate the expression of human YAP in transgenic *ApoE-rtTA, TRE-hYAP* mice, 0.2mg/ml doxycycline hyclate (Sigma) was diluted in filtered sterile drinking water supplemented with 2,5% sucrose and administered *ad libitum*. Doxycycline containing water bottles were protected from light and replaced every other day. Induction of hepatocyte-specific recombination of floxed alleles in *Yap*$^{flox/flox}$; *Taz*$^{flox/flox}$ and *Lats1*$^{flox/flox}$*; Lats2*$^{flox/flox}$ mice was achieved by injection of Adeno-associated virus serotype 8 (AAV8) expressing Cre recombinase under the hepatocyte specific TBG promoter which was purchased from UPenn (AAV8.TBG.PI.Cre.rBG, catalog AV-8-PV1091). Mice received $5x10^{11}$ GC (genome complements) of AAV8.TBG.PI.Cre.rBG diluted in 200µl of 1x phosphate-buffered saline (PBS) by tail vein injection. Acute liver injury was induced by intraperitoneal injection of carbon tetrachloride (CCl_4) at a concentration of 1ml/kg in corn oil.

Hepatocyte isolation

Mice were anesthetized by intraperitoneal injection of sodium pentobarbital (Nembutal, 50mg/kg). Livers were perfused for 5min with 40ml of perfusion medium SC-1 to remove the blood and for rapid destruction of intercellular junctions, followed by perfusion with 40ml of SC-2 medium containing 10mg collagenase for 5min to break up the supporting extracellular matrix. Each lobe was dissected off, and the tissue was disrupted inside of a beaker containing 50ml of SC-2 with 20mg collagenase (Roche) and 1ml DNase I (Sigma) followed by rotating incubation for 20min at 37°C. Cells were then filtered through a 100µm strainer and centrifuged at 50g for 2min at room temperature. Hepatocytes were washed once with 1X PBS and centrifuged again at 50g for 2min. Pellet was resuspended with 2ml of 1X PBS containing 0.04% BSA, filtered through a 70µm strainer and FACS sorted. 500,000 sorted cells were lysed for RNA extraction.

SC-1 and SC-2 medium preparation per liter:

	SC-1	**SC-2**
NaCl	8g	8g
KCl	400mg	400mg
NaH_2PO_4	98mg	98mg
Na_2HPO_4	151mg	151mg
HEPES	2.38g	2.38g
$NaHCO_3$	350mg	350mg
EGTA	190mg	-
D-Glucose	0.9g	-
$CaCl_2$ $2H_2O$	-	0.56g
Phenol red	1.2ml	1.2ml

***Drosophila* husbandry and stocks**

Crosses were raised at 25°C on standard media unless otherwise specified.

The following abbreviations are used:

FM7-GFP: FM7 P{w[+mC]=act-GFP)JMR3

CyO-RFP: CyO mhc-RFP w^+

yki^{3SA}*: attp2-UAS-*$yki^{S111A\ S168A,\ S250A\text{-}V5}$

yki^{1SA}*: attp2-UAS-*$yki^{S111A\text{-}V5}$

The stocks *sd^{47M} FRT19A*, *FRT42D hpo$^{42-47}$*, *FRT42D yki^{B5}* and *UAS-yki$^{1SA-GFP}$* were donated by Duoja Pan (Southwestern University, Dallas, TX). The stocks *attp2-UAS-yki$^{S111A-V5}$* and *attp2-UAS-yki$^{S111A\ S168A,\ S250A-V5}$* were donated by Kenneth D. Irvine (Waksman Institute, Rutgers University, Piscataway, NJ). The *yki-GFP^{KI}* was a gift from Nicolas Tapon. The *kibra-lacZ* stock was purchased from Bloomington (#11567). The following UAS-RNAi lines were used: *hpo^{RNAi}* (VDRC #7823), *sd^{RNAi}* (TRIP JF02514), *white^{RNAi}* (TRiP JF01793), *yki^{RNAi}* (KK 109756). The stocks used in the RNAi screen are listed in TableS10. Other stocks were *optix-Gal4 (67), C311-Gal4 (41),* and *GMR-Gal4* (*68*).

The following constructs were used:
sd^{+}w^{+}y^{+}: P[acman] clone #CH321-04K12 expressing the *sd* gene was inserted in the Bloomington stock #9736 *y w; PBac{y+-attP-9A}* on 2R (53B2).

Drosophila **genotypes by figure**

Fig. 1:

(E)

hpo^{-}: *y w sd^{47M} ey-FLP/w; FRT42D sd^{+}w^{+}y^{+} Ubi-GFP/FRT42D hpo$^{42-47}$*
hpo^{-} sd^{-}: *y w sd^{47M} ey-FLP/Y; FRT42D sd^{+}w^{+}y^{+} Ubi-GFP/FRT42D hpo$^{42-47}$*
ctrl: *y w sd^{47M} ey-FLP/y w; FRT42D sd^{+}w^{+}y^{+} Ubi-GFP/FRT42D*
sd^{-}: *y w sd^{47M} ey-FLP/Y; FRT42D sd^{+}w^{+}y^{+} Ubi-GFP/FRT42D*
yki^{-}: *y w sd^{47M} ey-FLP/y w; FRT42D sd^{+}w^{+}y^{+} Ubi-GFP/FRT42D yki^{B5}*
yki^{-} sd^{-}: *y w sd^{47M} ey-FLP/Y; FRT42D sd^{+}w^{+}y^{+} Ubi-GFP/FRT42D yki^{B5}*

(F)

ctrl GFP^{+}: *y w ey-FLP/y w; FRT42D/FRT42D tub-Gal80; +/tub-Gal4 UAS-GFP*
sd^{-} GFP^{+}: *sd^{47M} FRT19A/tub-Gal80 FRT19A; ey-FLP Act 5C<y^{+}<Gal4 UAS-GFP/+*
yki^{3SA} sd^{-} GFP^{+}: *sd^{47M} FRT19A/tub-Gal80 FRT19A; ey-FLP Act 5C<y^{+}<Gal4 UAS-GFP/+; UAS-yki^{3SA}/+*
yki^{3SA} GFP^{+}: *y w ey-FLP; FRT42D/FRT42D tub-Gal80; UAS-yki^{3SA}/tub-Gal4 UAS-GFP*

Fig. 2:

(B)(C)

ctrl GFP^{+}: *y w ey-FLP; FRT42D/FRT42D tub-Gal80; +/tub-Gal4 UAS-GFP*
sd^{-} GFP^{+}: *sd^{47M} FRT19A/tub-Gal80 FRT19A; ey-FLP Act 5C<y^{+}<Gal4 UAS-GFP/+*

(D)

ctrl: *y w sd^{47M} ey-FLP/y w; FRT42D sd^{+}w^{+}y^{+} Ubi-GFP/FRT42D*

sd^{-}: *y w sd^{47M} ey-FLP/Y; FRT42D sd^{+}w^{+}y^{+} Ubi-GFP/FRT42D*

hpo^{-}: *y w sd^{47M} ey-FLP/w; FRT42D sd^{+}w^{+}y^{+} Ubi-GFP/FRT42D hpo$^{42-47}$*

hpo^{-} sd^{-}: *y w sd^{47M} ey-FLP/Y; FRT42D sd^{+}w^{+}y^{+} Ubi-GFP/FRT42D hpo$^{42-47}$*

(E)

w/y v; optix-Gal4/+; UAS-w^{RNAi}/+

w/y v; optix-Gal4/+; UAS-sd^{RNAi}/+

w/+; optix-Gal4/UAS-yki^{RNAi}

w/+; optix-Gal4/UAS-yki^{RNAi}; UAS-sd^{RNAi}/+

(F)

ctrl: *w/y v; optix-Gal4 UAS-RFP/+*

sd^{-}: *w/y v; optix-Gal4/+; UAS-sd^{RNAi}/+*

(G-I)

y v/+;; C311-Gal4/UAS-w^{RNAi}

y v/+;;C311-Gal4/ UAS-sd^{RNAi}

Fig.S3:

(A)

ctrl: *w/y v; optix-Gal4, UAS-RFP/+*

sd^{-}: *w/y v; optix-Gal4/+; UAS-sd^{RNAi}/+*

(B)

y w; UAS-RFP/+; C311-Gal4/+

y w; UAS-RFP/UAS-yki^{RNAi}; C311-Gal4/UAS-p35

Fig.S9:

(A) *y w; ex-lacZ/+; hh-Gal4, UAS-GFP/+*

(B) *y w; ex-lacZ/UAS-yki^{RNAi}; hh-Gal4, UAS-GFP/+*

(C) *y w; ex-lacZ/UAS-yki^{RNAi}; hh-Gal4, UAS-GFP/ UAS-p35*

(D) *y w; ex-lacZ/UAS-yki^{RNAi}; hh-Gal4, UAS-GFP/ UAS-p35*

Fig.S11:

(H) *y w; Yki-GFP/+*

(I) *y w; ex-lacZ/CyO-RFP*

(K) *y w; +/+; DE-Gal4/UAS-GFP*

(L) *y w/ y v; +/+; DE-Gal4, UAS-wts^{RNAi}/kibra-lacZ*
(M) *y v; +/+; kibra-lacZ/TM3*

Drosophila **genotypes for RNA-seq analysis**

Yki^{3SA} overexpression in sd *mutant and* ctrl *clones – MARCM experiment (Fig.1, Fig.S2, Table S1)*

Using the MARCM system (*69*) allowed us to drive the overexpression of Yki^{3SA} in *sd* mutant clones. Full genotypes of this, as well as all of the appropriate control conditions, are listed below. Clones were generated in the entire eye imaginal discs using *ey-FLP*. however, *sd* mutant cells were not viable in the peripodial epithelium and their loss was compensated for by wildtype cells (see Fig.2B-C). Since, virtually no *sd* mutant cells were recovered in the peripodial epithelium, *sd^{-}* discs that were used for RNA-seq had almost entirely wildtype peripodia.

ctrl: 5 samples: *FRT19A/tub-Gal80 FRT19A; ey-FLP Act 5C<y+<Gal4, UAS-GFP/+; +/+*
2 samples: *y w ey-FLP/y w; FRT42D/FRT42D tub-Gal80; +/tub-Gal4 UAS-GFP*

sd^{-}: 5 samples: *sd^{47M} FRT19A/tub-Gal80 FRT19A; ey-FLP Act 5C<y^{+}<Gal4 UAS-GFP/+*

Yki^{3SA}, sd^{-}: 6 samples: *sd^{47M} FRT19A/tub-Gal80 FRT19A; ey-FLP Act 5C<y^{+}<Gal4 UAS-GFP/+; UAS-yki^{3SA}/+*

Yki^{3SA}: 5 samples: *FRT19A/tub-Gal80 FRT19A; ey-FLP Act 5C<y+<Gal4, UAS-GFP/+; UAS-yki^{3SA}/+*
1 sample: *y w ey-FLP; FRT42D/FRT42D tub-Gal80; UAS-yki^{3SA}/tub-Gal4 UAS-GFP*

Yki hyperactivation (Fig.5, Fig.S15, TableS8)

Yki^{3SA}: *FRT19A/tub-Gal80 FRT19A; ey-FLP Act 5C<y+<Gal4, UAS-GFP/+; UAS-yki^{3SA}/+*
Yki^{3SA} ctrl: *FRT19A/tub-Gal80 FRT19A; ey-FLP Act 5C<y+<Gal4, UAS-GFP/+; +/+*
wts^{-}: *y w ey-FLP/y w; +/+; FRT82B cl^{-}/FRT82B wts^{149}*
wts ctrl: *y w eyFLP/ y w; +/+; FRT82B cl^{-}/FRT82B wts^{149}*
optix>Yki^{3SA}: *w/y v; optix-Gal4/+; UAS-yki^{3SA}/+*
optix ctrl: *w/y v; optix-Gal4/+; UAS-luc^{RNAi}/+*

Larvae fed pupation-preventing diet

Both time points: *y w; +/+; +/+*

Pupation-preventing food

The YPH erg2Δ::TRP1 yeast strain unable to produce the hormone precursors necessary for the onset of pupation in *Drosophila* was cultured for 48h at 30°C, centrifuged at 4°C, 1500g for 3min, and the pellet was washed with PBS 3 times as described (*48*). The resulting yeast paste was stored at -20°C. For medium preparation, the yeast paste was boiled for 30 minutes and mixed with 10% sucrose, 1.5% agar solution and sterile water in the proportions 10:1:8:20. Nipagin and penicillin were added to prevent fungal and bacterial growth. Adult flies were left overnight to lay eggs, the medium was incubated at 25°C and the larvae were dissected on the day specified in the experiment (controls at day5, *ex-lacZ* and *kibra-lacZ* staining at day 8, samples for RNA-seq analysis at day 11).

RNAi-based genetic screens

To screen for targets required for Yki-driven overgrowth, we used fly lines with RNAi constructs targeting the high confidence Yki-Sd target genes as well as additional genes annotated as targets in reference (*55*). We obtained all available stocks with UAS-RNAi targeting these genes from the Vienna Drosophila Resource Center and the Bloomington Drosophila Stock Center (stock numbers listed in TableS10). We then crossed these stocks individually to *GMR>Yki^{1SA}* flies (full genotype: *w; GMR-Gal4/CyO-RFP; UAS-Yki^{1SA}/(TM6B)*) that overexpressed *Yki^{1SA}* (*70*) under the control of the *GMR-Gal4* driver (*68*). The crosses were raised at 29°C and scored for the size of the adult eyes. The confidence score was assigned based on the strength of the phenotype as well as its consistency among all the lines screened for a given gene.

We used the same collection of stocks expressing UAS-RNAi lines and screened them for requirement during normal growth. The UAS-RNAi stocks were individually crossed to *optix>w^{RNAi}* flies (full genotype: *w; optix-Gal4/CyO; UAS-white^{RNAi}/(TM3)*). The crosses were raised at 29°C and flies were scored for their adult eye phenotype. If the adults failed to eclose, pharate adults were pulled out from the pupal cases whenever possible. If the pupae died at earlier stages before the eyes could be discerned, the phenotype was described as lethal. The confidence score was assigned based on the strength of the phenotype as well as its consistency among all the lines screened for a given gene.

Imaging of adult *Drosophila* eyes

Images of adult flies were taken using a Zeiss Axioplan2 widefield microscope and processed using ImageJ with the Extended Depth of Field plugin.

Immunofluorescence stainings and image analyses

Drosophila larval imaginal discs were fixed in 4% formaldehyde for 30min at room temperature, then washed in PBT (PBS + 0.3% TritonX-100), subsequently blocked in 5% Normal Donkey Serum (NDS) in PBT for 15min. Tissues were incubated with primary antibody overnight at 4°C and then washed and incubated with secondary antibody and DAPI for 2h at room temperature and mounted in Vectashield (Vector Laboratories). Dissected eye imaginal discs were incubated with EdU (1:1000) for 45min at room temperature before fixation. EdU was detected using the "Click-iT EdU Alexa Fluor 555 Imaging Kit" (Life Technologies C10338).

Livers were collected and fixed in 4% paraformaldehyde (PFA) for 48h and then washed in PBS. For immunofluorescence analysis, livers samples were embedded in 4% agarose in PBS and then sectioned at 100µm thickness using a Vibratome (model Leica VT 1000S). The liver sections were permeabilized with 0,5% TritonX-100 for 10min and blocked in 3% Bovine Serum Antibody (BSA) in PBS for 2h at room temperature. The sections were then incubated in primary antibody overnight in 3% BSA in PBS. The following day the sections were incubated in a secondary antibody solution in 3% BSA in PBS for 2h at room temperature. Sections were then washed and mounted in Mowiol to be analyzed by confocal imaging.

Primary antibodies

Goat-anti-Osteopontin (1:1000, R&D systems #AF1433); rabbit-anti-Yap (1:100, abcam #52771); rabbit-anti-Ki67 (1:100, abcam #15580); rabbit-anti-cleaved Caspase 3 (1:250, Cell Signaling #9661S); rat-anti-ELAV (1:500, *Drosophila* studies hybridoma bank, DSHB 7E8A10); rabbit-anti-GFP (1:150, abcam #ab290); goat-anti-HNF4a (1:100, Santa Cruz Biotechnology 6556); rabbit-anti-Dcp1 (1:150, Cell Signaling #9578S); guinea pig-anti-Ato (1:2000, donated by Hugo Bellen, Baylor College of Medicine, Houston, TX); mouse-anti-Dlg (1:150, DSHB #4F3).

Secondary antibodies

All secondary antibodies were used at a concentration of 1:500. AlexaFluor 488-donkey-anti-rabbit; AlexaFluor 488-donkey-anti-goat; AlexaFluor 555-donkey-anti-goat; AlexaFluor 555-donkey-anti-rabbit; AlexaFluor 555-donkey-anti-rat; AlexaFluor 555-donkey-anti-mouse; Cy3-goat-anti-guinea pig (Jackson Immuno Research).

Drosophila and mouse samples were imaged on an Olympus FV1200 confocal microscope. Images were processed in ImageJ with the Bio-Formats Importer plug-in. All images were arranged using Adobe Photoshop CS6.

Quantifications and statistics

Quantifications of GFP-positive clones in eye imaginal discs (Fig.1G and Fig.2C) were done measuring the GFP^+ area using the ImageJ software. The fluctuating asymmetry (Fig.2F) is expressed as the difference in the number of ommatidia between a pair of pupal retinas from the same animal relative to the total number of ommatidia (average between the two retinas) = %(Left-Right)/avg (Left, Right). The ommatidia were counted manually on a confocal microscope image of mounted pupal retina stained with DAPI.

Quantification of the number of hepatocytes in liver sections from neonatal (P5) and adult (6-month-old) mice (Fig.S1C) was done by counting the number of hepatocytes over the total area of tissue in confocal images. Areas without DAPI, such as luminal spaces, were excluded in this measurement since these do not contribute to the tissue cell mass. Hepatocytes were quantified by counting 2 pictures from two liver sections per mouse (4 mice per condition). This amounted to about 1000 hepatocytes per section at P5 and 700 hepatocytes per section at 6 months of age. All quantifications were performed using the Cell Counter plugin in ImageJ software.

Statistical analyses were performed as follows:

Fig.1B: two-way ANOVA test. Statistical analysis of each time-point was performed using unpaired Student's t-test; CI=95%.

Fig.1G: ordinary one-way ANOVA test (P<0.0001). A multiple comparison test was subsequently performed (α=0.05). F=152, DF=3.

Fig.2F: two-sample equal variance t-test (P=0.25). A prior F-test (P=0.32) revealed no significant difference between the variance in both genotypes; N=10.

Fig.S1B: statistical analysis of each time-point was performed using unpaired Student's t-test; CI=95%. The data are presented as the mean ± SEM.

Fig.S1D: one-way ANOVA test and Dunnett's multiple comparison

Quantitative RT-PCR

Total RNA was isolated from mouse tissues using a RNAeasy Mini Kit (Qiagen) according to manufacturer's instructions. RNA samples were reverse transcribed to complementary DNA with oligo dT and RevertAid H Minus Reverse Transcriptase (Thermo Scientific). Real-time quantitative PCR was performed using LC 480 SYBR Green I Master (Roche) reaction. All runs were done in triplicate and expression levels were normalized to *Gapdh* levels. Primer sequences used:

Yap: FWD– CCTGATGATGTACCACTGCC; REV– GCCATGTTGTTGTCTGATCG;

Taz: FWD– CCTATGACGTGACCGACGAG; REV– TGCCATGTGGTGATTTTCTC;

Gapdh: FWD- CGTCCCGTAGACAAAATGGT; REV- TTGATGGCAACAATCTCCAC (*48*).

RNA sequencing and data analysis

Sample preparation and RNA sequencing

Dissection tools and surfaces were treated with RNAseZap (Sigma). *Drosophila* imaginal discs were dissected and transferred into RNAse-free 1xPBS on ice; a minimum of 30 discs per sample were used. Hepatocytes were isolated as described above. RNA was extracted immediately using the RNAeasy mini spin kit (Qiagen) and stored at -80°C. cDNA library preparation was performed according to the QuantSeq 3' mRNA-Seq Library Prep kit FWD (Lexogen) and the resulting library was sequenced on NovaSeq 6000 (100bp, single end, unstranded). Quality control and trimming of the sequencing reads was performed using FastQC and Cutadapt followed by mapping to the

Drosophila melanogaster genome assembly Release 6 (dm6) or *Mus musculus* genome assembly GRCm38 (mm10) using STAR. Raw sequencing reads and count matrices are deposited in GEO under the accession number GSE211461 with the following SubSeries: GSE211457 (Drosophila – non-pupating larvae), GSE211458 (Drosophila – Yki hyperactivation), GSE211459 (Liver – Yap hyperactivation) and GSE211460 (Liver – CCl4 in Yap/Taz KO).

RNA-seq data used

Conditions	**Source – complete results**
MARCM experiment: *yki^{3SA}; ctrl; sd^{-}; yki^{3SA} sd^{-}*	This manuscript – Table S1
Eye disc developmental time course: 72h, 96h and 120h	GSE94915 – Table S3
Larvae on pupation-preventing diet: 5 days and 11 days	This manuscript – Table S3
Eye imaginal discs – single cell dataset	GSE141589
Wing imaginal discs – single cell dataset	GSE127832 and GSE133204
ey-FLP wts^{-}; ey-FLP ctrl; optix>yki^{3SA}; optix ctrl	This manuscript – Table S8
Ubx-FLP wts^{-}	GSE71353 – Table S8
ap>Yki	GSE151935
Ras^{V12G} scrib^{RNAi} tumors in imaginal discs	GSE81272
Liver development – single cell dataset	GSE90047
Adult liver single cell atlas	GSE192740
Apo>YAP, Lats1/2 KO and controls (*Apo>YAP ctrl, Lats1/2 flox, BL/6, BL/6+Dox, BL/6*+AAV-Cre)	This manuscript – Table S4
Yap/Taz KO ± CCl_4; *Yap/Taz flox* ± CCl_4	This manuscript – Table S5

More details on genotypes and experimental conditions are listed in the corresponding supplemental tables. Other gene sets used in the analysis are listed in Table S7 for the liver and Table S9 for fly imaginal discs.

General analysis

After filtering lowly expressed genes, a differential gene expression analysis was performed using the DESeq2 R package(*71*), and results are reported in supplemental tables S1, S3, S4, S5 and S8.

In all bulk RNA-seq analyses, genes were considered significantly upregulated or downregulated, when adjusted p values were <0.05 and log2 fold changes were >1 or <-1, respectively. Heatmaps show log2 scale expression as obtained by 'regularized log' transformation from DESeq2. Clustering was done by hierarchical clustering using Euclidean distance and the ward.D2 method. All correlations were measured by Pearson's correlation coefficient.

Single cell RNA-seq of Drosophila imaginal discs

Single-cell RNA-seq data of wild type third instar eye-antennal discs together with cell type annotations was obtained from a loom file provided by the authors (*50*) at http://scope.aertslab.org/#/Bravo_et_al_EyeAntennalDisc. For our analysis, only cells originating from imaginal discs were kept, and cells of other identities such as brain, glia, hemocytes and *twi*$^{+}$ cells were discarded. A single-cell RNA-seq data set of wild type third instar wing discs was obtained by merging the two independent datasets GSE127832 (*72*) and GSE133204 (*73*) using the harmony R package (*74*). Cell types were annotated based on the expression of the marker genes listed in both publications. Data for both disc types was analyzed using the Seurat R package(*75*) with default settings. The UMAP was generated on 30 PCs. The average expression of gene sets was calculated using the Seurat function AddModuleScore and visualized on a UMAP (Seurat::FeaturePlot) or violin plot (Seurat::VlnPlot). The average expression per cell type (pseudobulk) was generated using Seurat::AverageExpression on SCT corrected counts. Cell cycle was assessed with the CellCycleScoring function.

Single cell RNA-seq of early liver development

Single-cell RNA-seq data of cells from embryonic mouse liver at E10.5-E17.5 was obtained from GEO Series GSE90047 (*47*). The time point annotation was extracted from the names of the cells. The data was analyzed using Seurat R package with default settings. Only genes with counts in at least 5 cells were included for further analysis. The UMAP was generated on 10 PCs. The cell populations were annotated based on the markers provided in the publication. Further analysis and visualization of gene expression was done as described for the imaginal disc datasets.

Single cell RNA-seq of adult livers

Single-cell RNA-seq data of cells from adult mouse liver together with cell type annotations was obtained from the Liver Cell Atlas (https://www.livercellatlas.org/download.php MouseStSt). The list of cell type specific marker genes was obtained from (*45*) Table S2.

Ras-scrib tumors

The gene expression from discs with *Ras-scrib* tumors (*UAS-scrib^{RNAi}, UAS-Ras^{V12G}/+; hh-Gal4, UAS-GFP/UAS-luc^{RNAi}*) was obtained from GEO Series GSE81272 published in (*44*). Based on the supplementary table provided by the authors, differentially expressed genes were defined by adjusted p value <0.05 and log2 fold change >1 (or <-1). The following comparisons were used in this publication:

- *Ras-scrib* tumors in eye discs vs. control eye discs
- *Ras-scrib* tumors in wing discs vs. control wing discs
- *Ras-scrib* tumors with *sd^{RNAi}* in eye discs vs. *Ras-scrib* tumors in eye discs

Full genotypes:

control: *hh-Gal4, UAS-GFP/UAS-luc^{RNAi}*

Ras-scrib tumors: *UAS-scrib^{RNAi}, UAS-Ras^{V12G}/+; hh-Gal4, UAS-GFP/UAS-luc^{RNAi}*

Ras-scrib tumors with *sd^{RNAi}*: *UAS-scrib^{RNAi}, UAS-Ras^{V12G}/+; hh-Gal4, UAS-GFP/UAS-sd^{RNAi}*

Gene ontology analysis

Biological Process, Molecular Function and Cellular Compartment Gene Ontologies from org.Mm.eg.db and org.Dm.eg.db were used for the mouse and *Drosophila* analyses, respectively. GO overrepresentation analysis was done using the enrichGO function from the clusterProfiler R package(*76*) with qvalue cutoff at 0.05 and otherwise default settings. The similarity between the enriched GO terms was calculated and visualized on a dendrogram using the enrichplot R package . Gene Set Enrichment Analysis (GSEA) was performed by the fgsea algorithm using clusterProfiler and visualized using enrichplot.

Chromatin accessibility and Sd binding sites

Single-cell ATAC-seq data of *Drosophila* third instar eye discs from (*50*) was obtained from SCope (http://scope.aertslab.org/#/Bravo_et_al_EyeAntennalDisc). The data was processed by the authors using cisTopic, a probabilistic framework that co-optimizes cell clustering and region clustering into topics. Among these topics, one of them represented regions uniquely accessible in the medial peripodial epithelium, with 1528 regions. To determine all accessible regions in medial peripodial epithelium cells, we performed peak calling on their pseudobulk profile using MACS2 (v2.1.2.1) with the following additional options: –nomodel –call-summits –nolambda. We performed motif enrichment in these regions using i-cisTarget (*77, 78*) using a ROC threshold of 0.01, a maximum rank of 5000, a NES threshold of 3, and the version 8 motif database, containing more than 20,000 transcription factor DNA binding motifs. Regions linked to Sd binding motifs were selected as peripodial epithelium peaks that contain the Sd binding site. Sd ChIP-Nexus data was obtained from GSE96868 published in (*79*). Sd motif enrichment in the ChIP-Nexus regions was performed as described above.

Yki-Sd target gene annotation

All protein-coding genes in the *Drosophila* genome were scored based on evidence generated by integrating data from Sd ChIP-seq (GSE54601 published in (*80*)) and Sd ChIP-Nexus (GSE96868 published in(*79*)), Sd motif enrichment (using i-cisTarget (*77, 78*) with ROC threshold of 0.01, a maximum rank of 5000, a NES threshold of 3 and the version 8 motif database), ATAC-seq (GSE59078), and RNA-seq of Yki hyperactivation (GSE71353 published in(*55*)). The selection criteria for target genes were weighted for the presence of Sd motifs in open chromatin regions with ChIP-seq peaks and accessible promoters. The scoring was done by visual assessment of tracks showing the above-mentioned data in UCSC genome browser.

Figure S1. Liver phenotypes of *Alfp-Cre; Yap/Taz KO* mice

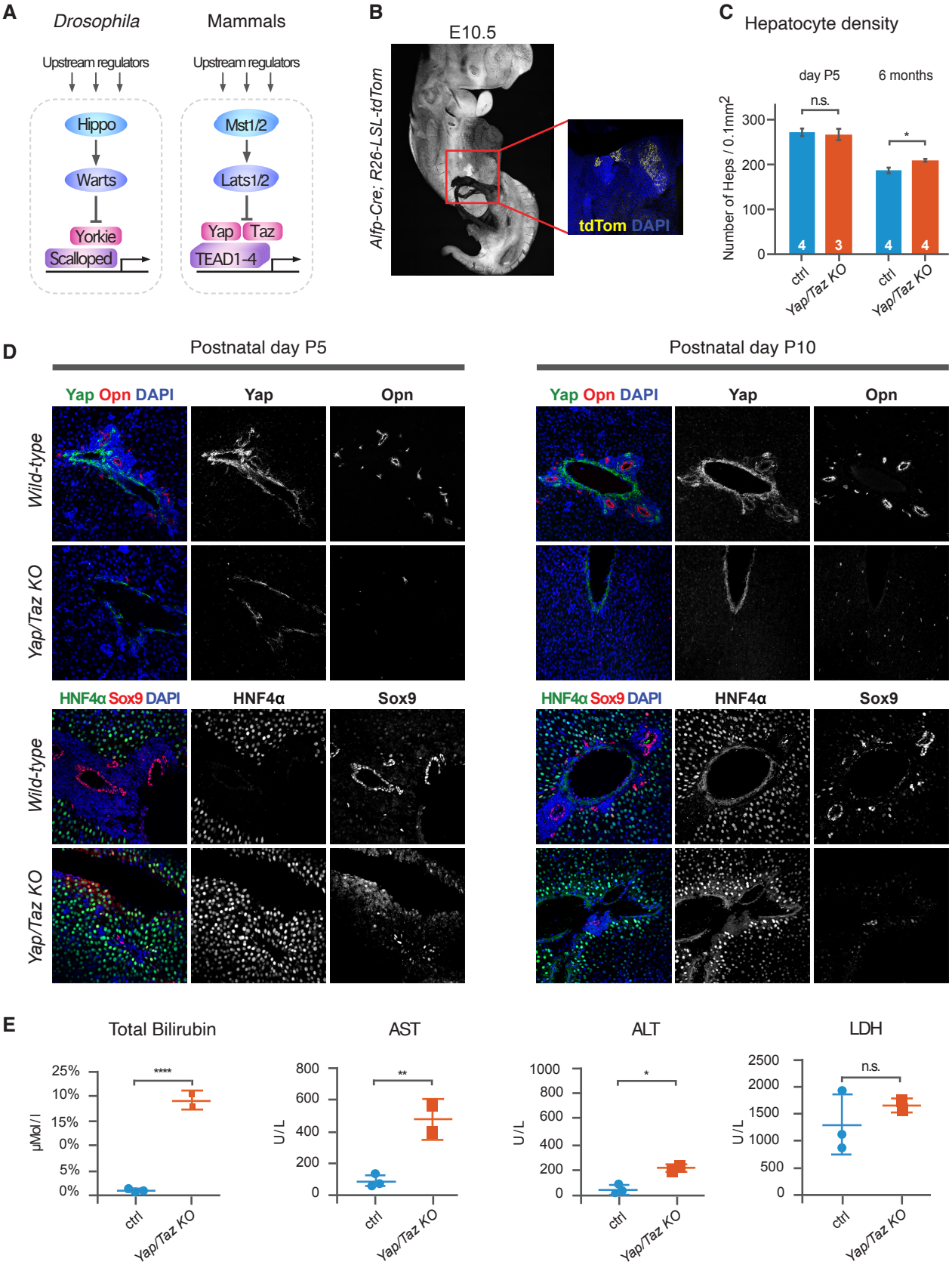

Supplemental Figure Legends

Fig. S1. Liver phenotypes of *Alfp-Cre; Yap/Taz* KO mice.

(**A**) Simplified schematic of the Hippo signaling pathway in *Drosophila* and mammals. Various mechanisms affect the activity of the Hippo pathway such as the state of the actin cytoskeleton, cell-ECM and cell-cell adhesion, and cell polarity. These mechanisms feed into the core of the Hippo pathway and activate the Hippo/Mst1/2 kinases and the Warts/Lats1/2 kinases, which phosphorylate and inactivate the Yorkie (Yki)/Yap/Taz co-activators. When not inhibited, Yki/Yap/Taz bind to Scalloped (Sd)/TEAD transcription factors to regulate the expression of target genes.

(**B**) Confocal image of a E10.5 *Alfp-Cre R26-LoxP-STOP-LoxP-tdTomato* mouse embryo stained for nuclei (DAPI, blue) and tdTomato (yellow) shows efficient recombination already at E10.5.

(**C**) Hepatocyte density in control and *Alfp-Cre; Yap/Taz KO* livers at postnatal day P5 and 6 months shows that loss of Yap/Taz does not affect the density of hepatocytes; number of samples shown on the bar; * = P <0.05; n.s. = not significant; data are mean ± SEM.

(**D**) Confocal images of liver sections of wild-type and *Alfp-Cre; Yap/Taz KO* mice at postnatal day P5 and P10 stained for nuclei (DAPI, blue), Yap (green) and the cholangiocyte marker Opn (red) in the top panels, or the hepatocyte marker HNF4α (green) and the cholangiocyte marker Sox9 (red) in the bottom panels. The lack of Opn and Sox9 expression shows impaired formation of the ductal plate and the complete absence of bile ducts in *Alfp-Cre; Yap/Taz KO* mutant embryos.

(**E**) *Alfp-Cre; Yap/Taz KO* mice have high blood serum levels of bilirubin, AST, ALT and LDH at 2 months of age compared to wild-type animals. One-way ANOVA test and Dunnett's multiple comparisons test were performed to calculate all p values.

Figure S2. Loss of Sd reverts the transcriptional changes induced by Yki^{3SA} overexpression

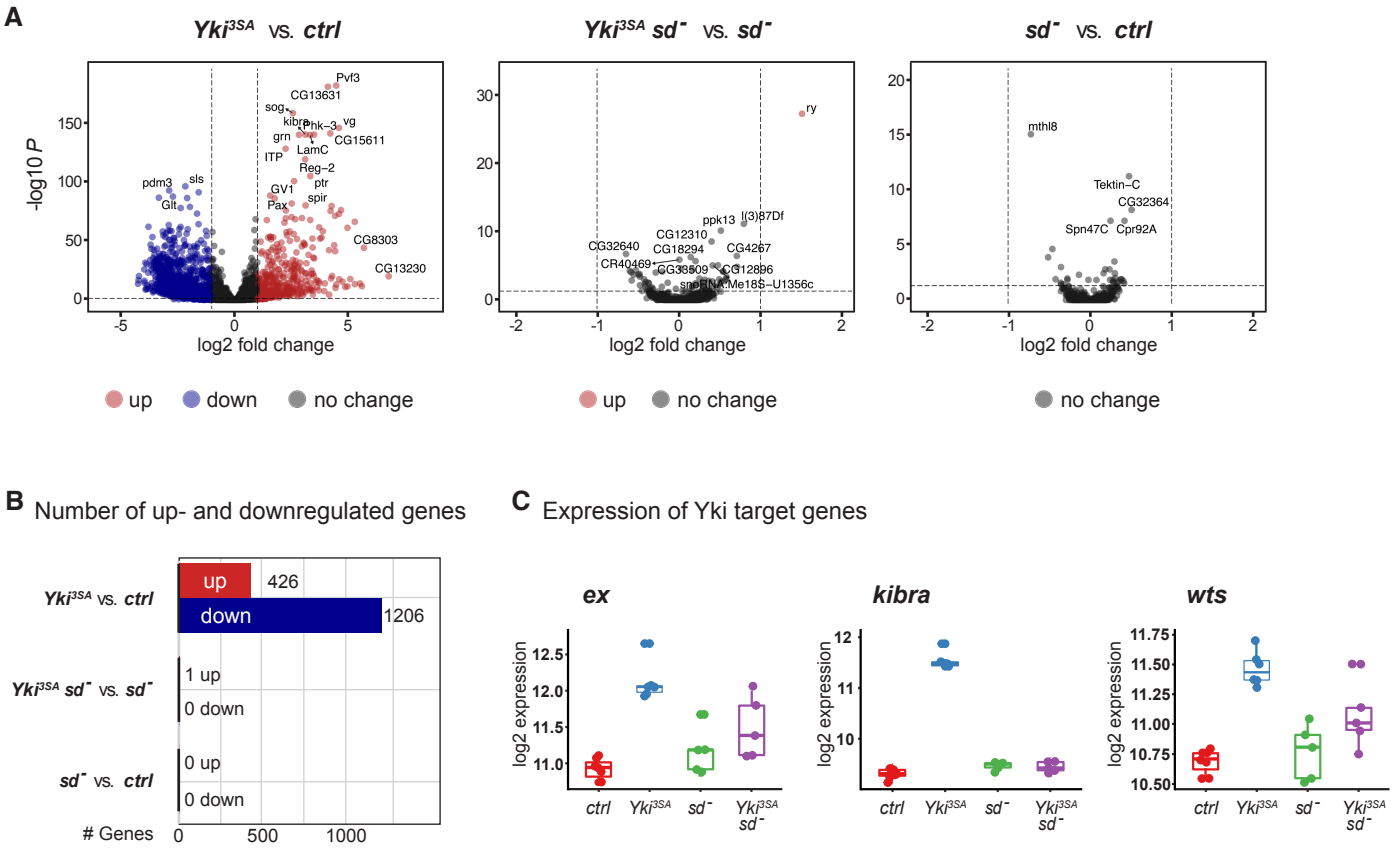

Fig. S2. Loss of Sd reverts the transcriptional changes induced by Yki^{3SA} overexpression.

(**A**) Volcano plots showing differentially expressed genes in the indicated comparisons. Upregulated genes (P adj. < 0.05; log2FC > 1) are marked in red and downregulated genes (P adj. < 0.05; log2FC < -1) are marked in blue.

(**B**) The number of up- or downregulated genes in the indicated comparisons.

(**C**) Absolute expression (in log2 scale) of selected Yki target genes in the indicated genotypes, each dot represents an individual sample; ctrl: N=7; *Yki^{3SA}*: N=6; *sd^{-}*: N=5; *Yki^{3SA} sd^{-}*: N=5.

Figure S3. Loss of Sd phenotypes

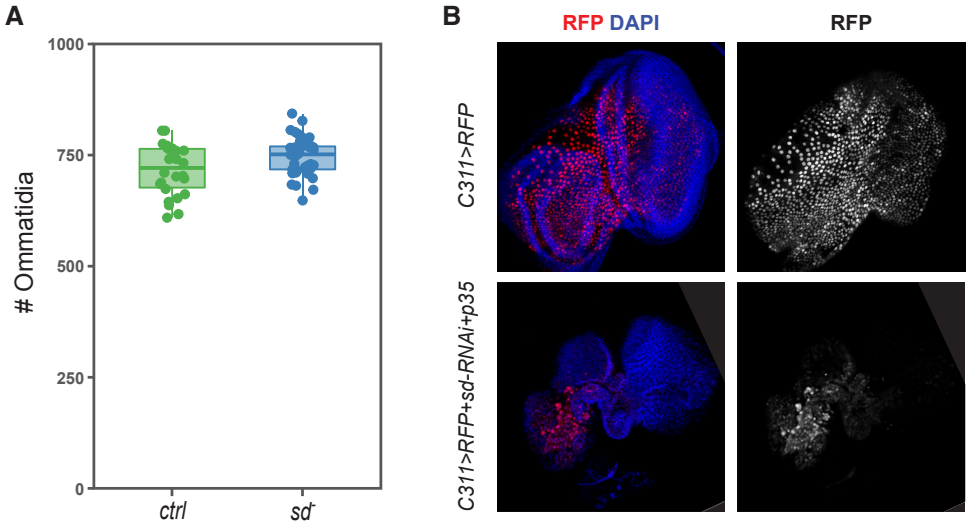

Fig. S3. Loss of Sd phenotype in the peripodial epithelium.

(**A**) Quantification of the number of ommatidia in adult control flies (*optix-Gal4 UAS-RFP*; N=26) and flies with sd^{-} mutant eyes (*optix-Gal4 UAS-*sd^{RNAi}; N=38).

(**B**) Confocal images of eye imaginal discs of the indicated genotypes showing nuclei (DAPI, blue) and RFP expression (red). The upper row shows the normal expression pattern of the *C311-Gal4* driver in the peripodial epithelium, marked by RFP, robustly expressed in peripodial cells. The bottom row shows the effects of *sd* knockdown in the peripodial cells rescued from cell death by co-expression of the anti-apoptotic protein p35. Prominent morphological defects of the sd^{RNAi} RFP^{+} cells indicate that Sd is essential not only for survival and growth, but also for the proper morphology of peripodial cells.

Figure S4. Validation of the Yap signature as a transcriptional readout for Yap/Taz activity

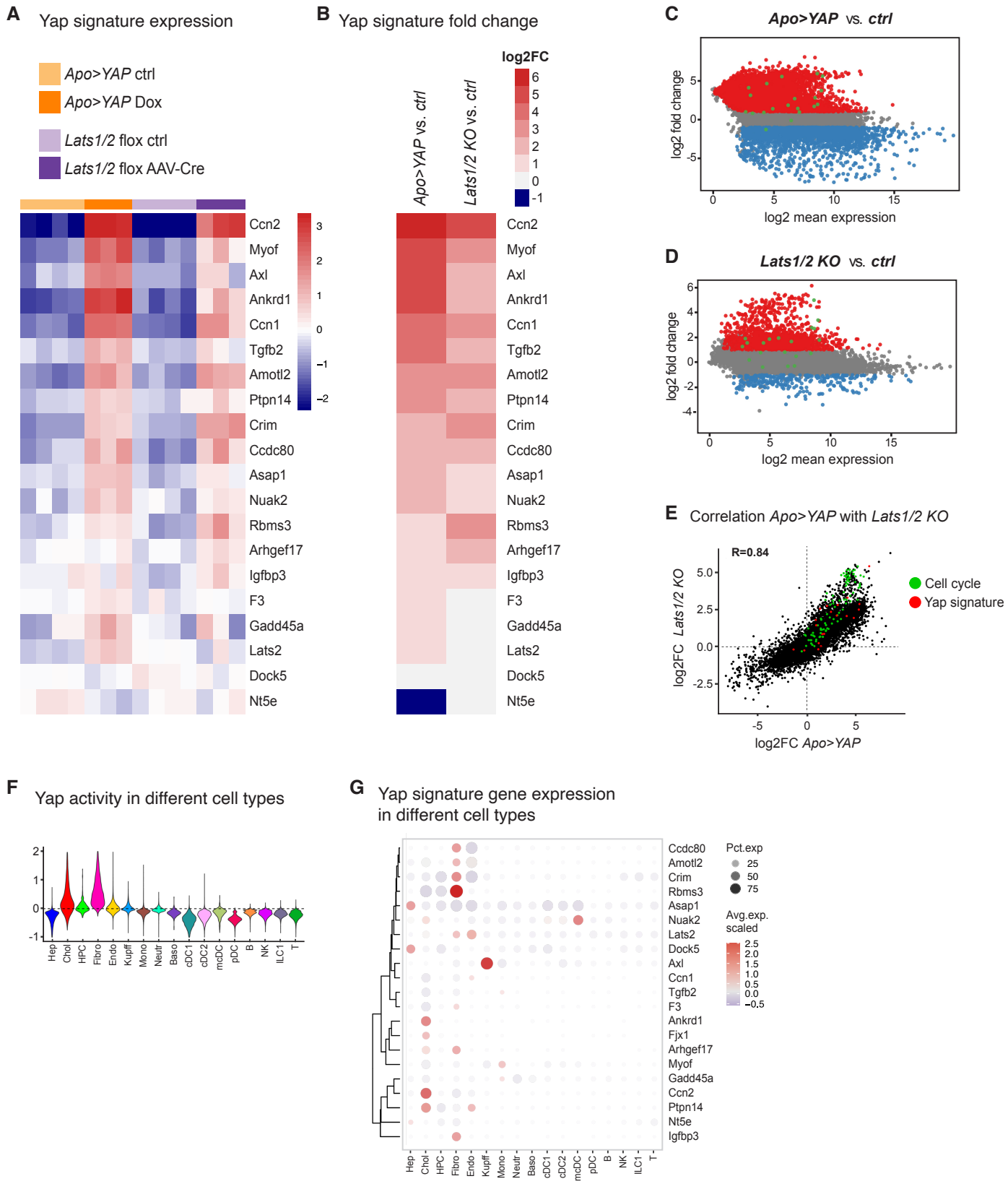

Fig. S4. Validation of the Yap signature as a transcriptional readout for Yap/Taz activity.

(**A** and **B**) Yap signature gene expression in purified hepatocytes one week after YAP overexpression or *Lats1/2* knockout. (A) Heatmap of the relative expression of Yap signature genes in *Apo>YAP*, *Lats1/2 KO* and their respective control samples and (B) log2 fold changes for the two genotypes showed upregulation of the majority of the signature.

(**C** and **D**) MA plots show how much Yap signature genes were induced in *Apo>YAP* and *Lats1/2 KO* hepatocytes relative to all differentially expressed genes; upregulated genes (P adj. < 0.05; log2FC > 1), downregulated genes (P adj. < 0.05; log2FC < -1) and Yap signature genes are marked in red, blue and green, respectively, and their distribution along the y-axis is shown by the density plot on the right side. The Yap signature was robustly induced in both genotypes.

(**E**) Correlation of the changes in gene expression induced by YAP overexpression versus *Lats1/2* knockout; cell cycle and Yap signature genes are marked in green and red, respectively, and their distribution along the axes is shown by the density plots. The effects on gene expression were highly correlated between *Apo>YAP* and *Lats1/2 KO*.

(**F** and **G**) Yap signature expression in the single cell atlas of the adult mouse liver. (F) Violin plot shows the distribution of averaged expression of all Yap signature genes in single cells grouped by cell identity. (G) Dotplot shows the expression of individual genes of the Yap signature averaged over all the cells in a given cell type; the color of the dots represents normalized expression, and the size represents the percentage of cells expressing a given gene for each cell type. Cell types with the highest expression of the Yap signature genes were fibroblasts, cholangiocytes and endothelial cells. Abbreviations are: Hep = hepatocytes; Chol = cholangiocytes; HPC = hepatic progenitor cells; Fibro = fibroblasts; Endo = endothelial cells; Kupff = Kupffer cells; Mono = monocytes; Neutr = neutrophiles; Baso = basophiles; cDC = conventional dendritic cells; mcDC = migratory conventional dendritic cells; pDC = plasmacytoid dendritic cells; B = B-cells; NK = natural killer cells; ILC1 = innate lymphoid cells; T = T-cells.

Figure S5. The pattern of cell proliferation and Yap/Taz activity in the embryonic mouse liver

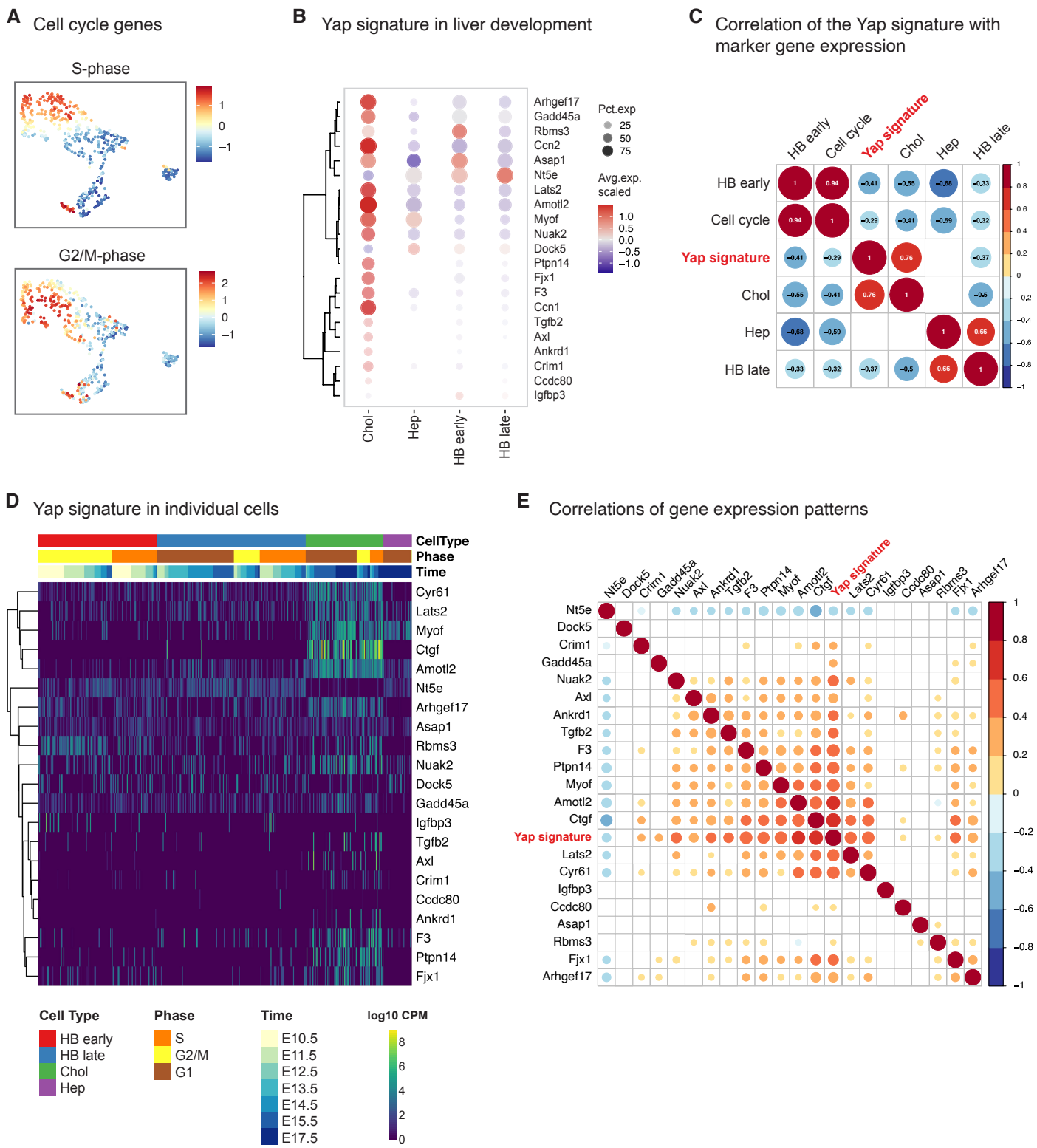

Fig. S5. The pattern of cell proliferation and Yap/Taz activity in the embryonic mouse liver.

(**A**) Normalized average expression of S-phase and G2/M-phase cell cycle genes in the single cell dataset of the mouse embryonic liver.

(**B**) Dotplot showing the expression of individual genes of the Yap signature averaged over all cells of each given cell type; the color of the dots represents normalized expression, and the size represents the percentage of cells expressing a given gene. Abbreviations in this and the other plots are: Hep = hepatocytes; Chol = cholangiocytes; HB early = early hepatoblasts; HB late = late hepatoblasts.

(**C**) Correlations between the normalized average expression of the indicated gene sets in the single cells of the embryonic liver; the size and the color of the dots represent correlation coefficient (R, Pearson's correlation), only statistically significant values are shown ($P<0.01$). The expression of cell cycle genes correlates with the expression of the marker genes for early hepatoblasts, and the expression of Yap signature genes correlates with that of cholangiocyte markers.

(**D**) Single cell heatmap of Yap signature genes showing their expression during liver development. Cells (columns) are grouped by cell type, cell cycle phase and developmental time; genes (rows) are grouped by similar expression pattern. At a single cell resolution, the majority of the Yap signature genes shows predominant expression in cholangiocytes.

(**E**) Correlations between the average expression pattern of the entire Yap signature and the expression of each individual gene in the single cells of the embryonic liver; the size and the color of the dots represent correlation coefficient (R, Pearson's correlation), only statistically significant values are shown ($P<0.01$). Genes with an expression pattern most similar to that of the entire signature (as seen in Fig.3D) are the canonical Yap target genes *Ctgf, Amotl2, Cyr61* and *Lats2*.

Figure S6. Sd binding to the direct target genes *kibra* and *expanded*

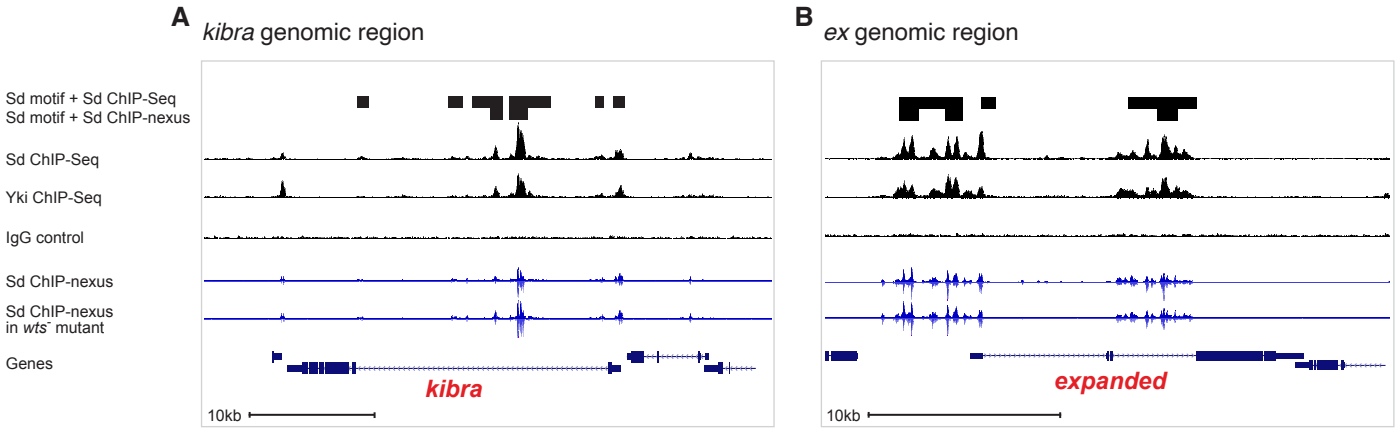

Fig. S6. Sd binding to the direct target genes *kibra* and *expanded*.

(**A** and **B**) Genome browser view of the genomic regions of the Yki target genes *kibra* and *ex* showing tracks of the overlap of Sd motifs with Sd ChIP-seq and Sd ChIP-nexus peaks (top); Sd-, Yki-, and IgG control-ChIP-seq peaks (middle); and Sd ChIP-nexus peaks in control and wts mutant discs (near bottom) above the location of the transcribed regions.

Figure S7. Expression of the Yki signature during eye disc development

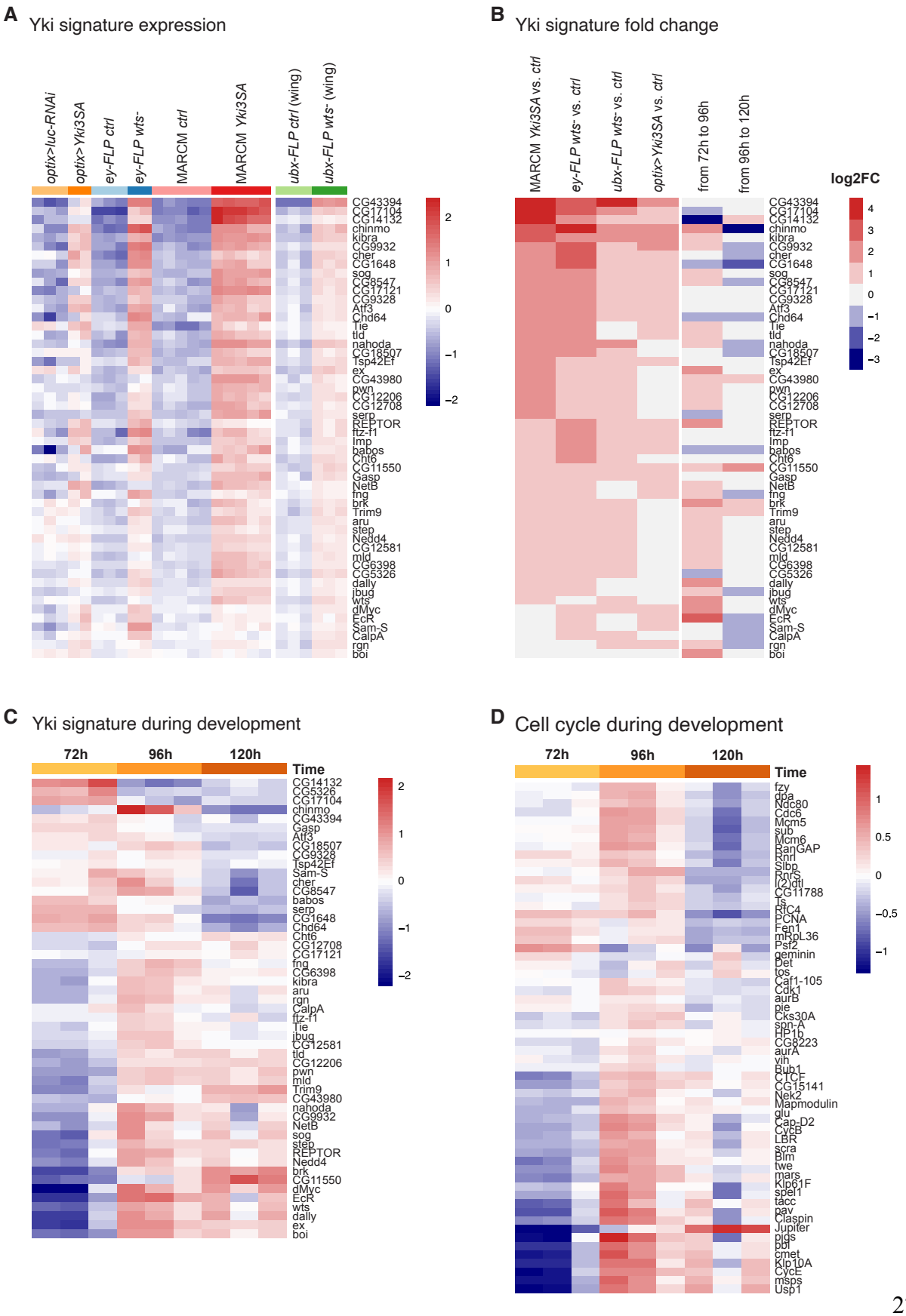

Fig. S7. Expression of the Yki signature during eye disc development.

(**A** and **B**) Yki signature gene expression in four genotypes with Yki hyperactivation in imaginal discs: Yki^{3SA} overexpression in clones in eye discs (MARCM *Yki3SA)*, *wts* knockout clones in eye discs *(ey-FLP wts^{-})*, Yki^{3SA} overexpression specifically in the eye disc proper (*optix>Yki^{3SA}*) and *wts* knockout in wing discs (*ubx-FLP wts^{-}*). (A) Relative expression levels of Yki signature genes in Yki hyperactivated samples and their respective controls, and (B) log2 fold changes for the four experimental conditions and during the developmental time course. The entire Yki signature was upregulated in the Yki hyperactivated samples, but the Yki signature was not strongly modulated during development. In (A), the expression values of the wing disc samples were normalized independently from those of the eye discs.

(**C**) Relative expression levels of the Yki signature genes at three time points during eye disc development showed multiple gene-specific temporal expression patterns with the majority of the genes having increased expression at later time points.

(**D**) Relative expression levels of cell cycle genes at three time points during eye disc development showed that cell proliferation does not obviously correlate with developmental stage in second and third instar larval eye imaginal discs.

Figure S8. The gene expression profile of growth completed eye discs

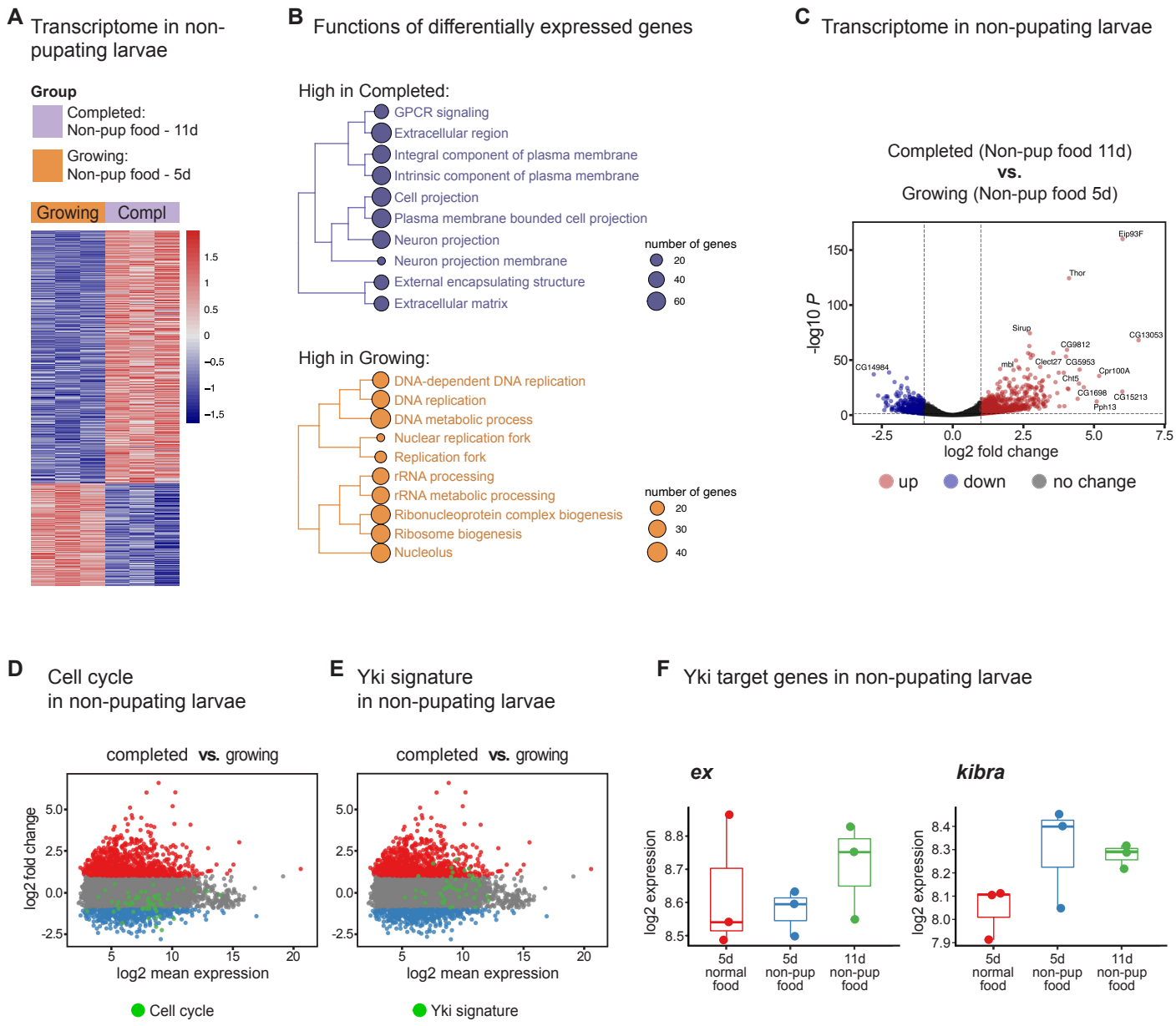

Fig. S8. The gene expression profile of growth completed eye discs.

(**A**) Heatmap showing the relative expression of all differentially expressed genes (P adj. < 0.05; |log2FC| > 1) between the eye discs of larvae kept on a diet preventing pupation at the time point of active growth (5 days = 120h AEL, after egg laying) and after growth completion (11 days AEL).
(**B**) Top 10 most significant GO terms enriched in the genes upregulated (top) and downregulated (bottom) in the growth completed discs as compared to actively growing discs. The size of the dots represents the number of genes overlapping between the given GO term and the differentially expressed genes.
(**C**) Volcano plot showing differentially expressed genes in the growth completed discs as compared to actively growing discs. Upregulated genes (P adj. < 0.05; log2FC > 1) are marked in red and downregulated genes (P adj. < 0.05; log2FC < -1) are marked in blue.
(**D** and **E**) MA plots showing how much the cell cycle and Yki signatures genes were changed in comparison to all differentially expressed genes in the growth completed discs versus actively growing discs; upregulated genes (P adj. < 0.05; log2FC > 1), downregulated genes (P adj. < 0.05; log2FC < -1) and cell cycle (D) or Yki signature genes (E) are marked in red, blue and green, respectively. Cell cycle, but not the Yki signature genes were downregulated upon growth termination.
(**F**) Absolute expression (in log2 scale) of the Yki target genes *ex* and *kibra* in growth completed (at 11 days AEL, green) and actively growing eye discs (at day 5 AEL) from larvae that were feed either standard (red) or pupation-preventing diet for 5 days (blue) or 11 days (green). Each dot represents an individual RNA-seq sample; N=3. Expression of *ex* and *kibra* is not affected by growth termination or the pupation-preventing diet itself.

Figure S9. Regulation of Yki activity in growth completed discs

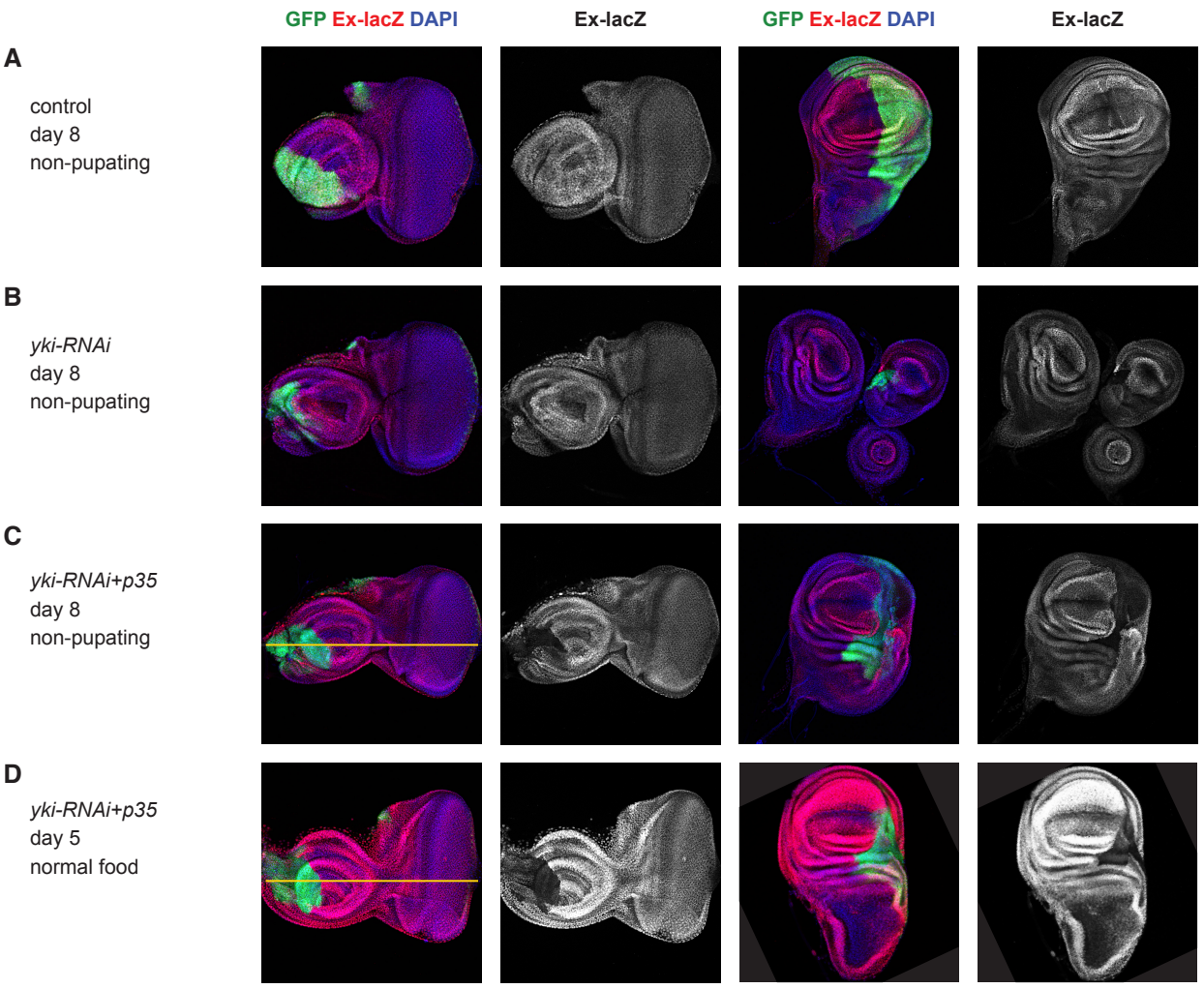

E

Quantification of *yki-RNAi+p35* on day 8 on non-pupating food

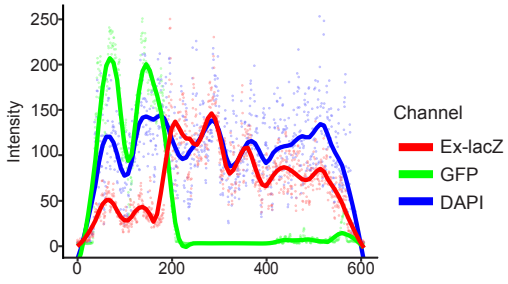

F

Quantification of *yki-RNAi+p35* on day 5 on normal food

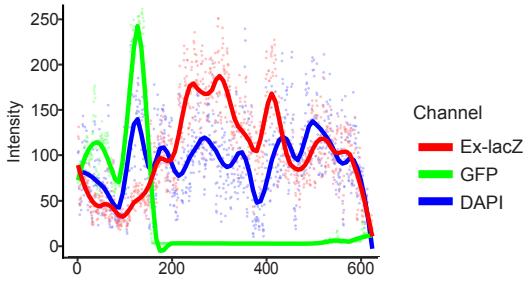

Fig. S9. Regulation of Yki activity in growth completed discs.

(**A** to **D**) Eye (left) and wing discs (right) of larvae fed the pupation-preventing diet (A-C) or normal diet (D) stained for the expression of *ex-lacZ* (red) as a measure of Yki activity and GFP (green) marking the expression domain (driven by *hh-Gal4*) of the *UAS-yki-RNAi* and *UAS-p35* transgenes. From the top: (A) Growth termination did not affect the normal expression pattern of *ex-lacZ* or *hh>GFP*; (B) Expression of *yki-RNAi* lead to cell death and loss of the GFP^+ posterior compartment; (C) Co-expression of *yki-RNAi* together with the anti-apoptotic protein p35 resulted in partial rescue of the posterior compartment and thus enabled the analysis of *yki* knockdown cells, which, even after growth termination, showed lower levels of Yki activity compared to the surrounding *yki* wild-type cells; (D) Discs from larvae of the same genotype as in (C) but where the larvae were fed a standard diet. These discs showed overall higher levels of *ex-lacZ* staining compared to larvae on the normal diet in (C) (all images taken with the same settings). However, knockdown of *yki* caused a similar downregulation of *ex-lacZ* expression in actively growing and growth completed discs. The overall lower levels of lacZ in growth completed discs might be more indicative of general lower translational activity of these discs rather than reflective of lower Yki activity. If growth termination would have been caused by an inhibition of Yki activity, then one would expect to see no difference in the levels of *ex-lacZ* expression between *yki* mutant and wildtype cells in growth completed discs. This was not the case, demonstrating that Yki was still active after growth terminated.

(**E** and **F**) Quantification of pixel intensity for each channel along the yellow horizontal lines marked on the images in panels (C) and (D). This showed that the differential expression of *ex-lacZ* (red) between *yki* mutant (GFP^+, green, on the left side of the plot) and wildtype cells (GFP^-, green, on the right side of the plot) is the same in growth completed (E) and actively growing discs (F). X-axis shows distance in pixels.

Figure S10. Expression of cell cycle and Yki signature genes in eye discs

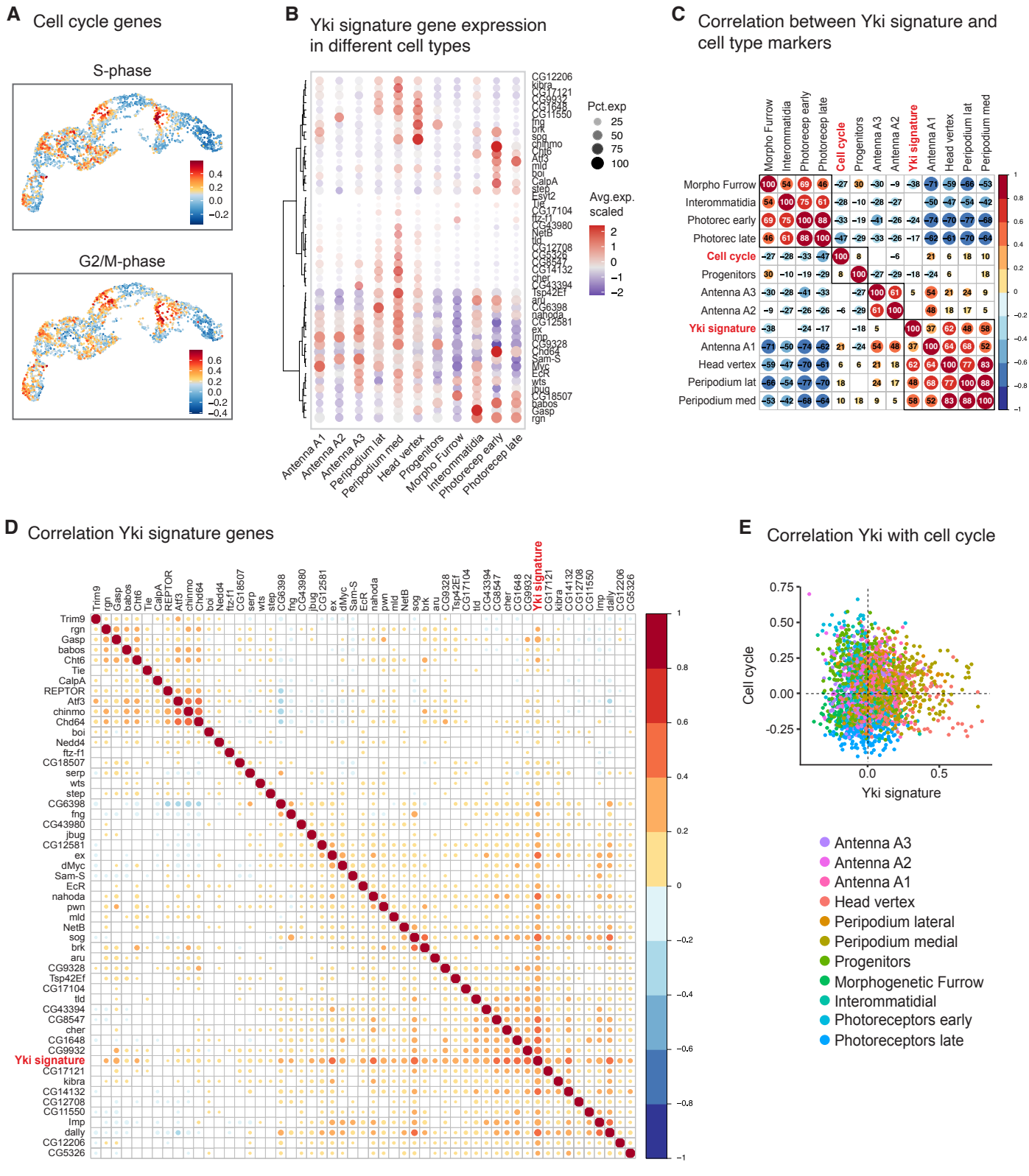

Fig. S10. Expression of cell cycle and Yki signature genes in eye discs.

(**A**) Normalized average expression of S-phase and G2/M-phase cell cycle genes in the single cell atlas of eye imaginal discs.

(**B**) Dotplot showing the average expression of the individual genes of the Yki signature in the cells of a given cell type; the color of the dots represents relative expression, and the size and transparency of the dots represent the percentage of cells expressing a certain gene. The majority of the genes had higher expression in the two subtypes of peripodial cells and cells of the head vertex.

(**C**) Correlations between the normalized average expression of the indicated gene sets in the single cells of eye discs, ordered by hierarchical clustering with k=4 clusters marked by thicker lines; the size and the color of the dots represent correlation coefficient (R, Pearson's correlation), only statistically significant values are shown (P<0.01). The expression of the Yki signature genes correlates best with the expression of marker genes for the peripodium and head vertex.

(**D**) Correlations between the average expression of the entire Yki signature and the expression of each individual gene in the single cells of the eye disc; the size and the color of the dots represent correlation coefficient (R, Pearson's correlation), only statistically significant values are shown (P<0.01). Among the genes with the expression pattern most similar to that of the entire signature (as seen in Fig.3J) are *ex*, *cher*, and *sog*.

(**E**) Scatter plot showing the correlation between the Yki signature and cell cycle gene expression in the single cells of the eye disc atlas, colored by cell identity. There was a complete lack of correlation between cell proliferation and Yki activity.

Figure S11. Yki signature expression in wing discs

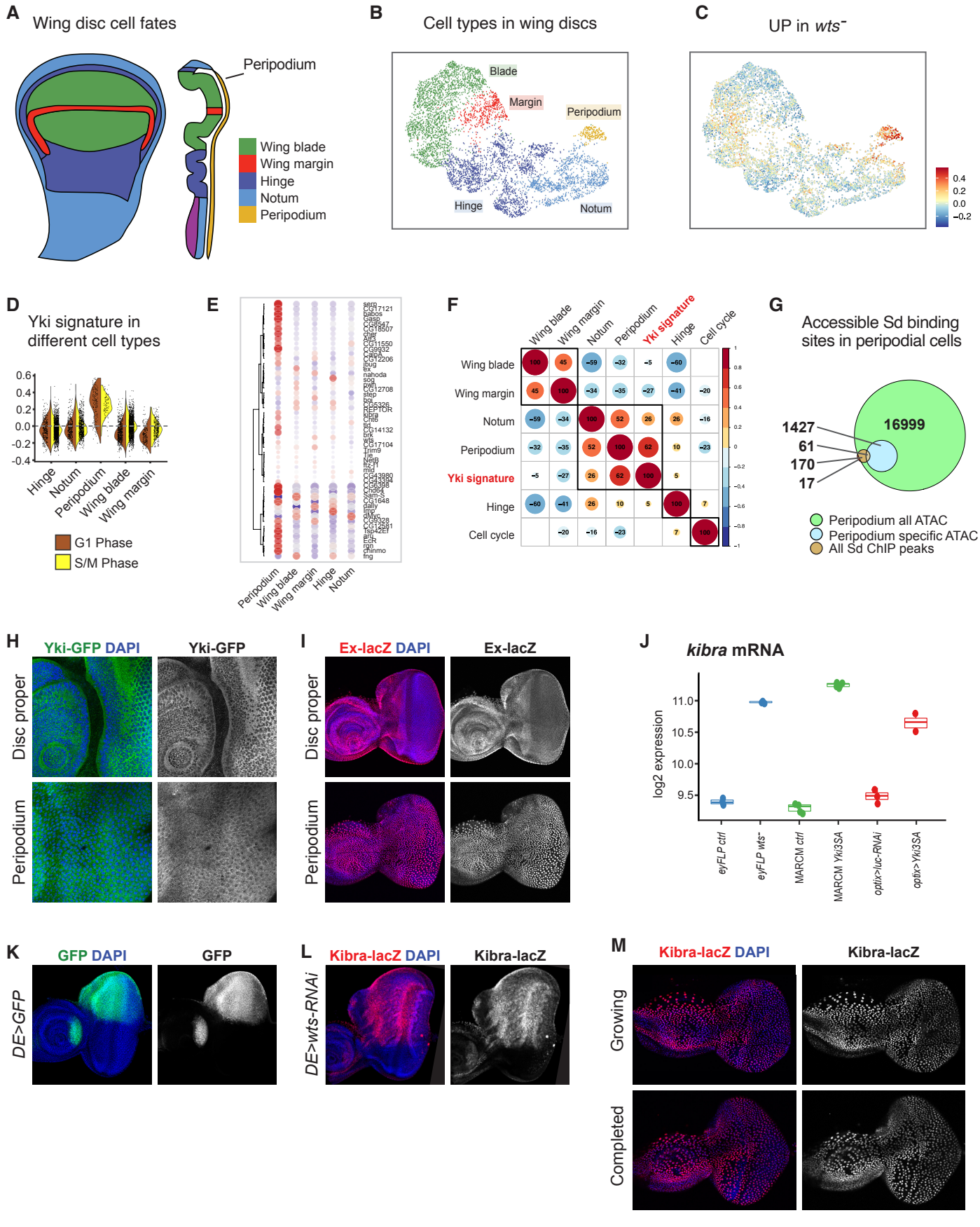

Fig. S11. Yki signature expression in wing discs.

(**A**) Schematic representation of a wild-type 3rd instar wing imaginal disc and its cross section showing the location of the major cell types.

(**B**) UMAP plot of single cell RNA-seq data with 8710 cells of the wing disc colored by assigned cell type.

(**C**) Normalized average expression of Yki signature genes in the single cells of the wing imaginal disc. The Yki signature showed highest expression in peripodial cells.

(**D**) Violin plot showing normalized average expression of Yki signature genes in single cells of the wing imaginal disc, grouped by cell type and then split and colored by cell cycle phase. Yki signature genes showed predominant expression in all peripodial cells regardless of whether they are cycling or not.

(**E**) Dotplot showing the expression of individual genes of the Yki signature averaged over all cells in a given cell type; the color of the dots represents relative expression, and the size and transparency of the dots represent the percentage of cells expressing a given gene. The majority of the genes had higher expression in peripodial cells.

(**F**) Correlations between the normalized average expression pattern of the indicated gene sets in the single cells of the wing disc, ordered by hierarchical clustering with k=4 clusters marked by thicker lines; the size and the color of the dots represent correlation coefficient (R, Pearson's correlation), only statistically significant values are shown ($P<0.01$). The expression pattern of the Yki signature genes showed very high correlation with the expression of marker genes for peripodial cells.

(**G**) Venn diagram showing the overlap between all accessible chromatin regions in peripodial cells (green), regions specifically accessible in peripodial cells (blue) and high confidence Sd ChIP-Nexus peaks with enriched Sd binding motifs (brown). Only 17 out of 248 Sd binding sites are not accessible in peripodial cells and 61 out of 248 Sd binding sites are accessible only in peripodial cells.

(**H** and **I**) Comparison of Yki activity in disc proper and peripodial cells of the eye disc assessed by standard read-outs – nuclear localization of Yki-GFP (H, green, grey, images at 40x magnification) and expression of *ex-lacZ* (I, red, grey, images at standard 20x magnification).

(**J**) Boxplot showing the absolute expression (in log2 scale) of *kibra* in the three genotypes with Yki hyperactivation in eye discs: Yki^{3SA} overexpression in clones in eye discs (MARCM *Yki3SA)*, *wts* knockout clones in eye discs *(ey-FLP* wts^{-}*)*, and Yki^{3SA} overexpression specifically in the eye disc proper (*optix>*Yki^{3SA}). Each dot represents an individual RNA-seq sample. Expression of *kibra* was robustly induced by Yki hyperactivation and showed stable expression in all of the control samples regardless of their genotype (i.e. its basal expression is not highly variable and not readily influenced by other transgenes such as GFP or non-targeting RNAi), which altogether makes it an excellent transcriptional read-out of Yki activity.

(**K**) Confocal image of an eye disc showing the expression pattern of GFP driven by *DE-Gal4* in the dorsal half of the eye disc. GFP (green, grey), nuclei (DAPI, blue).

(**L**) Confocal image of an eye disc with knockdown of *wts* by expression of *wts-RNAi* using the *DE-Gal4* driver (*DE>wts-RNAi*) stained for *kibra-lacZ* expression (red, grey) and nuclei (DAPI, blue). Knockdown of *wts* lead to tissue overgrowth and strong induction of *kibra-lacZ* expression. Yki hyperactivation was restricted to the dorsal part of the eye disc where it drove strong induction of *kibra-lacZ*, whereas the ventral part of the disc had wild-type levels of Yki activity and, concordantly, showed no expression of *kibra-lacZ*.

(**M**) Expression of *kibra-lacZ* is specific to peripodial cells regardless of their proliferation status. Actively growing (top) or growth completed (bottom) eye imaginal discs stained for *kibra-lacZ* expression (red, grey) and nuclei (DAPI, blue). This result suggests that Yki activity drives the identity of peripodial cells rather than their growth.

Figure S12. The transcriptional program of Yap hyperactivation in the adult liver

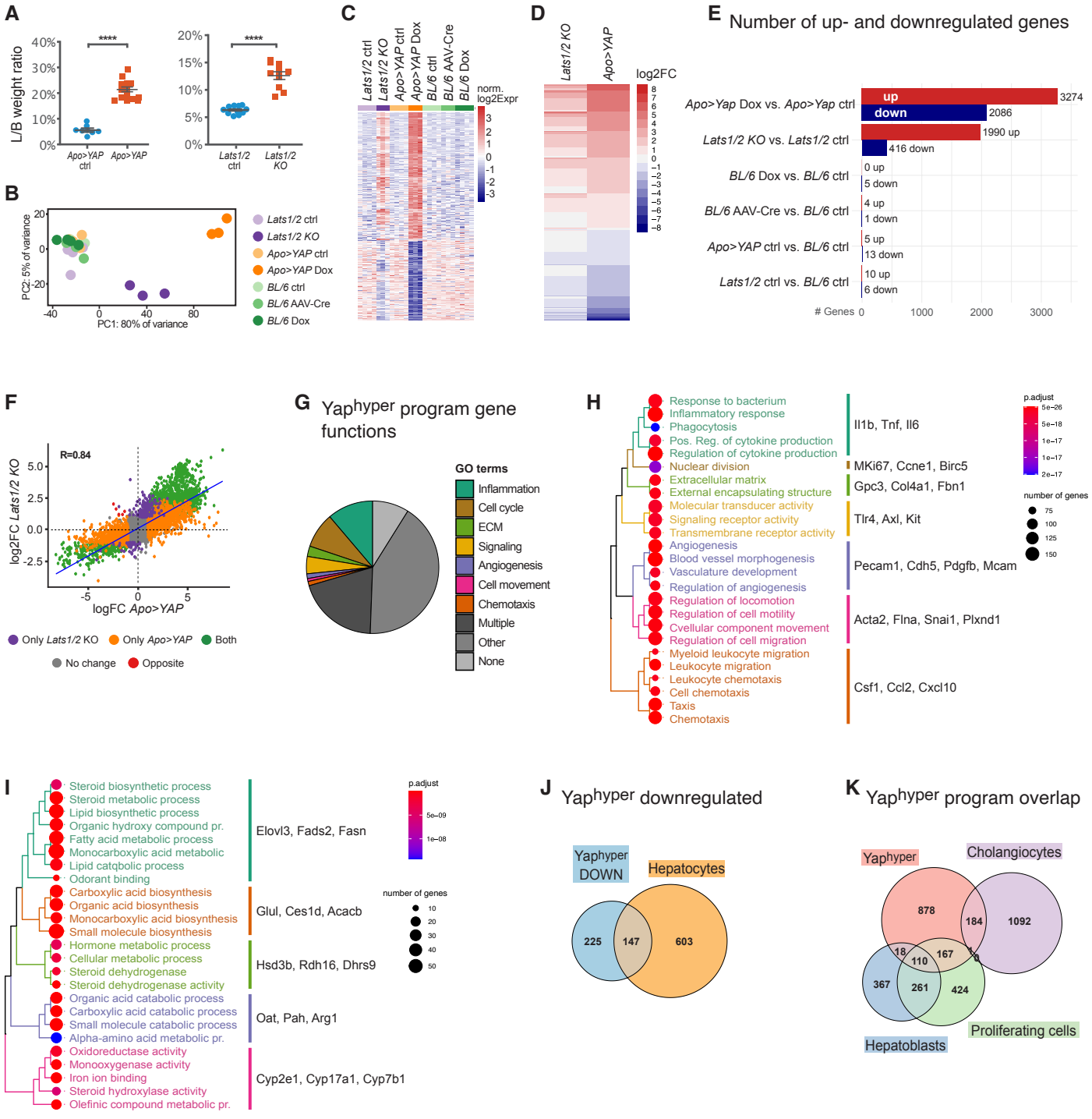

Fig. S12. The transcriptional program of Yap hyperactivation in the adult liver.

(**A**) Liver to body weight ratio was significantly increased upon Yap/Taz hyperactivation in both *Apo>YAP* (left) and *Lats1/2 KO* mice (right); N=10; **** P<0.001.

(**B**) Principal component analysis (PCA) plot showing the differences between the adult hepatocytes with hyperactivated Yap and control conditions. Experimental hyperactivation of Yap was the main source of transcriptional changes encompassing 80% of total variance along PC1, whereas the samples from all of the control conditions clustered closely together.

(**C** and **D**) Heatmaps of all differentially expressed genes (P adj. < 0.05; |log2FC| > 1) in purified hepatocytes from *Apo>Yap* and *Lats1/2 KO* mice. Relative gene expression in control and Yap hyperactivated samples (C) and respective log2 fold changes for the two comparisons (D) show overall similarity between *Apo>YAP* and *Lats1/2 KO* and that all of these changes can be attributed to Yap hyperactivation rather than the treatment with Doxycycline or AAV-Cre itself.

(**E**) Barplot showing the number of significantly up- or downregulated genes (P adj. < 0.05; |log2FC| > 1) for the indicated comparisons. Yap hyperactivation led to significant changes in expression of thousands of genes, whereas there were virtually no differences between the hepatocytes' transcriptome of different control strains and no overall effects of the Doxycycline or AAV-Cre treatments in BL/6 mice.

(**F**) Correlation of log2 fold change in gene expression induced by *Apo>YAP* or *Lats1/2 KO* (compared to their controls); significantly differentially expressed genes (P adj. < 0.05; |log2FC| > 1) in both genotypes, only in *Apo>YAP* and only in *Lats1/2 KO* are marked in green, orange and purple, respectively. 5 genes marked in red are downregulated in *Apo>YAP* but upregulated in *Lats1/2 KO*. There is an overall high correlation between the changes induced in the two genotypes.

(**G**) Functional classification of the Yap^{hyper} program genes - top 50 most significant GO terms have been grouped into 7 categories: Inflammation, Cell cycle, ECM, Signaling, Angiogenesis, Cellular movement and Leukocyte chemotaxis. The pie chart shows the proportion of the Yap^{hyper} program genes which belong to one of the given GO terms category, "multiple" for genes in more than one category, "other" for genes associated with GO terms outside of the top 50 and "none" for genes that do not belong to any enriched GO term.

(**H**) Treeplot showing the clustering of the top 25 GO terms enriched in the Yap^{hyper} program. The color of the dot reflects the adjusted P value, and the size is proportional to the number of genes in the overlap between the given GO term and the Yap^{hyper} program. The GO terms have been clustered by similarity and divided into 7 categories: (from the top) Inflammation, Cell cycle, ECM, Signaling, Angiogenesis, Cellular movement and Leukocyte chemotaxis. Representative genes from each category are listed on the right.

(**I**) Treeplot showing the clustering of the top 25 GO terms enriched in the genes downregulated in both *Apo>YAP* and *Lats1/2 KO*. The color of the dot reflects the adjusted P value, and the size is proportional to the number of genes in the overlap between the given GO term and the downregulated genes. The GO terms have been clustered by similarity and divided into 5 categories. Representative genes from each category are listed on the right.

(**J**) Venn diagram showing the overlap between the genes downregulated in both *Apo>YAP* and *Lats1/2 KO* (Yap^{hyper} DOWN) and hepatocyte markers (genes preferentially expressed in hepatocytes compared to other cell types of the adult liver). 40% of the genes downregulated upon Yap hyperactivation are hepatocyte markers and Yap hyperactivation leads to downregulation of 20% of hepatocyte-specific program.

(**K**) Venn diagram showing the overlap between the Yap^{hyper} program genes and markers of different cell populations in the developing liver: all hepatoblasts, all proliferating cells (in S or G2/M phase) and cholangiocytes. Many hepatoblast markers are actually specific to all proliferating cells and this is especially true for the hepatoblast markers that overlap with the Yap^{hyper} program.

Figure S13. The regeneration program in control and *Yap/Taz KO* hepatocytes

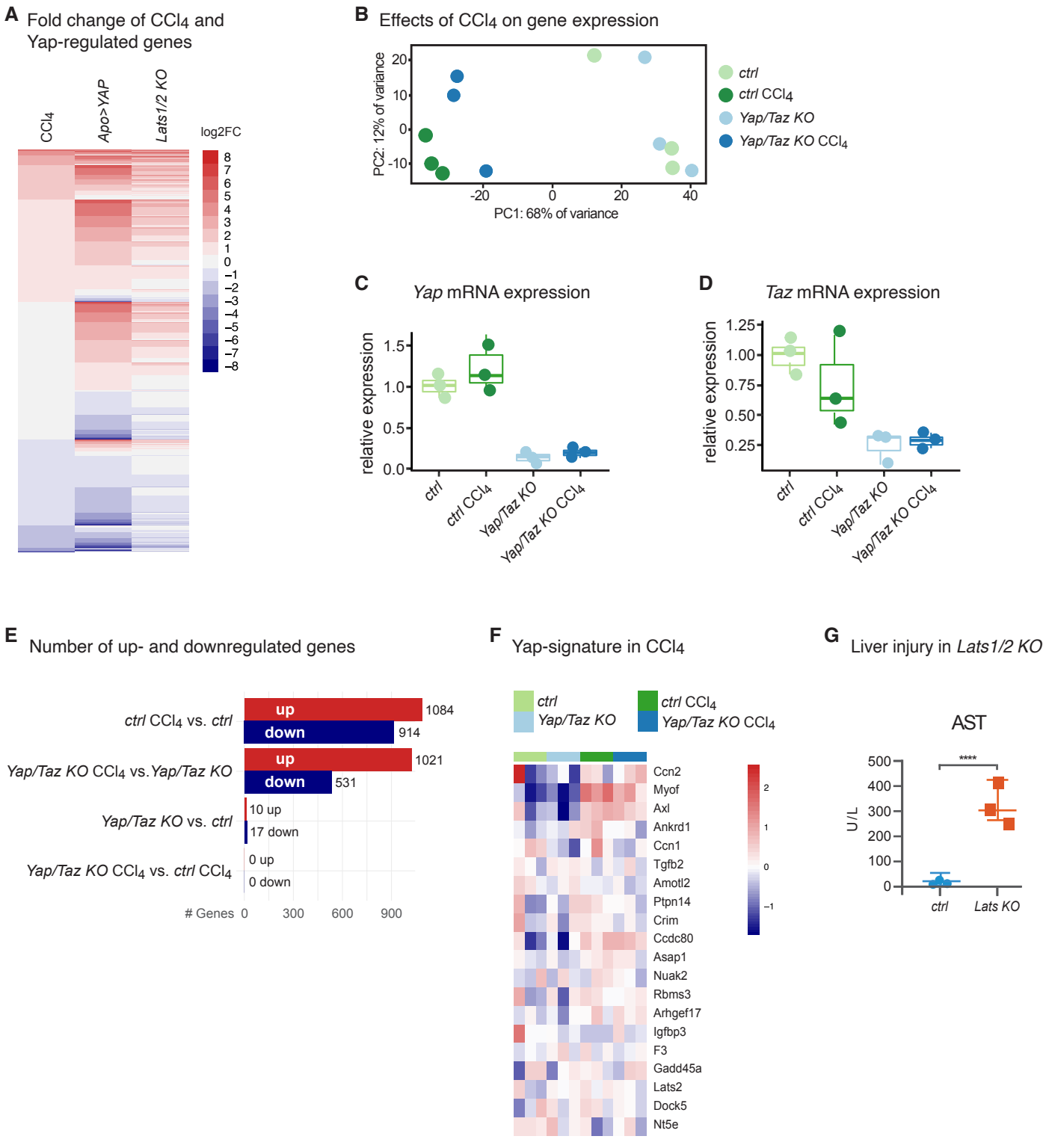

Fig. S13. The regeneration program in control and *Yap/Taz KO* hepatocytes.

(**A**) log2 fold changes in the expression of all differentially expressed genes for comparisons between the indicated conditions and their respective controls; values rounded to the nearest integer. Almost all of the genes induced by CCl_4 (red in the first column) are also upregulated by Yap hyperactivation (also red in *Apo>YAP* and *Lats1/2 KO*), similarly for the downregulated genes. In contrast, there are many genes changed by Yap hyperactivation but not by CCl_4 (white in the first column, but red or blue in *Apo>YAP* and *Lats1/2 KO)*.

(**B**) Principal component analysis (PCA) plot showing the differences in gene expression profiles between the hepatocytes of livers that are either *Yap/Taz* floxed (green) or *Yap/Taz KO* (blue) and are either before (brighter color) or 48h after CCl_4 injection (darker color). The effects of the toxic injury due to CCl_4 is the main source of changes to the gene expression with no major effects caused by the lack of *Yap* and *Taz*.

(**C** and **D**) Levels of *Yap* and *Taz* expression in *Yap/Taz KO* hepatocytes. Boxplots showing the relative expression of *Yap* (C) and *Taz* mRNA (D) in the indicated conditions, as measured by RT-qPCR. Each dot represents one sample, n=3.

(**E**) Barplot showing the number of significantly up- and downregulated genes (P adj. < 0.05; |log2FC| > 1) for the indicated comparisons. CCl_4 injection led to comparable changes in gene expression in *Yap/Taz* floxed and *Yap/Taz KO* hepatocytes. There were virtually no differences between the transcriptome of *Yap/Taz* floxed and *Yap/Taz KO* hepatocytes before CCl_4 injection and, strikingly, zero differentially expressed genes were identified between the regenerating *Yap/Taz* floxed and *Yap/Taz KO* hepatocytes at 48h after toxic injury.

(**F**) Heatmap showing the relative expression of Yap signature genes in the indicated conditions. The Yap signature is not induced at 48h after CCl_4 injection in neither *Yap/Taz* floxed nor *Yap/Taz KO* hepatocytes.

(**G**) *Lats1/2* KO mice have increased blood serum levels of AST compared to control animals, indicative of liver damage; N=3, **** P<0.001.

Figure S14. Gene functions of the Yap-specific and Yap-CCl_4 parts of the Yap^{hyper} program

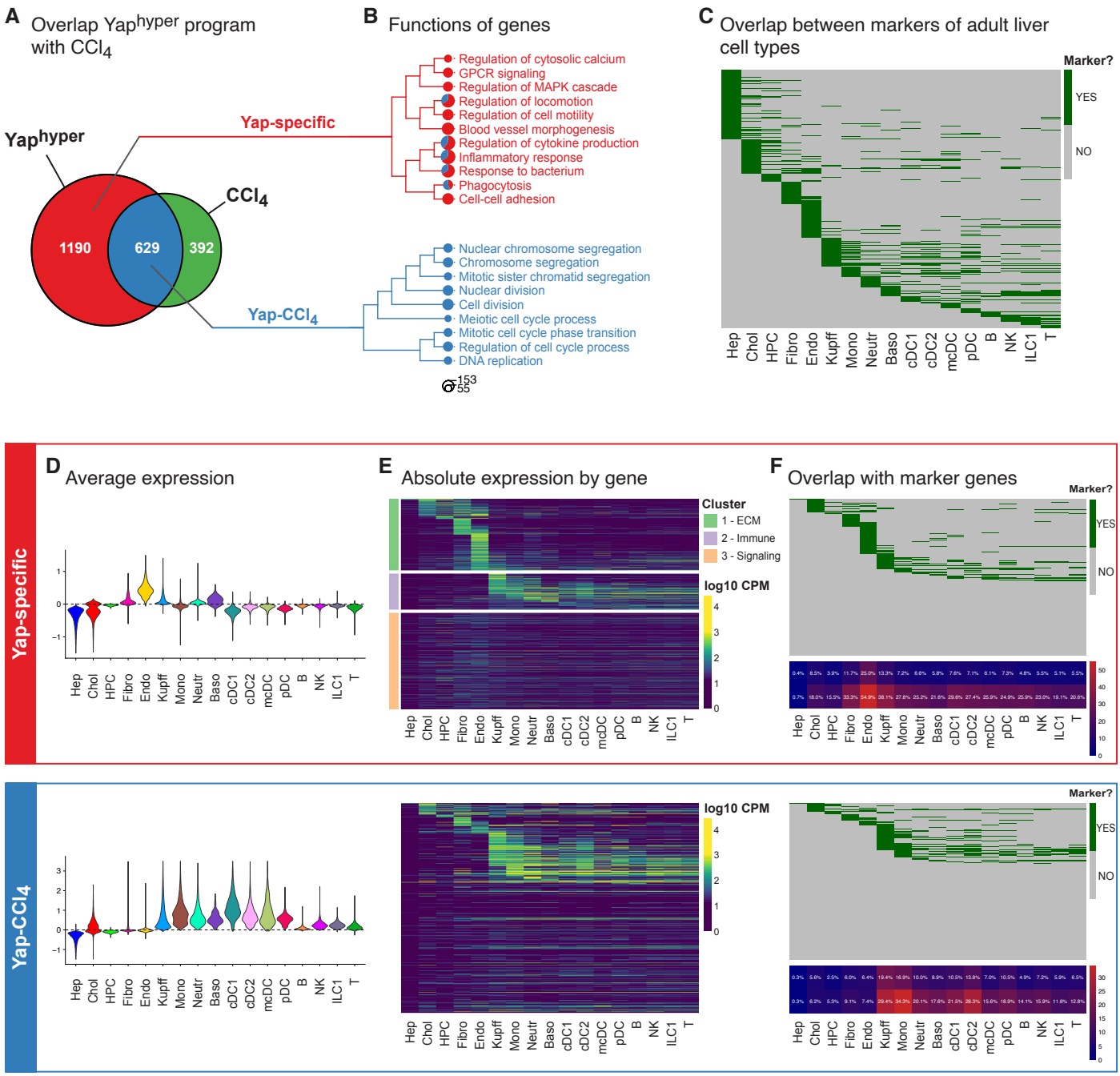

Fig. S14. Gene functions of the Yap-specific and Yap-CCl_4 parts of the Yap^{hyper} program.

(**A**) Venn diagram showing the overlap between the Yap^{hyper} program and genes induced by CCl_4. The shared Yap-CCl_4 part makes up 35% of the Yap^{hyper} program and 62% of the regeneration program.

(**B**) Treeplot showing the clustering of the top 10 most significant GO terms for the Yap-specific and Yap-CCl_4 parts of the Yap^{hyper} program, clustered by similarity. The size of the dots corresponds to the number of genes in the overlap between the given GO term and the Yap^{hyper} program and the dots are colored in red and blue to reflect the fractions of the genes belonging to the Yap-specific and Yap-CCl_4 parts of the program. Yap-CCl_4 shows enrichment in cell proliferation, whereas Yap-specific genes are enriched in the GO terms related to cell adhesion, blood vessels and inflammation.

(**C**) Visualization of the overlap between the marker genes of all cell types of the adult liver single cell atlas. The plot shows all of the marker genes (rows); a gene that is a marker for a given cell type (columns) is marked in green. The markers are ordered by cell type.

(**D**) Violin plots showing the distribution of the averaged expression of Yap-specific (top) and Yap-CCl_4 genes (bottom) in single cells of adult liver atlas grouped by cell identity. The Yap-specific program shows the highest expression in endothelial cells, whereas Yap-CCl_4 genes are enriched in the immune cell types.

(**E**) Absolute expression levels (log10 CPM) of Yap-specific (top) and Yap-CCl_4 (bottom) program genes. In each heatmap, the genes are ordered by their marker gene status, such that cluster 1 are genes that are markers of cholangiocytes, HPCs, fibroblasts or endothelial cells, cluster 2 are genes that are markers of the immune cell types and cluster 3 are genes that are not markers of any particular cell type.

(**F**) Visualization of the overlap between the marker genes of all cell types and the Yap-specific (top) and Yap-CCl_4 (bottom) programs. The genes that are markers for a given cell type are marked in green. The values below the main plot show, in the first row, the percent of the Yap-specific (or Yap-CCl_4) genes that are markers for a given cell type (e.g. 25% of Yap-specific genes are endothelial markers) and in the second row, the percent of the marker genes that belong to the Yap-specific (or Yap-CCl_4) program (e.g. 33% of all fibroblast markers belong to the Yap-specific program).

Figure S15. Yki hyperactivation in eye discs activates a portion of the peripodial cell program

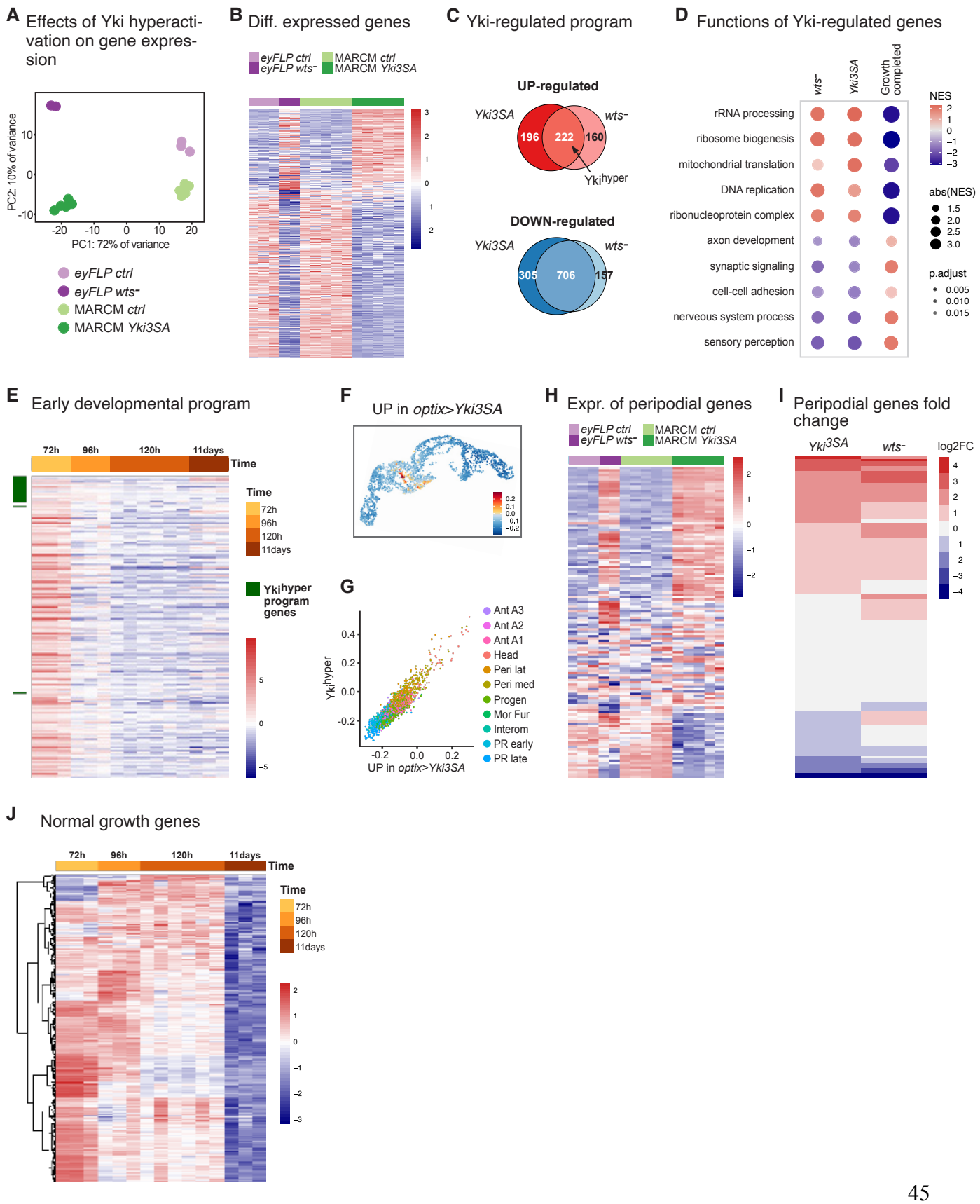

Fig. S15. Yki hyperactivation in eye discs activates a portion of the peripodial cell program.

(**A**) Principal component analysis (PCA) plot showing the differences in gene expression between eye discs with clones of cells with Yki hyperactivation (by Yki^{3SA} overexpression or *wts* KO) and their respective controls. Experimental hyperactivation of Yki is the main source of transcriptional changes encompassing 74% of total variance along PC1, whereas PC2 (15% variance) represents the differences between the two genotypes.

(**B**) Heatmap of all differentially expressed genes (P adj. < 0.05; |log2FC| > 1) in the two methods of Yki hyperactivation in the eye disc: Yki^{3SA} overexpression and *wts* knockout. Relative gene expression in control and Yki hyperactive samples shows overall similarity between Yki^{3SA} and *wts* knockout.

(**C**) Venn Diagram showing the overlap between the upregulated (top) and downregulated (bottom) genes in two methods of Yki hyperactivation: Yki^{3SA} overexpression and *wts* knockout.

(**D**) Dot plot representation of gene set enrichment analysis (GSEA) for the changes in gene expression caused by Yki hyperactivation shows enrichment for growth related GO terms in the upregulated genes and photoreceptor specific functions in the downregulated genes. The color of the dots corresponds to the Normalized Enrichment Score, NES, the size of the dot represents the absolute value of NES and the transparency reflects the adjusted p value.

(**E**) Heatmap showing relative expression of genes significantly upregulated in eye discs at 72h AEL (after egg laying) as compared to 120h AEL. Genes that belong to the Yki^{hyper} program are indicated by a green bar on the left side of the heatmap. Yki^{hyper} program genes make up only a small fraction of all the genes characteristic of the early eye development.

(**F** and **G**) Normalized average expression of the genes upregulated (P adj. < 0.05; log2FC > 1) upon Yki^{3SA} overexpression in the eye disc proper (*optix>*Yki^{3SA}) (F) and its correlation with the expression of Yki^{hyper} program genes (G). Genes induced by Yki^{3SA} overexpression in the eye disc proper are expressed in wild-type discs in the same peripodial cells as the genes induced by Yki^{hyper} program.

(**H** and **I**) Expression of marker genes (P adj. < 0.05; log2FC > 0.5) of all peripodial cells in two methods of Yki hyperactivation: Yki^{3SA} overexpression and *wts* knockout. (H) Relative expression in control and Yki hyperactive samples and (I) respective log2 fold changes for the two

comparisons show that less than half of the peripodial markers are induced by Yki hyperactivation.

(**J**) Expression of "normal growth" genes during the time course of eye disc development. Heatmap shows the relative expression of genes downregulated after growth termination (P adj. < 0.05; log2FC < -1) in growth-completed (day 11 AEL) eye imaginal discs as compared to actively growing discs (at 120h AEL). The majority of these "normal growth representing genes" are uniformly expressed at the three time points (72h, 96h, 120h AEL) of active growth rather than specifically in the late third instar (120h AEL), which validates this gene set as a general developmental growth signature.

Figure S16. Characterization of the Yki hyperactivation program in wing discs

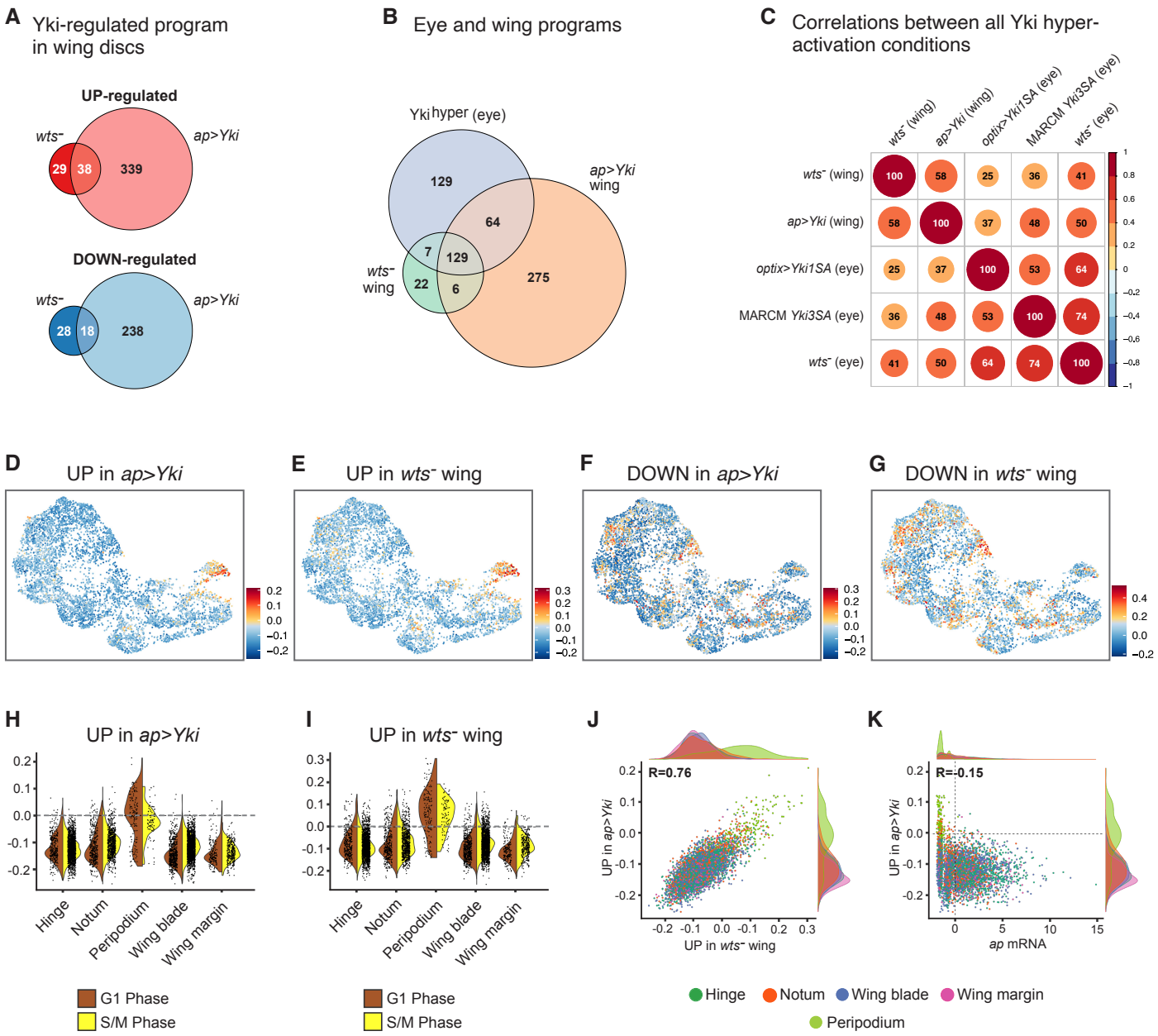

Fig. S16. Characterization of the Yki hyperactivation program in wing discs.

(**A**) Venn diagram showing the overlap between the upregulated (top) and downregulated (bottom) genes in two methods of Yki hyperactivation: Yki overexpression driven by *ap-Gal4* (*ap>Yki*) and *wts* knockout by *ubx-FLP* (*ubx-FLP wts*$^{-}$).

(**B**) Venn diagram showing the overlap between the genes of Yki^{hyper} program (upregulated upon Yki hyperactivation in eye discs) and genes induced (P adj. < 0.05; log2FC > 1) in wing discs in *ap>Yki* and *ubx-FLP wts*$^{-}$ discs.

(**C**) Correlation matrix showing correlations between the log2 fold changes in gene expression in the indicated conditions relative to their respective controls; the color and the size of each dot corresponds to the correlation coefficient (R); only significant values are shown (P<0.01). Overall, Yki hyperactivation causes similar changes to the transcriptome in eye and wing discs.

(**D** to **G**) Normalized average expression of the genes upregulated (left) and downregulated (right) in *ap>Yki* and *ubx-FLP wts*$^{-}$ discs visualized in the single cell atlas of the wing disc. Yki hyperactivation in wing discs leads to upregulation of genes normally expressed in peripodial cells, while downregulated genes are not specific to a single cell type of the wing disc. Cell type assignments are presented in Fig.S11B.

(**H** and **I**) Violin plot showing normalized average expression of the genes upregulated in *ap>Yki* and *ubx-FLP wts*$^{-}$ discs in single cells of the wing imaginal disc, grouped by cell type and then split and colored by cell cycle phase. Genes induced by Yki hyperactivation in wing discs show predominant expression in all peripodial cells regardless of whether they are cycling or not.

(**J**) Correlation between the average expression of the genes upregulated in *ap>Yki* and *ubx-FLP wts*$^{-}$ discs in the single cells of the wing imaginal disc colored by cell identity. The expression of the genes induced in both genotypes is highly correlated and characteristic of peripodial cells.

(**K**) Correlation between the average expression of the genes upregulated in Yki overexpression driven by *ap-Gal4* and the endogenous expression of *ap* in the single cells of the wing imaginal disc; colored by cell identity. Peripodial cells do not express *ap* (cells in green: distribution along the x-axis skewed to the left – very low expression), which means that *ap>Yki* drives the expression of peripodial genes in the wing disc proper. This is analogous to the genes induced by Yki^{3SA} overexpression driven by *optix-Gal4* in the eye disc proper being normally expressed in the peripodial cells (Fig.S15F-G).

Figure S17. The transcriptome of *Ras*^{V12G} *scrib*^{RNAi} tumors in eye and wing imaginal discs resembles that induced by Yki hyperactivation

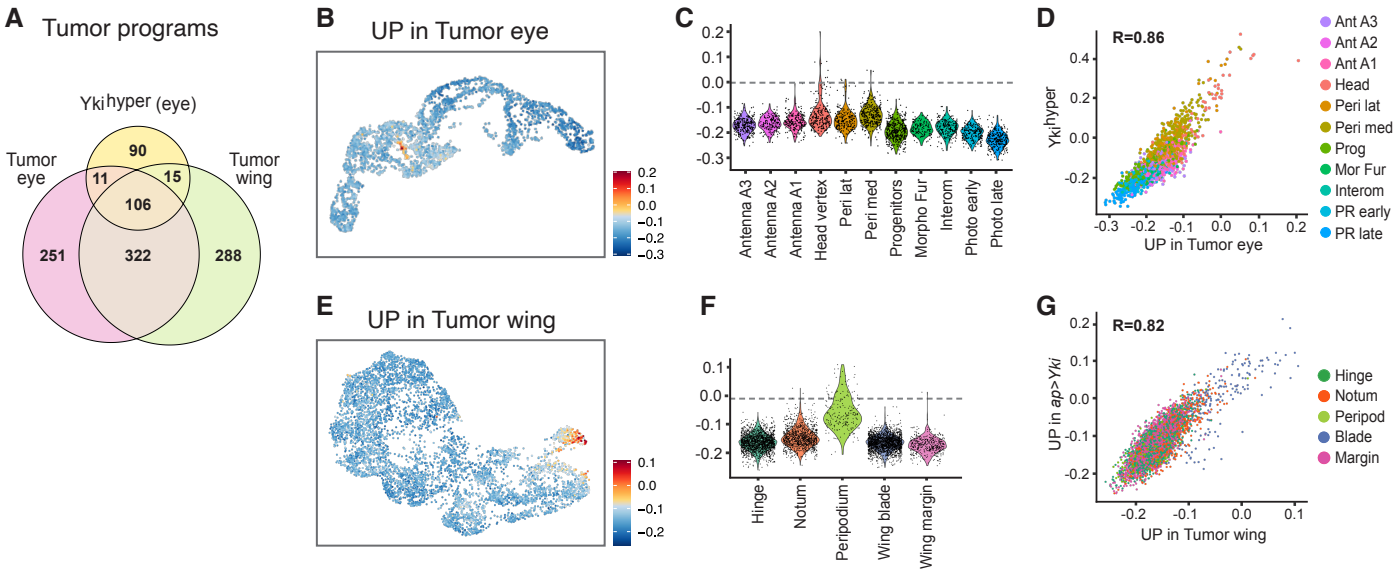

H Correlations between different types of growth: normal, Yki hyperactivation and tumors

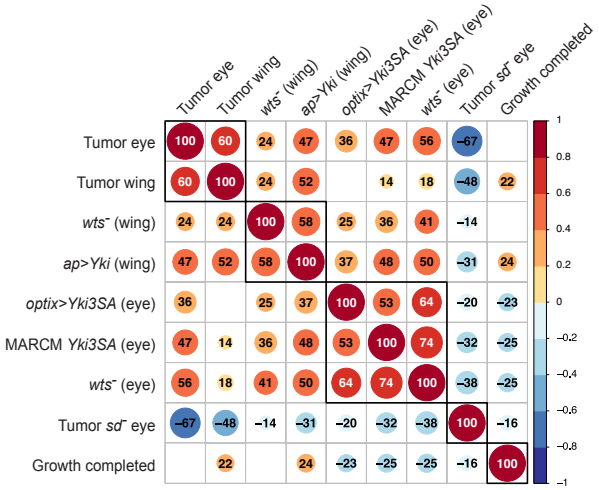

Fig. S17. The transcriptome of *Ras^{V12G} scrib^{RNAi}* tumors in eye and wing imaginal discs resembles that induced by Yki hyperactivation.

(**A**) Venn Diagram showing the overlap between the genes of Yki^{hyper} program (upregulated upon Yki hyperactivation in the eye disc) and the genes induced (P adj. < 0.05; log2FC > 1) in eye or wing discs with tumors (*hh*> *Ras^{V12G}, scrib^{RNAi}*). The tumors in the eye and wing discs are transcriptionally very similar to and encompass the majority of the Yki^{hyper} program.

(**B** to **D**) Tumors in the eye discs induce peripodial genes similarly to the Yki^{hyper} program. The normalized average expression of the genes upregulated (P adj. < 0.05; log2FC > 1) in the eye discs with tumors relative to control discs shown on the UMAP (B) and violin plot (C) show preferential expression in peripodial cells. The scatter plot (D) shows high correlation between the expression of the Yki^{hyper} and tumor program in the single cells of the eye imaginal disc; colored by cell identity.

(**E** to **G**) Tumors in wing discs also induce peripodial genes similarly to Yki hyperactivation. The normalized average expression of the genes upregulated (P adj. < 0.05; log2FC > 1) in wing discs with tumors relative to control discs shown on the UMAP (E) and violin plot (F) shows preferential expression in peripodial cells. The scatter plot (G) shows high correlation between the expression of the genes induced by tumors and Yki overexpression in the single cells of the wing imaginal disc; colored by cell identity.

(**H**) Correlation matrix showing correlations between the log2 fold changes in gene expression in the indicated conditions relative to their respective controls, ordered by hierarchical clustering with k=5 clusters marked by thicker lines; the color and the size of each dot corresponds to the correlation coefficient (R, Pearson's correlation); only significant values are shown (P<0.01). Overall, Yki hyperactivation causes similar changes to gene expression in eye and wing disc and the Yki hyperactivation gene expression profiles are much more similar to those of tumors than normal growth.

Table S1. (separate file)

Differential Gene Expression Analysis of Yki^{3SA} overexpression in *sd* mutant and *ctrl* clones.

Table S2. (separate file)

Establishment of a universal Yki signature.

Table S3. (separate file)

Differential Gene Expression Analysis of different time points of Drosophila eye disc development.

Table S4. (separate file)

Differential Gene Expression Analysis of Yap hyperactivation in adult hepatocytes.

Table S5. (separate file)

Differential Gene Expression Analysis of CCl4-induced liver injury in absence of Yap/Taz

Table S6. (separate file)

Expression, clustering and GO terms of Yap^{hyper} genes

Table S7. (separate file)

Markers and other gene sets – liver

Table S8. (separate file)

Differential Gene Expression Analysis of Yki hyperactivation in Drosophila imaginal discs

Table S9. (separate file)

Markers and other gene sets – Drosophila

Table S10. (separate file)

Results of in vivo RNAi screen of the growth phenotypes of Yki target genes